BROADBAND SOLAR RADIOMETRIC MEASUREMENTS IN THE GREATER DURBAN AREA

By Khulisile Kunene

Supervisor: Mr. M. J. Brooks

Co-supervisor: Prof. L. W. Roberts

University of KwaZulu-Natal

31 October 2011

Declaration

In fulfillment of the Master of Science in Engineering (MSc Eng), University of Kwa-Zulu Natal

Date: 31 October 2011

Supervisor: Mr. M. J. Brooks

As the candidates supervisor I agree/do not agree to the submission of this thesis.

I ..... declare that

(i) The research reported in this dissertation/thesis, except where otherwise indicated, is my original work.

(ii) This dissertation/thesis has not been submitted for any degree or examination at any other university.

(iii) This dissertation/thesis does not contain other persons" data, pictures, graphs or other information, unless specifically acknowledged as being sourced from other persons.

(iv) This dissertation/thesis does not contain other persons" writing, unless specifically acknowledged as being sourced from other researchers. Where other written sources have been quoted, then:

a) their words have been re-written but the general information attributed to them has been referenced;

b) where their exact words have been used, their writing has been placed inside quotation marks, and referenced.

(v) Where I have reproduced a publication of which I am an author, co-author or editor, I have indicated in detail which part of the publication was actually written by myself alone and have fully referenced such publications.

(vi) This dissertation/thesis does not contain text, graphics or tables copied and pasted from the Internet, unless specifically acknowledged, and the source being detailed in the dissertation/thesis and in the References sections.

Signed:……

On Year……. Month…….. Day…… at …….

Acknowledgements

This work has been a joint collaboration of the University of KwaZulu-Natal (UKZN), Westville and Howard College stations, and Mangosuthu University of Technology (MUT).

I gratefully acknowledge my supervisor, Mr. Michael Brooks and my co-supervisor Prof. Lance Roberts, for their knowledge and insight. To Mr. Michael Brooks, thank you for your patience, time, advice and encouragement throughout my research work.

I would also like to acknowledge the following,

- Eskom and UKZN High Voltage and Direct Current centre (HVDC) for their financial support for my studies.
- Mr. Markus Nowotny from Check IT Systems. Thank you for your assistance and knowledge in LabVIEW you shared with me.
- A special thank you to Mrs. Ewa Zawilska, a dear friend and colleague. Thank you for managing the station in MUT.
- Dr. Richard Loubser at the Sugar Milling Research Institute. Thank you for your assistance in MATLAB.

Last but most importantly, I would like to thank my mother and late father. If it were not the dream you instilled in me, I would not be here today. You have taught me to excel in all I do. You ignited a spark, which tomorrow will be a roaring fire, the benefits of which you shall reap. To my friends and family, thank you for believing in me. I am indebted to God, my creator. Thank-you God for the thirst of knowledge, successes and blessings you have bestowed upon me.

Abstract

This work comprises a radiometric study of Durban‟s solar resource, utilizing data from the Howard College campus of the University of KwaZulu-Natal (UKZN), and the Solar Thermal Applications Research Laboratory (STARlab) at Mangosuthu University of Technology (MUT), located 17 km away.

The study has three aims: first to establish a solar radiometric monitoring network for the greater Durban area, comprising the UKZN Howard College and Westville stations, and the STARlab facility at MUT. The UKZN Westville station is under refurbishment and should be operational by the end of 2011. Data from this station are not included in the study. The instrumentation and acquisition software in use at Howard College and STARlab are described. The stations record global horizontal irradiance (GHI), direct normal irradiance (DNI) and diffuse horizontal irradiance (DHI), measured by an unshaded pyranometer, a normal incidence pyrheliometer and a pyranometer shaded with a stationary band respectively.

Second, to test a number of existing radiometric models against measured data gathered at the stations. Radiometric models assist in estimating missing components of radiation at stations that do not measure all three components separately, for reasons of cost. The models investigated included Erbs et al. (1982), Orgill and Hollands (1977), Reindl et al. (1990), Boland et al. (2001), and Skartveit and Olseth (1987) and correction models by Drummond et al. (1956), Le Baron et al. (1990), Batlles et al. (1995), and Muneer and Zhang (2000) to correct the shadow band effect.

Third, to compare data from the two operational stations and to investigate potential spatial differences in sun strength arising from micro-climate effects in the greater Durban area. This takes the form of a statistical analysis of the differences in radiometric data recorded simultaneously at the UKZN and STARlab stations. The study found that the recorded difference in GHI over one year was 0.72%, which lies within the instrument measurement accuracy. Therefore no measurable radiometric differences due to microclimate could be detected and, for the period in which data were collected, measurements from Howard College could be used to estimate irradiance patterns for MUT, and vice versa.

Table of contents

List of symbols and abbreviations

A	Air mass
b	Width of shadow band (m)
b_1	Sky condition containing the sun as described by Muneer and Zhang
b_2	Sky condition opposing the sun as described by Muneer and Zhang
C_B	Shadow band correction factor by the Batlles et al. model
C_D	Shadow band correction factor by the Drummond model
C_L	Shadow band correction factor by the Le Baron et al. model
C_M	Shadow band correction factor of Muneer and Zhang model
D	Diameter of particle in Mie"s theory
DHI	Diffuse horizontal irradiance (W/m^2)
DNI	Direct normal irradiance (W/m^2)
E	Global horizontal irradiance from reference pyranometer during calibration
E_i	Error of the i^{th} data point
E_o	Eccentricity correction factor of the earth
E_{off}	Thermal offset error
E_{IR}	Net infra red radiation
f	Portion of hemisphere blocked by shadow band
GHI	Global horizontal irradiance (W/m^2)
HC	Howard College station
I_b	Hourly beam/direct irradiance incident (W/m^2)
I_d	Hourly diffuse irradiance incident on a horizontal surface (W/m^2)
I_{Db}	Diffuse horizontal irradiance by the Batlles et al. model (W/m^2)
I_{dD}	Diffuse horizontal irradiance by the Drummond model (W/m^2
I_{dL}	Diffuse horizontal irradiance by the Le Baron et al. model (W/m^2)
I_{dM}	Diffuse horizontal irradiance by the Muneer and Zhang model (W/m^2)
I_{dUn}	Uncorrected diffuse horizontal irradiance (W/m^2)
I_g	Hourly global irradiance incident on a horizontal surface (W/m^2)
$I_g(cal)$	Reference global horizontal irradiance from calibrated sensor at NREL (W/m^2)
I_{Ghc}	Sum of global horizontal irradiation calculated at Howard College (kJ/m^2h)

I_{gMUT}	Sum of global horizontal irradiation calculated at MUT (kJ/m^{2}h)
$I_g(new)$	Newly calibrated global horizontal irradiance
$I_g(uncal)$	Uncalibrated global horizontal irradiance
I_n	Normal beam component calculated from the closure equation 1.1 (W/m^2)
I_O	Hourly extraterrestrial irradiance incident on a horizontal surface (W/m^2)
I_{sc}	Solar constant (W/m^2)
K	Hourly diffuse fraction
k_t	Hourly clearness index
MBE	Mean bias error
MUT	Mangosuthu University of Technology
N	Day number of the year or index of refraction
N	Number of data points
NREL	National Renewable Energy Laboratory
PSP(1)	Pyranometer at STARlab to be calibrated, currently measuring DHI.
PSP(2)	Pyranometer at STARlab to be calibrated, currently measuring GHI.
PSP(3)	Recently calibrated pyranometer at STARlab in July 2009
R	Radius of shadow band (m)
R^2	Coefficient of determination
RMSE	Root mean square error
RS	Responsivity or calibration factor (μV/W/m^2)
RS_g	Calculated minute responsivity from test radiometers (μV/W/m^2)
$RS_{45\text{-}55}$	Responsivity in the zenith range 45°-55° (μV/W/m^2)
S	Output voltage when pyranometer is shaded (V)
SST	Total sum of squares
SSE	Sum of squares
STARlab	Solar Thermal Applications Research Laboratory
U	Output voltage when pyranometer is unshaded (V)
V_u	Voltage of each pyranometer signal during component summation method (V)
W	View angle of shadow band subtended at diffuse irradiance sensor

Greek symbols

δ	Declination, north positive, south negative
Φ	Latitude, north positive, south negative

θ_z	Average zenith angle
ω	Hour angle, solar noon zero, mornings positive and afternoons negative
ω_i	Hour angle at middle of an hour, solar noon zero, mornings positive and afternoons negative
ω_s	Sunset hour angle
α	Solar altitude
ε	Function of the sky clearness

List of figures Page

List of tables

CHAPTER 1: INTRODUCTION

The study describes the set up of stations with common instrumentation and software format in the greater Durban area of KwaZulu-Natal. Data generated at the stations are analysed and compared with a set of well-known solar radiometric models. An inter-station comparison is performed to establish any spatial variations that may be ascribed to micro-climate effects. Variations in the sun‟s intensity at the earth‟s surface are caused by local geography, latitude and seasonal changes.

Coastal regions in particular are affected by micro-climate effects causing variations in sun strength over relatively small distances [1]. With the new focus on renewable energy, accurate knowledge of sun strength is vital. Engineers, financiers and project planners require information of the breakdown of irradiance into its different components namely; global horizontal irradiance (GHI), direct normal or beam irradiance (DNI) and diffuse horizontal irradiance (DHI). This aids in evaluating the technical and economic aspects of solar energy systems they intend to implement. Sun strength data are obtainable in various ways, for example, radiometric models. Radiometric models are simplified versions of mathematical concepts to predict solar irradiance values for any location, other than the place in which they were derived. They are based on experimental data that has been collected and analyzed. Other sources of sun strength measurements include satellite data and ground-based data. Solar radiation data derived from geostationary satellites produces estimates with high root mean square errors of 20-25% or about 80-100 W/m^2 [2]. Three reported sources of error are i) the difference between single point measurements and pixels extended in space, ii) errors due to pyranometric measurements and iii) assumptions made in deriving models to convert satellite data into ground radiation [3]. Ground-based data are potentially the most accurate when all three components of irradiance are measured separately. For various radiometric schemes, explained in Chapter 4, estimating the „missing‟ component based on the measurement of a single radiometric quantity is common. This is because of the high cost of radiometric equipment, which has led to the development of a selected number of radiometric models. In characterizing Durban‟s solar resource, this study aims to quantify the limitations by comparing ground data with modelled values.

Measurement of energy from the sun is an expensive practice. This is why few stations in the world have reliable, long-term measured irradiance databases [4]. Accurate solar radiation data are also limited with respect to geographic location and patchy in terms of long-term history [5]. Therefore,

more accurate measuring ground stations are required in South Africa and this study is a contribution in this regard. Direct measurements of ground-based data were used in this work to measure the local solar resource.

Research question

The eThekwini Municipality, which incorporates the greater Durban region, has expressed interest in large-scale use of solar water heaters, off-grid photovoltaics and related solar energy technologies in an attempt to reduce the reliance on the main electricity grid. Solar energy technologies are an ideal option for rural electrification in sparsely located homesteads. Accurate knowledge of sun strength is required for the technical and economic evaluation of solar energy technologies. Sun strength measurements are obtainable in various ways such as:

1. Ground data
2. Long term maps
3. Satellite sensors
4. Mathematical models

Of the various ways stated above, ground-based data are potentially the most accurate although establishing a radiometric station is expensive. The high cost of radiometric facilities has resulted in the development of mathematical radiometric models that are often inaccurate when applied other than where they were derived. The study aims to quantify the accuracy of a set of models as they apply to the solar resource available in Durban. Mathematical models require certain adjustments of regression constants to suit the new location in which they are to be implemented. Some authors tend to use the models as they are with no alterations as in [6] and [7]. Adopting the works of [6] and [7], a similar exercise is executed at two operational stations located on the South African East coast. These stations are the Solar Thermal Applications Research Laboratory (STARlab) located in uMlazi at the Mangosuthu University of Technology (MUT) and at the University of KwaZulu-Natal (UKZN), Howard College campus. The results of the analysis are shown in Chapter 4.

Another aspect that is addressed is that of whether two radiometric stations located approximately 20 km apart in a coastal region should experience measurable variations in solar radiation. Ocean activity affects weather, climate and hence solar radiation patterns of nearby locations. Changes in ocean activity result from the earth‟s rotation that accounts for the Coriolis force [8]. The tilt of the earth accounts for the seasons that exist which modulate the intensity of radiation incident at any

location on the earth‟s surface. Coastal regions are greatly affected as ocean currents and sea clouds blowing onto shore modify the local weather, and hence, climate patterns of locations nearby.

Aims

The aims of this work were

1. To establish solar radiometric stations with similar data acquisition software and instrumentation to accurately measure solar irradiance. Using similar equipment aids in valid comparisons of data between stations. The LabVIEW software tool was used to write code for data acquisition and storage.
2. To process and analyse data gathered at HC and MUT for the period May 2010 to April 2011. Well-known solar radiometric models were used for analysis. The models chosen for use in this study include predictive models by Erbs et al. (1982), Orgill and Hollands (1977), Reindl et al. (1990), Boland et al. (2001), and Skartveit and Olseth (1987) . Shadow band correction models by Drummond et al. (1956), Le Baron et al. (1990), Batlles et al. (1995), and Muneer and Zhang (2000) were also investigated.
3. To gather and compare twelve months worth of data at both the HC and MUT stations to answer the question of any spatial variations of sun strength between the two stations. The comparison also involves a statistical analysis between measured and modelled data from Durban.

1.1 Solar radiometry

Solar radiometry is the study of solar irradiance, measured as an energy flux in watts per square metre (W/m^2) or as radiation in joules per square metre (J/m^2). Solar radiation describes radiation emitted from the sun in the visible and near-visible (ultra-violet and near-infrared) regions with wavelengths between 0.2 μm and 4.0 μm (microns) [9]. Not all of the energy emitted by the sun reaches the earth‟s surface as shown in Fig. 1-1 [10]. A fraction of it is absorbed or scattered by constituents of the atmosphere such as ozone, water vapor, Mie scattering, mixed gases, clouds and aerosols. Obtaining true solar measurements is important in assessing the available solar resource for a particular location. Solar irradiance incident at the earth‟s surface is typically measured as diffuse horizontal irradiance (DHI) made up of all indirect radiation falling on a horizontally located sensor, and as direct normal irradiance (DNI) comprising the beam radiation emanating from the solar disk itself, measured normal to the beam. A third commonly measured value is global

horizontal irradiance (GHI) made up of the DHI and a component of DNI, measured by a horizontally located sensor. The work undertaken here encompasses shortwave radiation in the bandwidth 0.3-2.5 μm and includes the visible spectrum. Pyranometers and pyrheliometers measure shortwave radiation whilst a pyrgeometer measures long wave radiation. Pyrgeometers are not used in this study.

1.2 Types of solar radiation

1.2.1 Diffuse horizontal irradiance (DHI)

Diffuse horizontal irradiance is the energy that is scattered in the atmosphere and which is measured on a horizontal surface. All particles in nature scatter radiation. The larger the particle, the greater is the scattering effect and the greater is the diffuse irradiance measured [10]. From [10], for a scattering particle of size πD/λ, Mie‟s theory applies when $\frac{0.6}{n} < \frac{\pi D}{\lambda} < 5$ where λ is the wavelength in micrometers, D is the diameter of the particle in metres and n is the index of refraction. Diffuse irradiance is typically measured using a pyranometer shaded with a shadow band, as described in 1.3.1.

1.2.2 Direct normal irradiance (DNI)

The beam or DNI component is the energy incident on the earth‟s surface that emanates from the solar disk. This is the only component of the sun that can be concentrated because it is directional or collimated and is used in solar collectors for thermal heating and storage. The magnitude of this component is attenuated by reflection, and absorption by atmospheric constituents. Fig. 1-1 shows the distribution of solar radiation in the atmosphere. Direct normal irradiance is measured using a normal incidence pyrheliometer.

1.2.3 Global horizontal irradiance (GHI)

Global horizontal irradiance is the total solar radiation on a horizontal surface as measured within a hemispherical view of 180°. It includes the scattered rays as well as collimated direct rays. GHI is calculated as the sum of DHI and the component of the direct irradiance normal to the surface. For a horizontal surface, the three components are related by the following closure equation

$$I_g = I_d + I_b \cos\theta_z \tag{1.1}$$

where I_g, I_b and I_d represent the global horizontal, direct normal and diffuse horizontal irradiances respectively. The parameter θ_z is the solar zenith angle that is the angle of incidence of beam radiation on a horizontal surface [11].

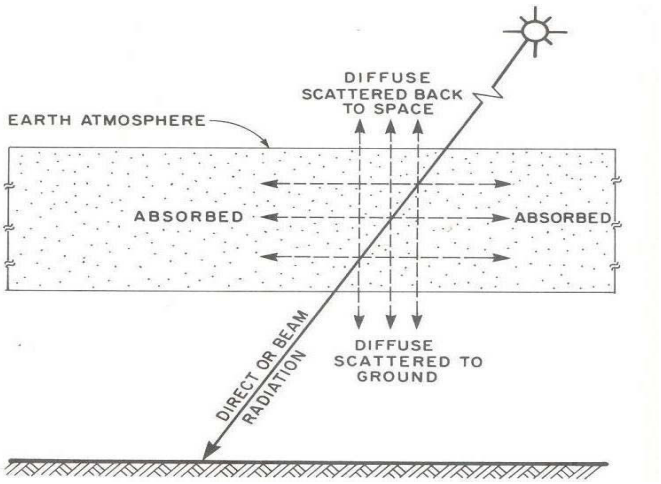

Fig. 1-1 Distribution of direct normal, diffuse horizontal and absorbed solar radiation [10].

1.3 Radiometric instruments

1.3.1 Pyranometer

Routine measurements of GHI on ground level are primarily made with pyranometers. These hemispherically sensitive sensors measure the downward solar radiation flux on a horizontal surface over a given time. Total radiation thus measured is the sum of the beam and diffuse components. For inclined surfaces, diffuse radiation constitutes two components: sky diffuse and ground-reflected radiation [11]. Pyranometers mounted on an angled plane experience a tilt effect, which is caused by heat exchange between the interior and exterior atmospheres of the glass domes. The effect is known to vary with the angle of inclination. The variation should not exceed 2% for well-designed pyranometers [10]. In this study, all GHI measurements were made with horizontal unshaded pyranometers. When mounted facing upwards, a pyranometer measures the global horizontal irradiance and when shaded using a stationary shadow band (SBS), it measures diffuse horizontal irradiance. Various shadow bands are available. For example, the Eppley shadow band stand (SBS) is made of anodized aluminum with a diameter of 635 mm and a width of 76.3 mm [12] (Fig. 1-2). The Eppley Precision Spectral Pyranometer (PSP) was used in this work. It has two circular domes made of Schott optical glass. The domes absorb energy between 0.285 μm to 2.8 μm

and reduce thermal exchange between the detector and the environment [13]. The pyranometer has a black thermopile sensor that absorbs the incident solar irradiance. The sensor, shown in Fig. 1-3a, measures the heat difference between the inner and outer surrounding of the pyranometer housing. This heat difference generates a millivolt analogue signal that is directly proportional to solar irradiance measured. Each radiometric sensor is supplied with a temperature dependence curve and a calibration certificate that is traceable to the World Radiometric Reference (WRR), as discussed in Chapter 2.

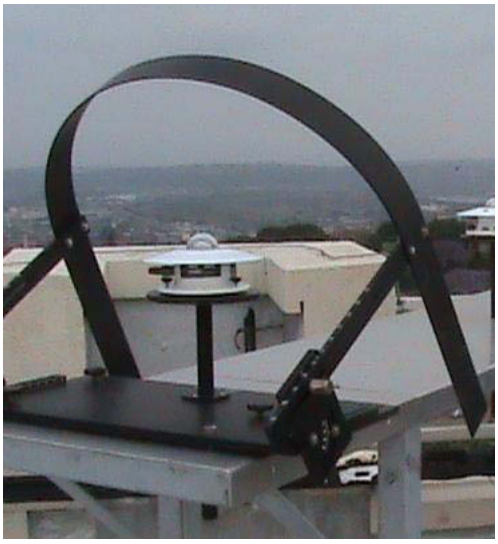

Fig. 1-2 Eppley PSP installed under a shadow band and in use at the UKZN Howard College station.

1.3.2 Pyrheliometer

A pyrheliometer measures the beam irradiance at normal incidence. The Eppley Normal Incidence pyrheliometer (NIP) shown in Fig. 1-3b, has a multijunction thermopile as its sensing element that is coated in 3M velvet black paint [10]. Its design consists of a collimated tube that is painted black in the inside and filled with dry air at atmospheric pressure with a view angle of five degrees [10]. This angle is small so as to limit the pyrheliometer to measure strictly the direct normal component. The pyrheliometer is used in conjunction with a solar tracker, which may be mechanical or automated. The equatorial tracker is driven by a motor and enables the pyrheliometer to track the sun as it traverses across the horizon. Mechanical trackers such as the Eppley model ST-1 and ST-3 are electrically driven (Fig. 1-3b). They operate on a clock-based motor that makes one revolution

each day. Mechanical trackers are adjusted manually for changes in declination. During equinoxes, alignment should be regularly performed as declination changes more rapidly [12].

Pyrheliometers mounted on mechanical trackers are aligned on clear days. The rotary movement of an NIP as it tracks the sun causes coiling of the cable joining the NIP to the data logger. To prevent fouling of the cable, it is useful to wind the cable in the opposite direction such that it unwinds itself during rotation. Weekly disconnection of the cable from the NIP is suggested to relieve the cable from any stress that might result in breakage of the wires from the connector. Automated trackers such as the SOLYS2 model manufactured by Kipp and Zonen automatically configure the location of the sun through an integrated Global Positioning System (GPS) receiver. A SOLYS tracker can be configured as a complete radiometric station as it can mount up to three pyranometers and one pyrheliometer [14], Fig. 1-4. Shading disks are included to enable measurement of the diffuse component. Global horizontal irradiance is measured by an unshaded pyranometer.

a) b)

Fig. 1-3 a) Eppley Precision Spectral Pyranometer (PSP) and b) Eppley Normal Incidence Pyrheliometer (NIP) mounted on green manual tracker, ST-1 model at the UKZN (Howard College) station.

Fig. 1-4 Kipp and Zonen SOLYS tracker configured as a complete radiometric station. Three CM22 pyranometers and one CHP 1 pyrheliometer are mounted on the tracker.

1.4 Instrument errors

Solar irradiance measurements are meaningless if they are not traceable to a reference standard such as the World Radiometric Reference [15]. Numerous methods and models have been devised in improving solar irradiance measurements. Recently, Reda [15] has demonstrated a method that can reduce uncertainty by at least 50%. All radiometric instruments have errors associated with their measurement of sun strength [16]. Two commonly reported errors are the thermal offset and cosine response error. Cosine errors occur at high zenith angles and are mainly due to specular reflection from the sensor near grazing incidence, when the DNI is almost parallel to the sensor surface [17]. The effect is observed in the early morning and late afternoon hours (Fig. 1-5). For an ideal instrument, the cosine response should be equal to one around midday when the incident angle is zero degrees. Bias error of more than +/-5% have been reported for zenith angles greater than 60°, both in the early morning (negative incidence angles) to late afternoon (positive incidence angles) [18]. Percentage uncertainties of Eppley pyranometers are reported to be in the range 3-4% as shown in Table 2-2. Measurements of irradiances corresponding to zenith angles greater than 70° should be avoided as the error is high in this range [10]. Gueymard and Myers [19] suggest using *a posteriori* corrections that depend on each specific instrument or using an incidence-angle-dependent calibration method described in [20]. The cosine error is known to be large at zenith angles greater than seventy degrees and causes errors in irradiance measurements. Eppley stipulates a maximum of zenith angle of 75° for their instruments upon calibration. For these two reasons,

irradiance measurements corresponding to zenith angles less than seventy-five (75°) degrees are used in this work.

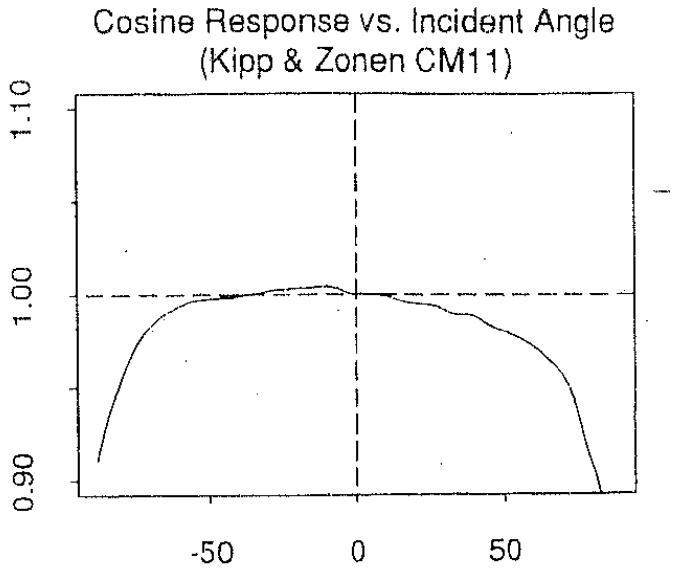

Fig 1-5 Cosine error in diffuse measurement using a Kipp and Zonen CM11 pyranometer.

A second error is that due to thermal offset. This is a thermal infrared (IR) induced error that results from differences between the internal surface temperature of the instrument, and that of the sky. The exchange of infrared radiation between the thermopile sensor, its hemispherical glass domes and external environment during nighttime causes reduced output signals, which in turn cause negative bias errors, reducing the accuracy of radiometric sensors [21]. As discussed in [22], small bias errors can become large percentage errors in diffuse measurements during daylight periods. Adding ventilation (Fig. 2-4) to the instrument minimizes this error, although at additional expense. Authors in [19] suggest using a method, in which the offset is calculated using the equation,

$$E_{off} = a_0 + a_1 E_{IR} \tag{1.2}$$

where E_{off} and E_{IR} are the offset error and net infra-red irradiance respectively, as measured by a pyrgeometer. The coefficients, a_1 and a_0 are obtained using least squares fitting of data. This method proves costly, as an additional instrument has to be purchased. Radiometers with low sensitivity to dome and convective temperature variations, for example, the CM22 or black and white sensors which have a longer time response can be used to eliminate this cost.

1.5 Summary of work done

The flowchart (Fig. 1-6) summarizes the work discussed in the dissertation. Data acquisition for the two active stations comprising GRADRAD utilizes the software tool LabVIEW. The Solar Position Algorithm (SPA) [23] developed by NREL and discussed in Chapter 3, was used to obtain sun parameters defining the solar vector such as the Julian day, solar declination angle, solar zenith angle, the obliquity of the ecliptic (the earth‟s axial tilt), solar azimuth angle and hour angle. Solar irradiance values gathered at both stations are time-stamped with parameters defining the solar vector to establish the true location of the sun when irradiance values were recorded.

The first block in Fig. 1-6 explains how the LabVIEW software is exploited to obtain yearly hour values of DNI, DHI and GHI. The LabVIEW code starts writing to file when the computer clock is greater or equal to twenty minutes before sunrise and stops writing to file twenty minutes after sunset. Sampling of data is at six-second intervals. Ten values of each of the ten outputs (six solar vector quantities and four irradiance measurements) are recorded over a sixty-second interval and stored temporarily in a buffer from which an average value is saved and written to a file for each separate day. The program repeats the averaging sequence and appends data onto the same file for the same day. Daily data processing is performed by integrating minute values over hourly periods. The process is repeated over a twelve month period so as to have hourly values over a yearly period for both active stations of GRADRAD.

Before any data can be analyzed, it is imperative that the dataset is cleaned (second block in Fig. 1-6). Three filters were proposed in this study to filter the data set from both stations, discussed in Chapter 4. The first filter eliminates all solar irradiance values with corresponding zenith angles greater than 75°. The filter eliminates data that contain the cosine effect which is present at high zenith angles. The second filter is that proposed by the European Daylight Commission where various bounds are set for GHI, DNI and DHI. The filter eliminates values of irradiance outside the following intervals:

1. $0 < I_d < 0.8I_o$
2. $I_g < 5\ W/m^2$
3. $0 < I_d < 1.1I_g$
4. $0 < I_g < 1.2I_o$
5. $0 < I_b < I_o$

where I_o is the hourly horizontal extraterrestrial solar irradiation, given by equation 4.1. The third filter removes outliers in the dataset. Outliers are data points that lie unusually far removed from the bulk of the data population [3]. They should be eliminated from the dataset as they cause skew in the distribution. Processing and analysis of the cleaned dataset follows and it is divided into two parts. As mentioned earlier in Chapter 1, an ideal radiometric station is one in which all three components are measured separately, that is, GHI is measured with an unshaded pyranometer, DNI is measured with a NIP, and DHI is measured with a shaded pyranometer. A setup of this nature allows a crosscheck of any of the components using the closure equation 1.1. The flowchart summarizes how either the DHI or DNI can be calculated.

Diffuse horizontal measurements can be obtained in two ways, that is, the direct and indirect method (third block). The direct method measures DNI with a shadow band and uses four well-known shadow band correction models by Drummond [24], Le Baron et al. [25], Batlles et al. [26] and Muneer and Zhang [27] to correct the shadow band effect. The shadow band effect results from a portion of the sky blocked by the band and as a consequence, blocking off DHI obscured by the band. The indirect method calculates the DHI from the closure equation 1.1, where GHI measurements are with an unshaded pyranometer and DNI is measured with a NIP. This way a cross check can be made to compare the results obtained by either method (Fig. 4-17 and Fig. 4-18).

Similarly, the DNI is obtained in two ways, that is, the direct and indirect method (fourth block in Fig. 1-6). The indirect method requires knowledge of atmospheric constituents such as the ozone optical depth, humidity, temperature and cloud cover, as inputs in estimating DNI. Knowledge of these parameters is not often available as a majority of radiometric ground stations do not measure weather data and solar data concurrently. These models of the indirect method are very complex and will not be investigated in this study. An example is the fast atmospheric signature code (FASCODE) [28]. The direct method utilizes equation 1.1 after correcting DHI for the shadow band effect using any of the previously mentioned correction models. Models that do not require knowledge of atmospheric data to estimate DNI are known as decomposition models. The models are derived by developing relationships between the clearness index, k_t which is the ratio of GHI to the extraterrestrial radiation and the diffuse fraction, k that is defined as the ratio of DHI to GHI. Parameters such as temperature, humidity, cloud cover, and solar altitude are used to augment the k-k_t correlation. They are, however, quite often not accurate as compared to spectral models that have atmospheric data as inputs. In this study, decomposition models have been implemented on data acquired at Howard College and STARlab to estimate the direct normal irradiance. The modelled

values are then compared with the directly measured DNI to quantify their accuracy. The comparison is through graphical and statistical analyses. Decomposition models investigated in this study include models by Erbs et al. [29], Orgill and Hollands [30], Reindl et al. [31], Boland et al. [32] and Skartveit and Olseth [33].

The final output of the work is to determine any spatial differences between the Howard College and MUT station (fifth block). This was achieved by performing a calibration exercise at MUT and running a PSP from HC at MUT to observe the difference when measuring GHI. The difference obtained was 1.36%. The calculated value indicates the difference in the instruments when run at one location. To establish the existence of micro-climate effects, the difference in the GHI when all instruments are run separately at either location was calculated (section 4.2.4) to be 0.72%. Measurable results of any potential spatial variations will exist only if the difference in GHI when run at separate locations is greater than 4% (greater than the instrument accuracy, Table 2-2). Based on the calculated results, no measurable spatial effects seem to exist between the two stations.

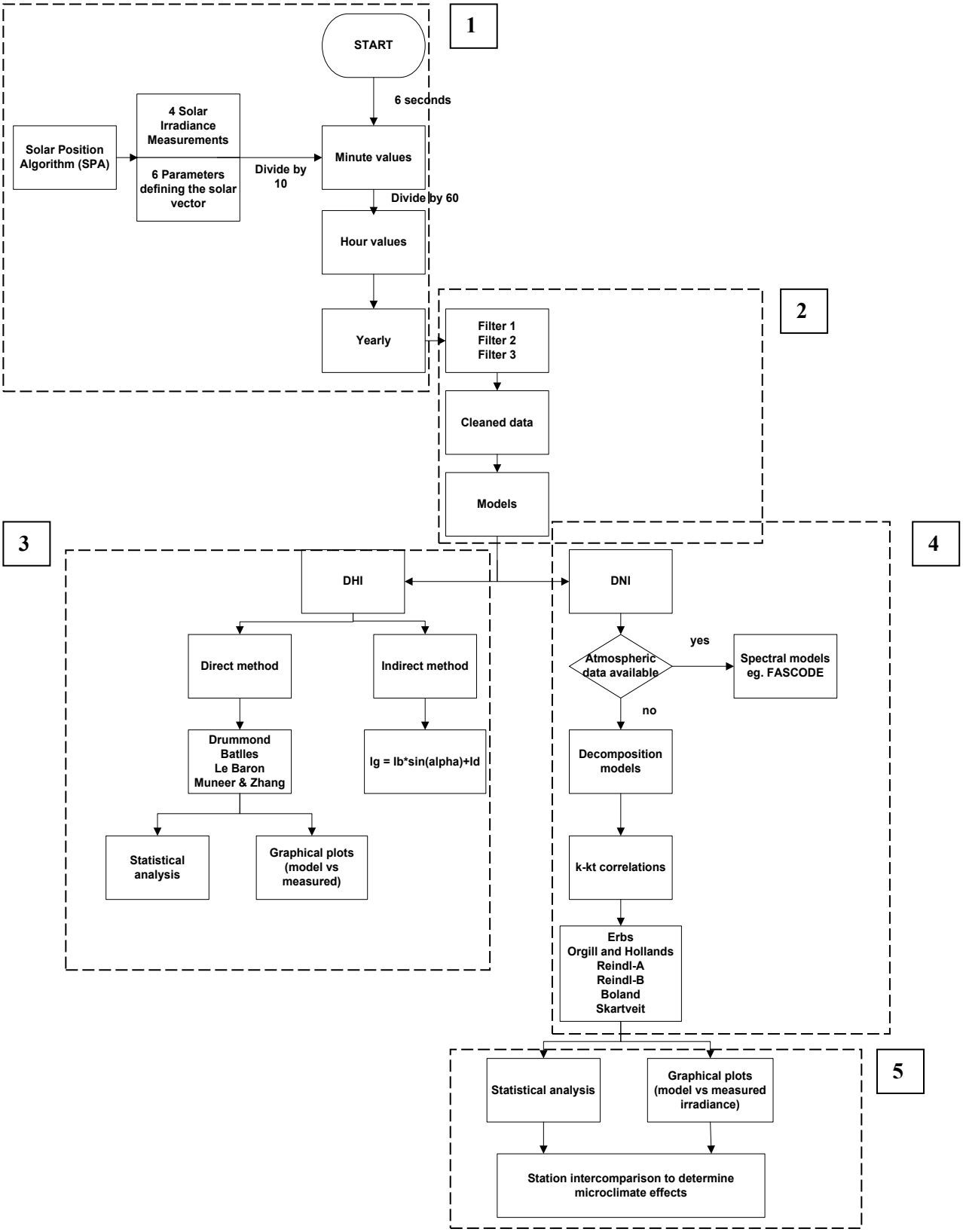

Fig. 1-6 Flowchart of a summary of the work performed for this study.

CHAPTER 2: The Greater Durban Radiometric Network (GRADRAD)

The GRADRAD Network is an ongoing initiative aimed at gathering solar radiometric data for South Africa as a whole and publishing the data on one dedicated website at no fee to the global research community. Although the network currently consists of two active (plus one under development) ground stations located within the metropolitan boundaries of Durban (Fig. 2-1), the project aims to eventually expand beyond provincial boundaries of South Africa [34]. The network stations are: Mangosuthu University of Technology (MUT) station also known as the Solar Thermal Applications Research Laboratory (STARlab) (Fig. 2-2), UKZN Howard College station (Fig. 2-3), and UKZN Westville station (Fig. 2-4). The UKZN Westville station is currently undergoing refurbishment and is expected to be operational by the end of 2011. Figure 2-1 shows the three stations located on the South African east coast. Durban experiences a subtropical climate, characteristic of mild to warm winters and hot humid summers. Midwinter temperatures are as low as 16°C and can rise to a high of over 33°C [35]. To ensure easy comparison of data gathered at the network, similar data acquisition software and similar acquisition hardware is used. A list of the present equipment and measured irradiance components are given in Table 2-1. Table 2-2 gives the specifications of the Eppley pyranometer and pyrheliometer in use at GRADRAD.

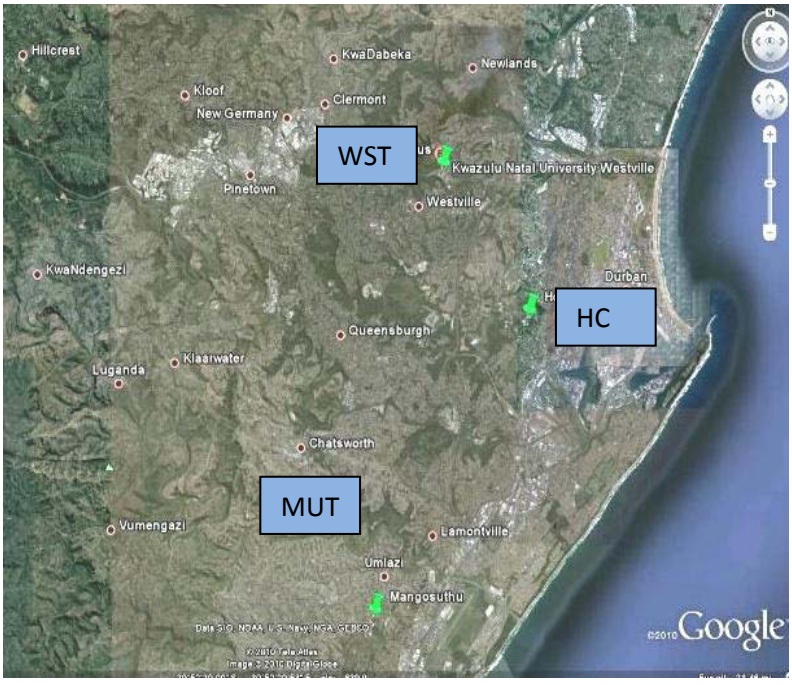

Fig. 2-1 Relative positions of the three stations viewed from Google Maps.

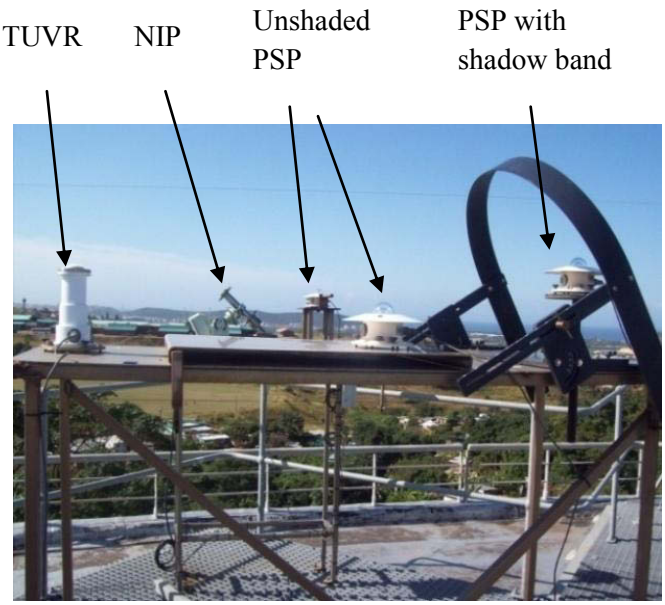

Fig. 2-2 STARlab solar radiometric station at MUT. Shown are three Eppley pyranometers: two unshaded and one shaded by an SBS, one NIP mounted on an ST-1 tracker and a ultra-violet radiometer.

Fig. 2-3 UKZN Howard College solar radiometric station. Shown is an unshaded PSP, shaded pyranometer with solid band to measure DHI, an unshaded PSP (to measure GHI) with a perforated band and a NIP to measure DNI.

Fig. 2-4 UKZN Westville solar radiometric station. Shown are an Eppley PSP with a ventilation mask and an Eppley NIP.

2.1 Development of the UKZN station

The UKZN School of Mechanical Engineering established a new radiometric station in December 2009. It went into full operation in February 2010 [36]. UKZN has acquired three Eppley Precision Spectral Pyranometers (PSP) and one Normal Incidence Pyrheliometer (NIP) for the routine measurements of the global horizontal, diffuse horizontal and direct normal components. The site is located on the rooftop of the Desmond Clarence building at the University of KwaZulu-Natal, Howard College Campus. The solar platform is at latitude 29.52° South, longitude 30.62° East, at an elevation of 151.3 meters. The choice of location for a site is crucial and a number of factors were considered, such as safety and ease of access to the site for daily maintenance. The site should be away from electrical disturbances that could cause difficulty in detecting and processing the actual required signal thus reducing its clarity. It should also be free from artificial obstructions such as tall buildings and natural obstructions such as tall trees above the plane of the sensing element that could cast shadows over the sensors.

The instrumentation bench at Howard College consists of a table mounted facing true north, shown in Fig. 2-5. The orientation is to enable the instruments to track the sun in an east-west axis as the sun traverses the horizon. The instrumentation consists of three Eppley Precision Spectral Pyranometers (PSP) and a Normal Incidence Pyrheliometer (NIP) that is mounted on an Eppley ST-1 solar tracker. Due to power cuts and surges from the national grid, the station has suffered loss of data on certain number of days as it is presently without an Uninterruptible Power Supply unit

(UPS). Lost data are noted on the GRADRAD solar calendars. A UPS unit has since been purchased and reliability of data is likely to improve. Plans are in place to acquire a weather station for the Howard College station to provide measurements of humidity and temperature. With the availability of such weather data, spectral models can be implemented in future on GRADRAD data to give higher accuracy estimates of the direct normal irradiance.

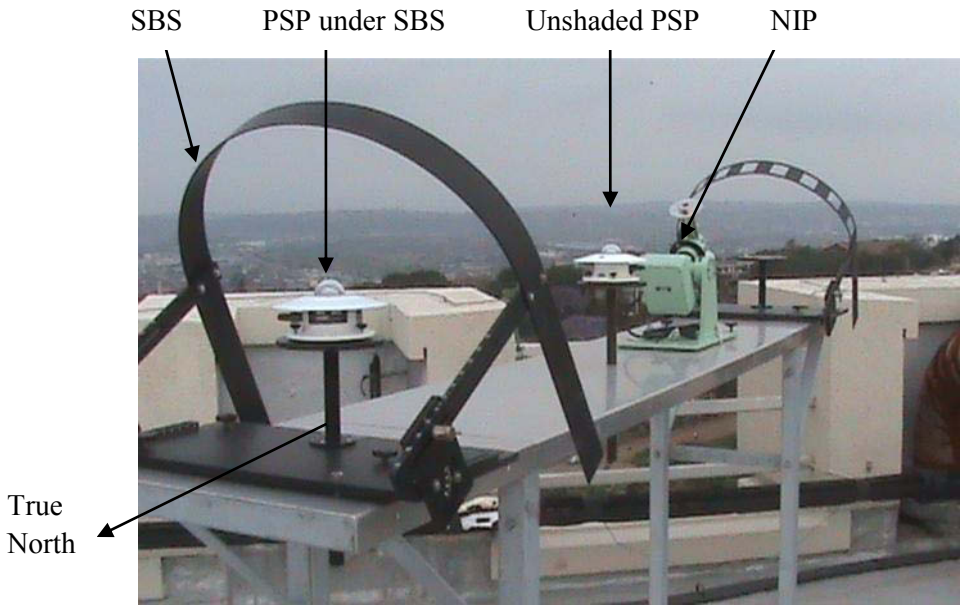

Fig. 2-5 UKZN Howard College solar radiometric ground station.

2.3 MUT station

The station was established between July 2002 and February 2003 [37]. The collection of high quality global horizontal, direct normal and diffuse horizontal irradiances, as well as ultra-violet radiation has been ongoing since its establishment. STARlab also houses an outdoor solar thermal test facility to characterize the performance of a solar collector described in [38]. The instrumentation bench is located at 29.97° South and 30.92° East. It is 105.5 m above sea level and consists of five radiometers: Eppley models of a shaded PSP mounted with a shadow band, an unshaded PSP, a tilted PSP for measurement of global irradiance on a tilted plane, an Eppley NIP and a Total Ultra Violet Radiometer (TUVR) shown in Fig. 2-2. In addition, the station also gathers weather data. Continuous data gathering at the site is ensured by the presence of a UPS in situations where there are power cuts and surges.

(UPS). Lost data are noted on the GRADRAD solar calendars. A UPS unit has since been purchased and reliability of data is likely to improve. Plans are in place to acquire a weather station for the Howard College station to provide measurements of humidity and temperature. With the availability of such weather data, spectral models can be implemented in future on GRADRAD data to give higher accuracy estimates of the direct normal irradiance.

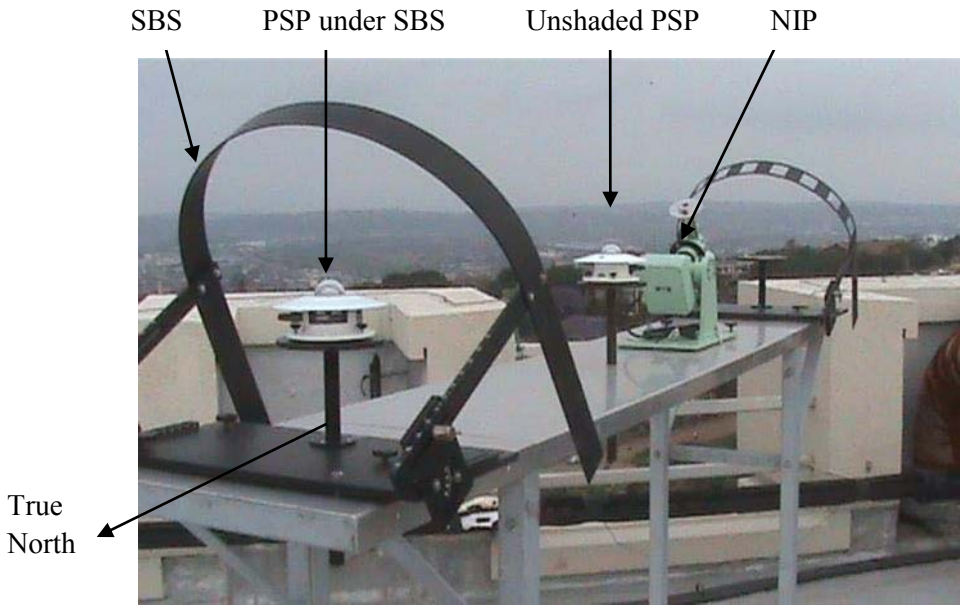

Fig. 2-5 UKZN Howard College solar radiometric ground station.

2.3 MUT station

The station was established between July 2002 and February 2003 [37]. The collection of high quality global horizontal, direct normal and diffuse horizontal irradiances, as well as ultra-violet radiation has been ongoing since its establishment. STARlab also houses an outdoor solar thermal test facility to characterize the performance of a solar collector described in [38]. The instrumentation bench is located at 29.97° South and 30.92° East. It is 105.5 m above sea level and consists of five radiometers: Eppley models of a shaded PSP mounted with a shadow band, an unshaded PSP, a tilted PSP for measurement of global irradiance on a tilted plane, an Eppley NIP and a Total Ultra Violet Radiometer (TUVR) shown in Fig. 2-2. In addition, the station also gathers weather data. Continuous data gathering at the site is ensured by the presence of a UPS in situations where there are power cuts and surges.

2.4 Westville station

The station (Fig. 2-4) was established in 1996 and is currently being refurbished. It is expected to be operational by the end of 2011. It is located at latitude 29.51° South and longitude 30.6° East at an elevation of 205 m above sea level. Instruments include a ventilated Eppley PSP, NIP and two PSP"s which have been recently purchased. A state of the art automated solar tracker and additional radiometers from Kipp and Zonen are currently on order for the station. To date, various work has been produced using data from the station including a radiometric study undertaken by Lysko [39] in conjunction with the Norwegian University of Science and Technology.

Table 2-1 Equipment and measured irradiance components present at the stations that currently comprise GRADRAD.

Station	Instrument	Serial no.	Measurement	Conversion factor (μV/W/m^2)
Howard College	Shaded pyranometer	35662F3	Diffuse	8.73
	Unshaded pyranometer	35622F3	Global	7.59
	Pyrheliometer	35649E6	Beam	8.12
	Perforated shadow band	35663F3		9.18
Westville	Pyrheliometer	Not operational	Beam	Not operational
	Unshaded pyranometer	Not operational	Global	Not operational
MUT	Shaded pyranometer	34332F3	Diffuse	8.36
	Unshaded pyranometer	34332F3	Global	8.10
	Unshaded pyranometer	33583F3	Global	8.01
	Pyrheliometer	31955E6	Beam	8.45
	Total Ultra Violet Radiometer (TUVR)	34623	Ultra violet	213

Table 2-2 Specifications of Eppley PSP and NIP radiometers [11].

Specification	PSP	NIP
Sensitivity	9 μV/W/m^2	8 μV/W/m^2
Impedance	650 Ω	200 Ω
Temperature	±1%	±1%
Linearity	±0.5% from 0-2800 W/m^2	±0.5% from 0-1400 W/m^2
Response time	1 second	1 second
Cosine response	±1% from 0°-70° zenith angle, ±3% 70°-80° zenith	None
Weight	3.18 kg	2.27 kg
Orientation	Not affected by tilt	Affected by tilt
Accuracy	±3-4%	±3-4%

2.5 Intercomparison of instruments

One of the objectives of this work is to compare data from ground stations located a short distance apart, but before a comparison can be made the measurement differences between the instruments at each station must be established. This is to verify whether the difference observed when the instruments are run at the different locations, (STARlab and UKZN Howard College) is due to spatial variations in sun strength or just merely due to instrument differences. To confirm this, a calibration exercise was performed at STARlab. A pyranometer from Howard College station was run alongside three pyranometers present at STARlab. All four pyranometers were run measuring GHI. The reference, noted in the text as PSP(3) was taken as the standard as it was previously calibrated outdoors at the National Renewable Energy Laboratory (NREL) in the USA. Even though instruments from Howard College are relatively new, purchased in 2009, it would be less than ideal to use them as a basis because they were calibrated indoors with an integrating hemisphere. This refers to an artificial sky whereby diffuse radiation of approximately 700 W/m^2 is produced by a series of tungsten-filament lamps. The calibration factor obtained by the artificial method degrades when the instrument is run under field or real sky conditions [40].

Regular radiometer calibration is necessary to ensure data quality. A measurement standard has been in use since 1980 in Davos, Switzerland. The standard is the World Radiometric Reference (WRR) and is an internationally accepted System Internationale des Unites (SI units) traceable measurement of terrestrial solar radiation. The WRR ensures homogeneity of solar irradiance measurements around the world. A series of Absolute Cavity Radiometers (ACR) form the WRR.

These instruments, also referred to as primary instruments, have an estimated accuracy of 0.3% and give radiation measurements within 0.1% stability [41]. Secondary or field instruments (the instruments used in GRADRAD are examples of field instruments) are calibrated against the reference (Fig. 2-6b) by running side-by-side comparisons. The Eppley Normal Pyrheliometer (NIP) and Eppley Precision Pyranometer (PSP) are examples of secondary instruments. Figure 2-6a shows an Absolute Cavity Radiometer (ACR) of the Automatic Hickey-Frieden (AHF) type with serial number AHF AWF 31117.

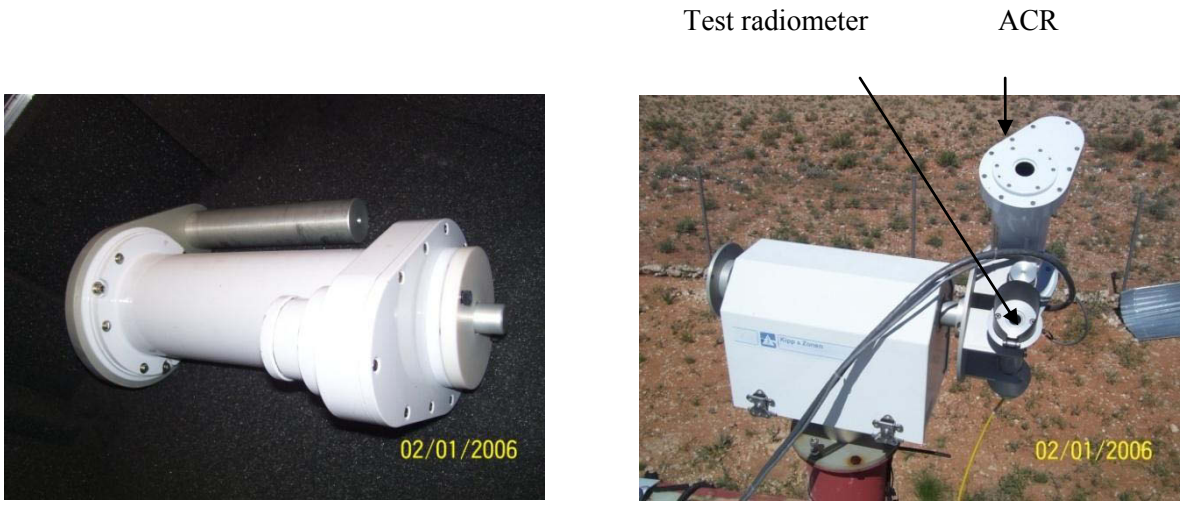

a) b)

Fig. 2-6 a) An Absolute Cavity Radiometer (ACR) and b) a side-by-side calibration process of a test Kipp and Zonen radiometer using the ACR as a reference.

Calibration of radiometric instruments is important to ensure accuracy in the measured quantities. Although Eppley recommends a minimum calibration cycle of five years, the manufacturer encourages annual calibrations for highest measurement accuracy. A calibration exercise was performed at STARlab in July 2010. Two Eppley Precision Spectral Pyranometers (PSP) currently in use at the Solar Thermal Research Laboratory (STARlab) in uMlazi were calibrated against a pyranometer (PSP(3)) recently calibrated at the National Renewable Energy Laboratory (NREL) in the USA in July 2009. Data from two clear days, 22-23 July 2010 were used. The two pyranometers, PSP(1) and PSP(2) measure diffuse horizontal irradiance and global irradiance on a tilted plane respectively. The shadow band was removed resulting in all three instruments measuring the global quantity on a horizontal surface. The previous calibration factors (shown in

Table 2-3) were used to calculate the irradiance in W/m^2 from the uncalibrated instruments by the equation,

$$Irradiance = \frac{1}{RS}V \tag{2.1}$$

where *RS* is the known responsivity in W/m^2 and *V* is the voltage in volts. The responsivity is calculated using a method adopted by Wilcox and Myers [18] from the equation,

$$RS_g = \frac{V}{E} \tag{2.2}$$

where *E* is the global horizontal irradiance from the reference pyranometer, PSP(3) and RS_g is each calculated minute responsivity in (μV/W/m^2) from the test radiometric sensors ((PSP(1) and PSP(2)). A zenith angle interval of 45° to 55° was used, as per the National Renewable Energy Laboratory (NREL) to reduce cosine error. Mean responsivity was obtained as follows:

$$RS = \frac{\sum_{g=0}^{h} RS_g}{N} \tag{2.3}$$

where N is the number of data points in the selected range.

Table 2-3 Responsivities of the STARlab pyranometers before calibration.

Instrument	**PSP**	**Calibrated**	**Responsivity (μV/W/m^2)**	**Measurement**
Eppley PSP	PSP(3)	YES	8.10	Global
Eppley PSP	PSP(2)	NO	8.01	Global (tilted plane at 30°)
Eppley PSP	PSP(1)	NO	8.36	Diffuse

In the calibration procedure, solar irradiance data from the zenith range 45° to 55° were used as this interval is less affected by the cosine response. Equation 2.1 was used to calculate the output voltage from the uncalibrated instruments (PSP(1) and PSP(2)) where *Irradiance* is the known GHI measured by either instrument using the known calibration factors. The minute responsivities for both instruments were calculated for each day, 22 July and 23 July. A resultant responsivity was calculated from the average of the two daily responsivities for either instrument, shown in Table 2-4. To check the applicability of the newly calculated responsivity values, two days on which all three pyranometers measured the global horizontal irradiance were used. Figure 2-7 and Fig. 2-8 show plots for 24 July 2010 and 25 July 2010.

Table 2-4 Summary of calculated responsivities of MUT pyranometers over two day period at STARlab.

Date	Pyranometer	N	Mean RS ($\mu V/W/m^2$)	Previous RS ($V/W/m^2$)	New RS ($V/W/m^2$)
22 July	PSP(2)	187	7.17		
	PSP(1)	187	7.67		
23 July	PSP(2)	190	7.16		
	PSP(1)	190	7.65		
	PSP(1)			8.36	7.66
	PSP(2)			8.01	7.16

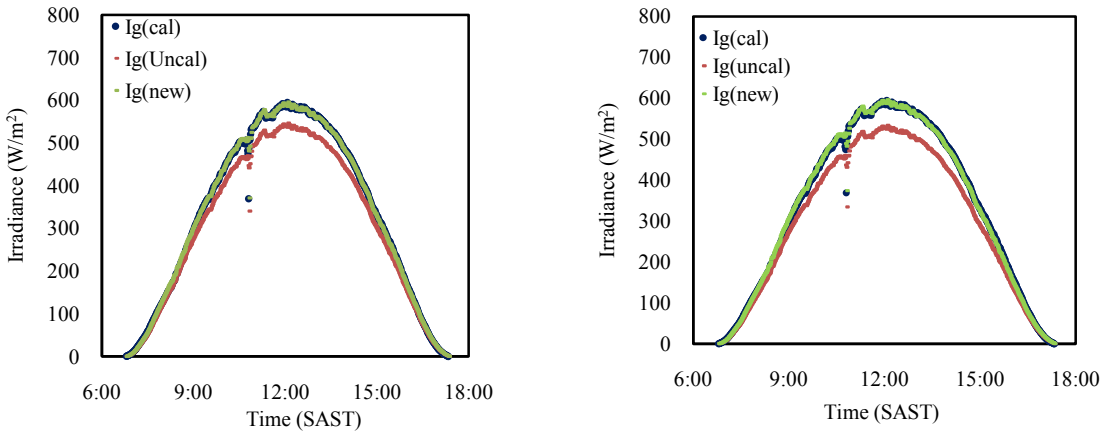

a) b)

Fig. 2-7 Calibration checks of global horizontal irradiance (Ig) for a) PSP(1) and b) PSP(2) on 24 July 2010.

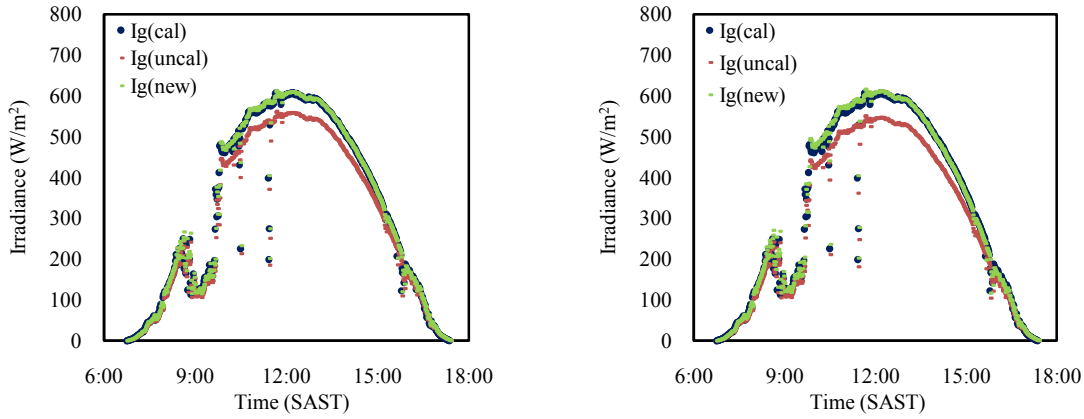

Fig. 2-8 Calibration checks of global horizontal irradiance (Ig) for a) PSP(1) and b) PSP(2) on 25 July 2010.

Table 2-4 is a summary of the final responsivities averaged over the two-day calibration process. It should be noted that this is not an ideal method to use for calibration. The Broadband Outdoor Radiometer Calibration (BORCAL) used by the National Renewable Energy Laboratory (NREL) is suggested for a more accurate calibration procedure [42]. BORCAL uses either of two methods for calibration: component summation or the shade/unshade method. These methods can characterize and calibrate up to one hundred radiometers on a clear day [43], [44]. In the shade/unshade method, a pyranometer is exposed to alternating periods of shade (blocked of the beam irradiance using a shading device thus measuring diffuse irradiance) and unshade of beam irradiance thus measuring global irradiance. For a pyranometer with responsivity *RS*, global irradiance is given as *U/RS* where *U* is the output voltage when it is unshaded. Diffuse irradiance equals *S/RS* where *S* is output pyranometer voltage during periods of shading. Equation 1.1 becomes

$$\frac{U}{RS} = I_b \cos\theta_Z + \frac{S}{RS} \tag{2.4}$$

from which the responsivity is calculated as

$$RS = \frac{U - S}{I_b \cos\theta_z} \tag{2.5}$$

The equation is valid only when *U* and *S* are measured simultaneously, which is not possible if reference instruments are absent, as the pyranometer cannot measure global and diffuse irradiance concurrently. The equation above is known as the shade/unshade equation where the parameters I_b,

θ_z, and S are measured after a settling time after shading [45]. The parameter U is measured when the pyranometer is unshaded and measuring global irradiance. A question that stands with this method is „how long should the shade and unshade period be" since different pyranometers have different time constants, thus different settling times. An improved shade/unshade method uses a control pyranometer that is constantly shaded and the test pyranometer that is exposed to periods of shade and unshade [43].

In the component summation method, a pyranometer shaded to measure the diffuse component is used under clear-sky conditions. The pyranometer is previously calibrated using the shade/unshade method. An absolute cavity pyrheliometer traceable to WRR measures the direct beam radiation. Using equation 1.1, the global radiation is obtained as the sum of the measured diffuse (shaded pyranometer) and direct beam radiation (measured by absolute cavity pyrheliometer) multiplied by the cosine of the zenith angle. The responsivity from this method is calculated as

$$RS = \frac{V_u}{I_d + I_b \cos \theta_Z} \tag{2.6}$$

where V_u is the voltage of each pyranometer signal. I_d and I_b are DHI and DNI components obtained from a shaded pyranometer and a pyrheliometer respectively. Proper calibration of radiometric sensors using methods such as BORCAL requires technical training and an absolute cavity pyrheliometer which were not available at the time the instruments were calibrated [42]. Thus neither the shade/unshade or the component summation methods were used in this work. In this study, the errors in the estimation of the global solar irradiance for PSP(2) for the two random test days were calculated as follows,

$$E_i = Measured - Model \tag{2.7}$$

where E_i is the error of the i^{th} data point, *Model* is the reference global irradiance from PSP(3) and *Measured* is the actual measured GHI. Statistical indicators such as the mean bias error (MBE) and root mean square error (RMSE), were used to measure the relationship of the measured and predicted irradiances using the formulae,

$$MBE = \frac{\sum E_i}{N} \tag{2.8}$$

$$RMSE = \sqrt{\frac{\sum (E_i)^2}{N}} \tag{2.9}$$

$$\% MBE = \frac{MBE}{Measured\ \ average} 100 \tag{2.10}$$

$$\% RMSE = \frac{RMSE}{Measured\ \ average} 100 \tag{2.11}$$

where N is the number of data points.

Figures 2-7 to Fig. 2-8 show an improvement of the global irradiance estimations after calibration, where the notations $I_g(cal)$, $I_g(Uncal)$, and $I_g(new)$ represents the reference global horizontal, uncalibrated and newly calibrated global horizontal irradiances respectively. A statistical analysis of the MBE and RMSE indicate a close match from the reference value as the errors are less than 1% for a clear day for both PSP(1) and PSP(2) (Table 2-5 and Table 2-6). A selection of more clear days is advised to be used to check the validity of the results. This was not possible in this procedure as the weather was cloudy and unfavorable. Table 2-5 and Table 2-6 show an increased magnitude of errors for a cloudy day (25 July) as compared to a clear day (24 July).

Table 2-5 Errors resulting from using $RS_{45\text{-}55}$ for PSP(1) after calibration.

Date	N	MBE (W/m^2)	MBE %	RMSE (W/m^2)	RMSE %
24 July	194	0.55	0.1	3.40	0.61
25 July	198	2.92	0.51	4.20	0.74

Table 2-6 Errors resulting from using $RS_{45\text{-}55}$ for PSP(2) after calibration.

Date	N	MBE (W/m^2)	MBE %	RMSE (W/m^2)	RMSE %
24 July	194	1.13	0.20	5.13	0.92
25 July	198	4.70	0.83	6.91	1.21

Figure 2-9 shows plots of two clear days of a pyranometer from each of the stations, run concurrently at STARlab. The plots show the difference between the instruments when run at one location. The observed difference is calculated to be 1.36% in the global quantity over the interval $\theta_z \leq 75°$. A clear day 23 July was used to calculate the percentage difference since calibration is performed during clear skies. Taking (PSP(3)) as the reference, a sample calculation is shown below,

$$\%\ difference = \frac{\sum I_{gMUT} - \sum I_{gHC}}{\sum I_{gMUT}} * 100$$

$$\%\ difference = \frac{442 - 436}{442} * 100$$

$$= 1.36$$

In this study, one of the aims is to verify whether this difference increases when the instruments are run separately at Howard College and STARlab. The calculated value of 1.36% is indicative of the pyranometric difference between the two instruments when run at one location. From this, it is assumed that all comparisons of global horizontal data between the two stations will possess a 1.36% difference due to instrument differences alone. Any excess difference greater than 4% (as Eppley pyranometers have an uncertainty of 3-4% (Table 2-2)) is assumed to be to some degree, to micro-climate effects. This will be investigated in Chapter 4 where an assessment of spatial differences is performed to establish any variations on the total irradiation incident at the two locations. No comparisons can be made with the diffuse horizontal and direct normal measurements, as neither was run concurrently at one location to establish the relationship.

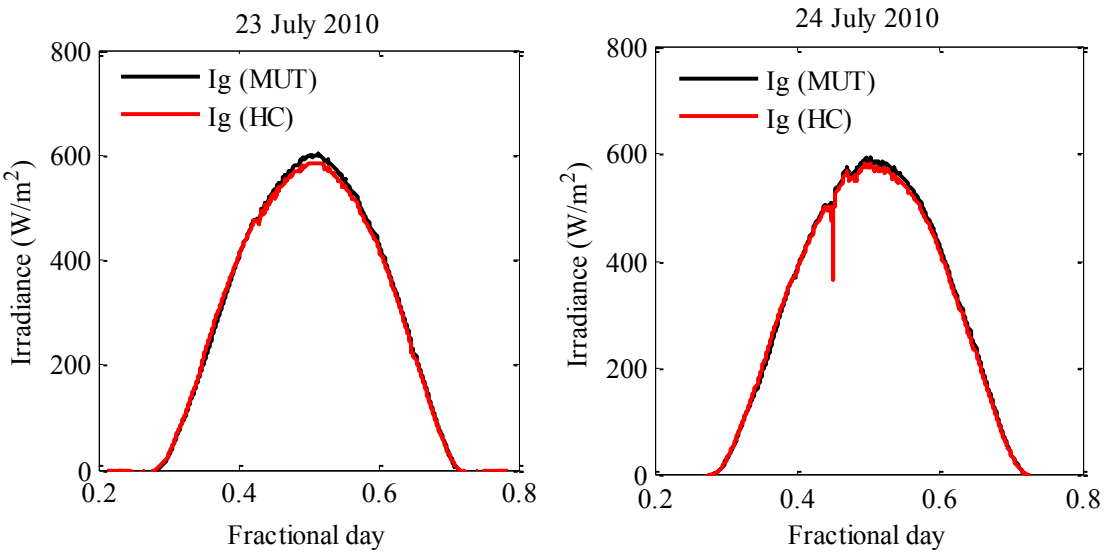

Fig 2-9 Comparison of global irradiances at STARlab on 23 July 2010 and 24 July 2010 when unshaded pyranometers PSP(1) and PSP(2) were run concurrently at one location.

CHAPTER 3: DATA ACQUISITION

Hallmarks of a successful monitoring network include data reliability, consistency and accuracy. GRADRAD employs the software tool LabVIEW for signal acquisition at the UKZN HC and STARlab stations. High quality diffuse horizontal, direct normal and global horizontal irradiance measurements are sampled at six-second intervals from which one-minute averages are obtained. Solar position data are time-stamped and written to file together with irradiance values. Project engineers and solar energy researchers require such information in implementing renewable energy projects and it is appropriate to include solar vector data in the station output files.

Locating the true position of the sun is important to obtain the sun parameters necessary for solar radiometric applications. Numerous algorithms are available in the literature that estimate the true position of the sun with varying degrees of accuracies [46, 47, 48]. An example is the Plataforma de Almeria (PSA) [49] which is valid until 2015. The Solar Position Algorithm (SPA) developed by the National Renewable Energy Laboratory (NREL) [23] was selected for use in this work. This algorithm has low uncertainties of +/- 0.0003 degrees and is valid for a wider period (year -2000BC to 6000AD). Although originally developed in C++ Language, it has been reprogrammed in MATLAB to make it compatible with the LabVIEW software used in this work. Data acquired from the LabVIEW application is sampled every six seconds and averaged over one-minute intervals. Figure 3-1 shows a schematic of a ground-based solar monitoring station.

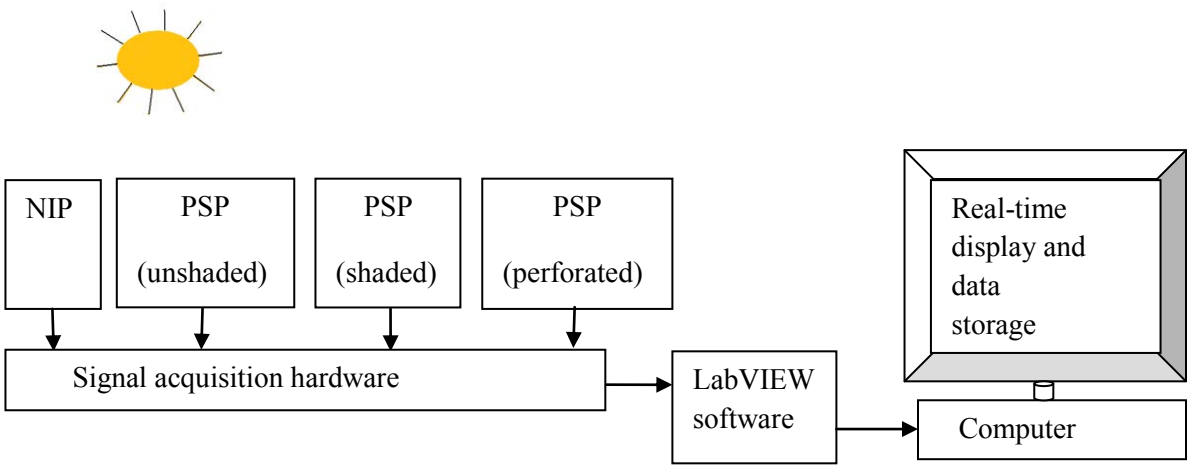

Fig. 3-1 Data acquisition schematic in use by stations comprising the GRADRAD network.

3.1 LabVIEW data acquisition system

LabVIEW, an acronym for Laboratory Virtual Instrument Engineering Workbench, is a graphical programming language from National Instruments for data acquisition and instrument control software. The developed code in Appendix A illustrates how the readings from the radiometric instruments are acquired. The code is implemented in two interfaces; the front panel and the block diagram. The front panel (in grey), shown in Fig. 3-2a is the interface through which the user interacts with LabVIEW. The block diagram, shown in Fig. 3-2b is the source code containing the necessary drop-and-drag icons for implementing the logic governing data acquisition.

The LabVIEW math script node (Fig. 3-3), which is similar to the MATLAB language syntax, is used to import files from a MATLAB developed code using the Solar Position Algorithm [23]. The current date and time are supplied as input variables to the SPA [23], imported into the math script node (Appendix B). A series of math script nodes are used to output the parameters defining the solar vector. Ten values representing one minute"s worth of data are read and the average is saved before being written to a spreadsheet file in the format, YYYYMMDD, where Y represents the year, M represents the month and D represents the day number for the respective day.

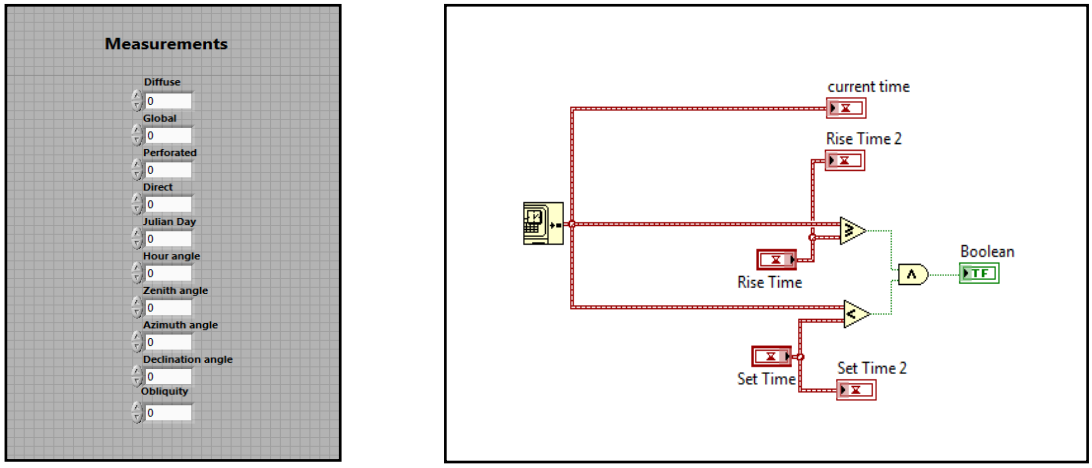

a) LabVIEW front panel b) LabVIEW block diagram

Fig. 3-2 Two user interfaces of LabVIEW a) the front panel in grey and b) the block diagram showing drag-and-drop icons for coding.

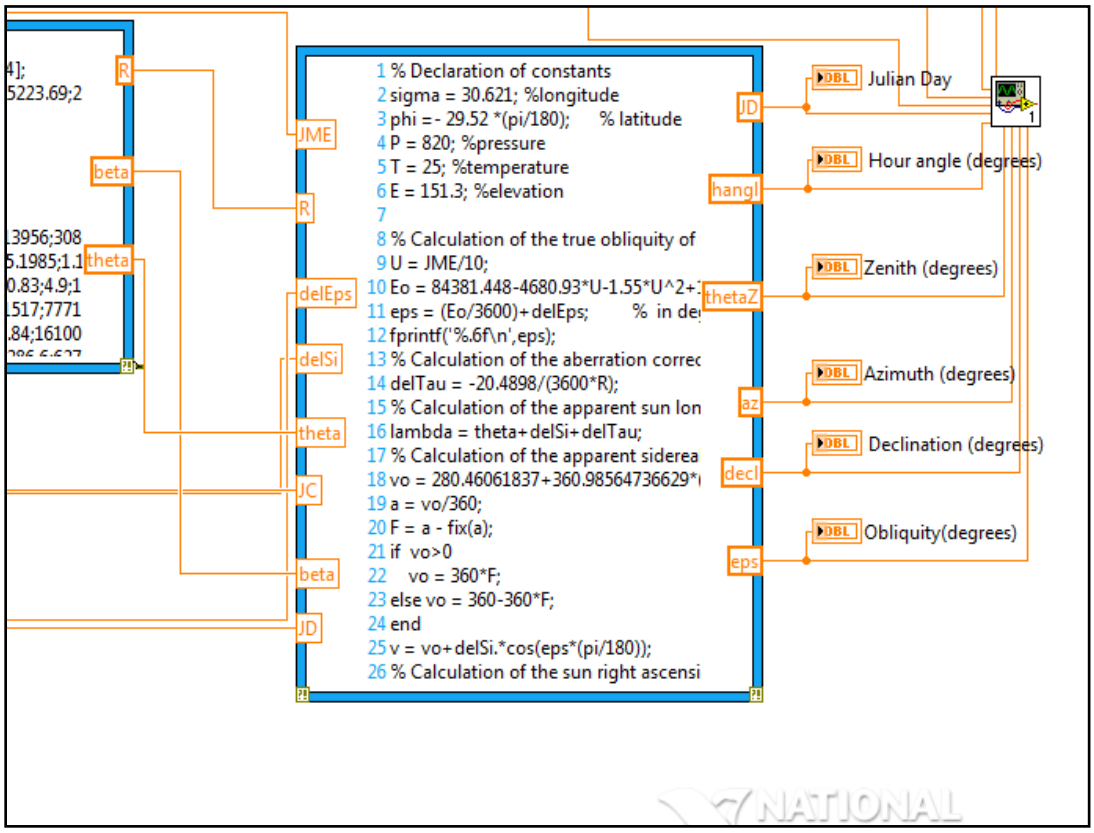

Fig. 3-3 An illustration of a LabVIEW math script node carrying embedded MATLAB code. This code implements the Solar Position Algorithm for locating the sun"s position [23].

3.2 Sampling scheme

Four physical channels are selected as analogue voltage inputs for the four instruments. These signals are indexed into an array to which a conversion factor (Table 2-1) is applied that converts the millivolt signals into an irradiance flux, measured in W/m^2. The SPA [23] written in MATLAB and imported into LabVIEW, calculates six parameters defining the position of the sun at any instant. These are the solar zenith angle, azimuth angle, Julian day, hour angle, angle of declination and the obliquity of the ecliptic. Ten data points (four irradiance values and six parameters defining the solar vector) are stored temporarily in a buffer system (Fig. 3-4) over a sixty-second interval. Averaged minute values are written and saved to a spreadsheet file for each day. Data obtained are updated in real-time and displayed as a waveform chart on the GRADRAD graphical interface via the LabVIEW front panel shown in Fig. 3-5.

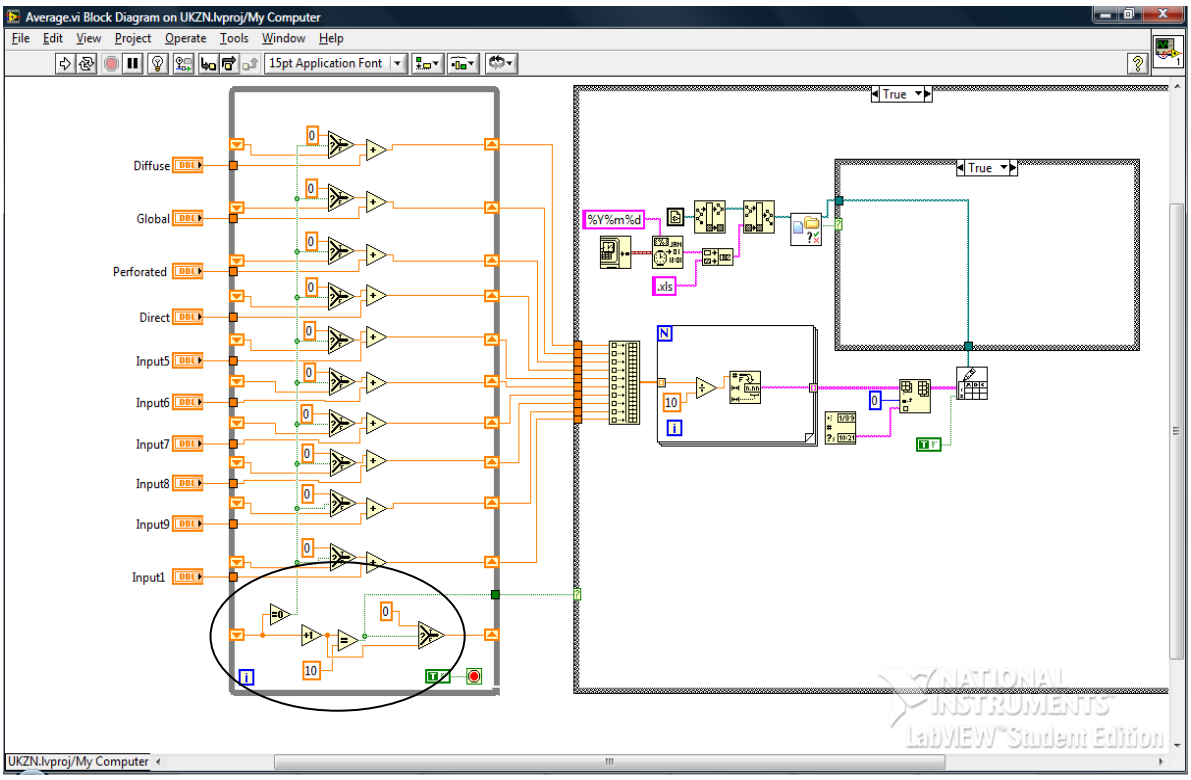

Fig. 3-4 A buffer system showing temporal storage (circled) of data for a count of ten values in a minute. The second block averages the ten-input array to obtain one value per output. The ten averaged values are written and saved into a spreadsheet file. The loop is repeated, appending the results until it stops writing to file twenty minutes after sunset.

The GRADRAD software utility is automated to start writing to file twenty minutes before sunrise and stop twenty minutes after sunset each day. Twenty minutes was chosen arbitrarily to eliminate uncertainties surrounding the calculation of the sunrise and sunset times using the equation by Cooper [39] given below,

$$\delta = 23.45 \sin\left[(n+284)\frac{360}{365}\right] \tag{3.1}$$

where n defines the day number of the year.

After sunset, the code continues executing without writing to file. This prevents the accumulation of unnecessary data collected during the night. Appendix A shows the front panel and block diagram of the LabVIEW code required for daily acquisition and storage of recorded data at either of the two

operational stations that comprise the network. The code operates sequentially through four modes namely; wait, initialize, main and reset, as explained below:

Wait – The program awaits the detection of the following day at midnight to compute the sunrise time. The program starts executing and writes to a spreadsheet file when the local South African standard time (SAST) read by the computer clock is greater or equal to twenty minutes before sunrise.

Initialise - Starts the main mode. Input variables of the SPA Algorithm are the geographical location and current date and time of the solar radiometric station.

Main – This mode contains the SPA [23] that calculates parameters defining the solar vector. Live updates of the six defined parameters defining the solar vector along with four measured irradiances are displayed on the front panel. Data acquisition at the Howard College station is through a National Instruments data acquisition chasis whilst a stand-alone Agilent HP34970A switch unit is in use at the MUT station.

Reset – After sunset, the program is reset to stop writing to file. Thereafter, it executes in idle mode and reverts to the wait function for the next day.

3.3 GRADRAD Webpage

Data gathered from GRADRAD are published at http://gradrad.ukzn.ac.za. Users of the website have the option to navigate through various features. These include a live display of the data and a download option to download raw daily data files. A history of the instruments is also shown along with a maintenance log sheet. An additional feature is the solar calendar, which is a graphical summary of the solar irradiance for a given month. Figure 3-6 shows a screenshot of the live webpage along with the above mentioned features. This webpage is similar to that developed by the United States National Renewable Energy Laboratory (NREL) in Colorado. NREL is the primary renewable energy research facility in the United States [51]. The GRADRAD website is intended to be user-friendly and is one of relatively few resources that provide free solar radiation data to the global research community. Similar resources are provided by NREL and the University of Oregon.

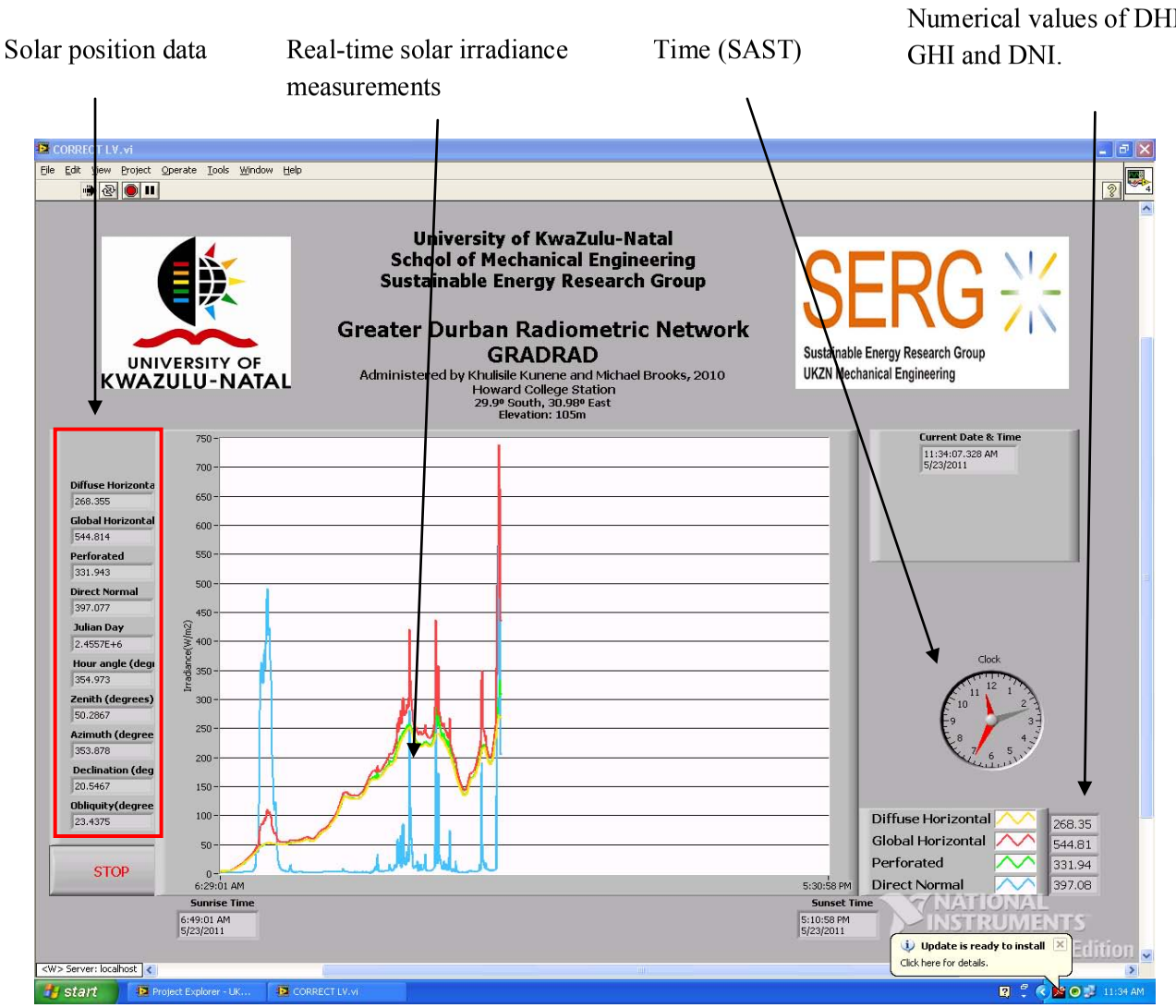

Fig. 3-5 Screenshot of GRADRAD real-time display for the Howard College station.

The following figures illustrate the navigation through the GRADRAD website. The navigation bar (circled in Fig. 3-6) gives the user an option to select any of the three stations that currently comprise the network although available data are presently limited to the Howard College station. The following can be viewed for the operational station: live display of the data, downloads of raw daily data files, views of the instrument history, maintenance log sheet and the solar calendar. Figure 3-7 shows download options for raw daily data files in any given month. A sample of a complete data file for 1 June 2010 of the HC station is available in Appendix C. These spreadsheet files are presented in the Microsoft Word 97-2003 format. By clicking on the download link, the user is able to download raw daily data files which have not been filtered by any quality control filter scheme. Diffuse horizontal measurements are from a shaded pyranometer and a correction is to be applied to correct the „shadow band effect" discussed in Chapter 4. Various models are available in the literature and are discussed in Chapter 4.

The data files are archived into monthly summaries known as solar calendars. A solar calendar shows the irradiance profiles for the three measured components of solar radiation: direct normal, global horizontal and diffuse horizontal irradiances for a given month. This summary makes it possible to view irradiance patterns for any given month without viewing large spreadsheet files of numerical values. The solar calendar (Fig. 3-8) has an empty profile for 16 June. This is due to power interruption at the site. This has caused gaps in the data acquired at the station and a calculated 8.22% of data has been lost. A sample of each data file is shown in Fig. 3-9 for all three irradiance components and the six outputs defining the solar vector as calculated by the SPA [23]. The figure shows minute values of the ten outputs from the LabVIEW code described in section 3.1. A complete file is shown in Appendix C.

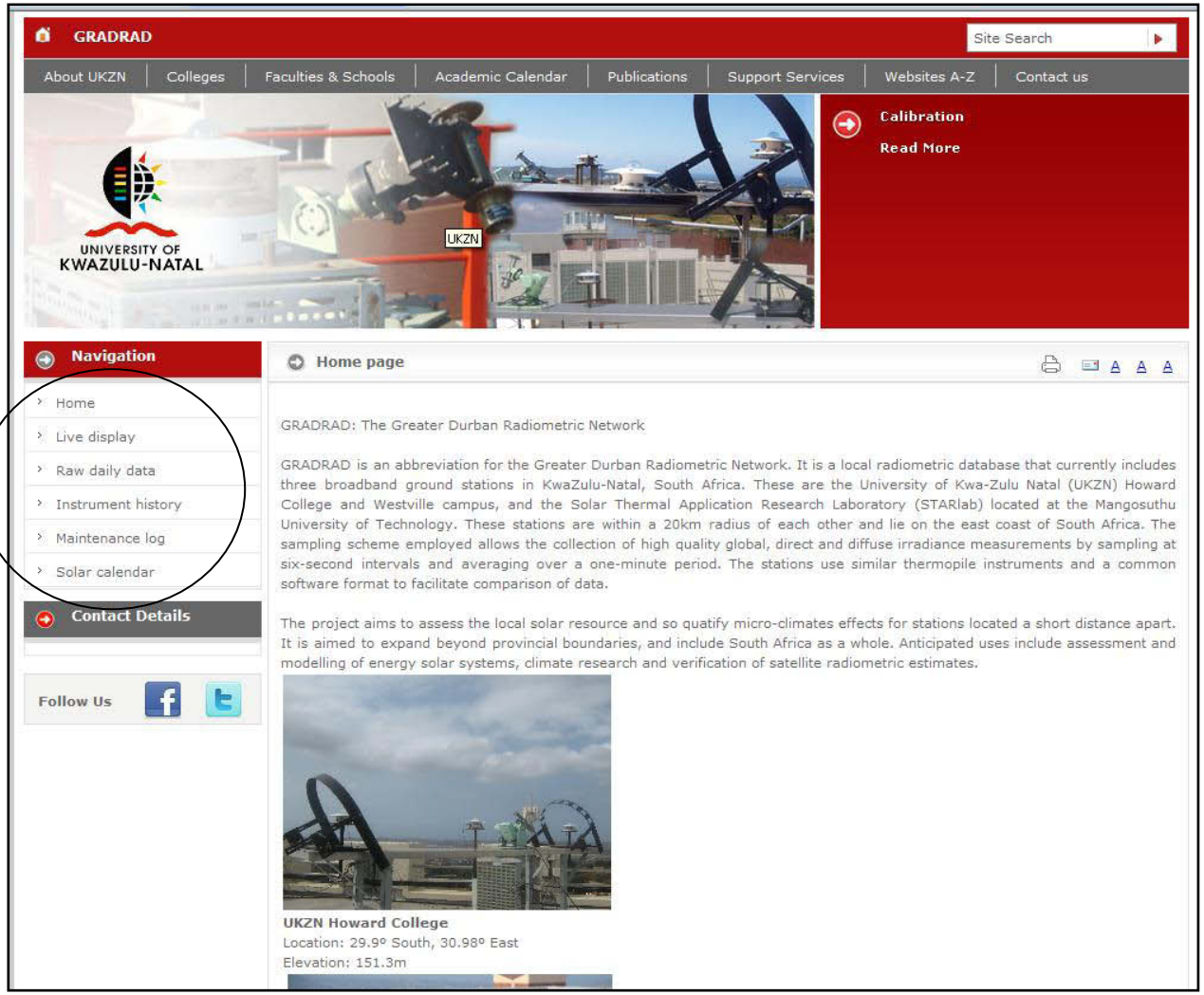

Fig. 3-6 A screenshot of the live GRADRAD webpage. The navigation bar (circled) allows users to explore data from each of the stations comprising the network.

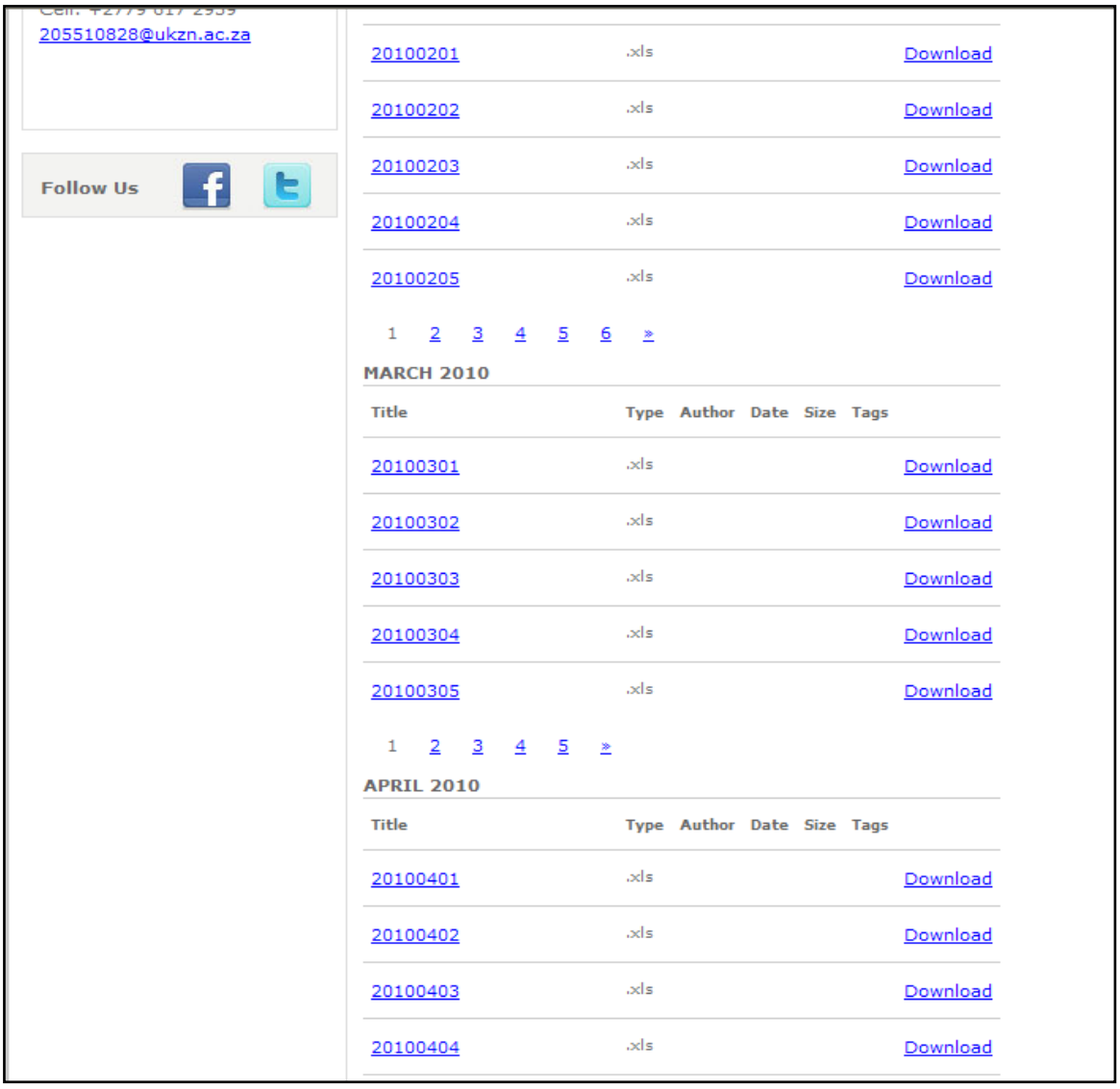

Fig. 3-7 Illustration of download option of raw daily data files for the months April, May and June, extracted from the GRADRAD webpage.

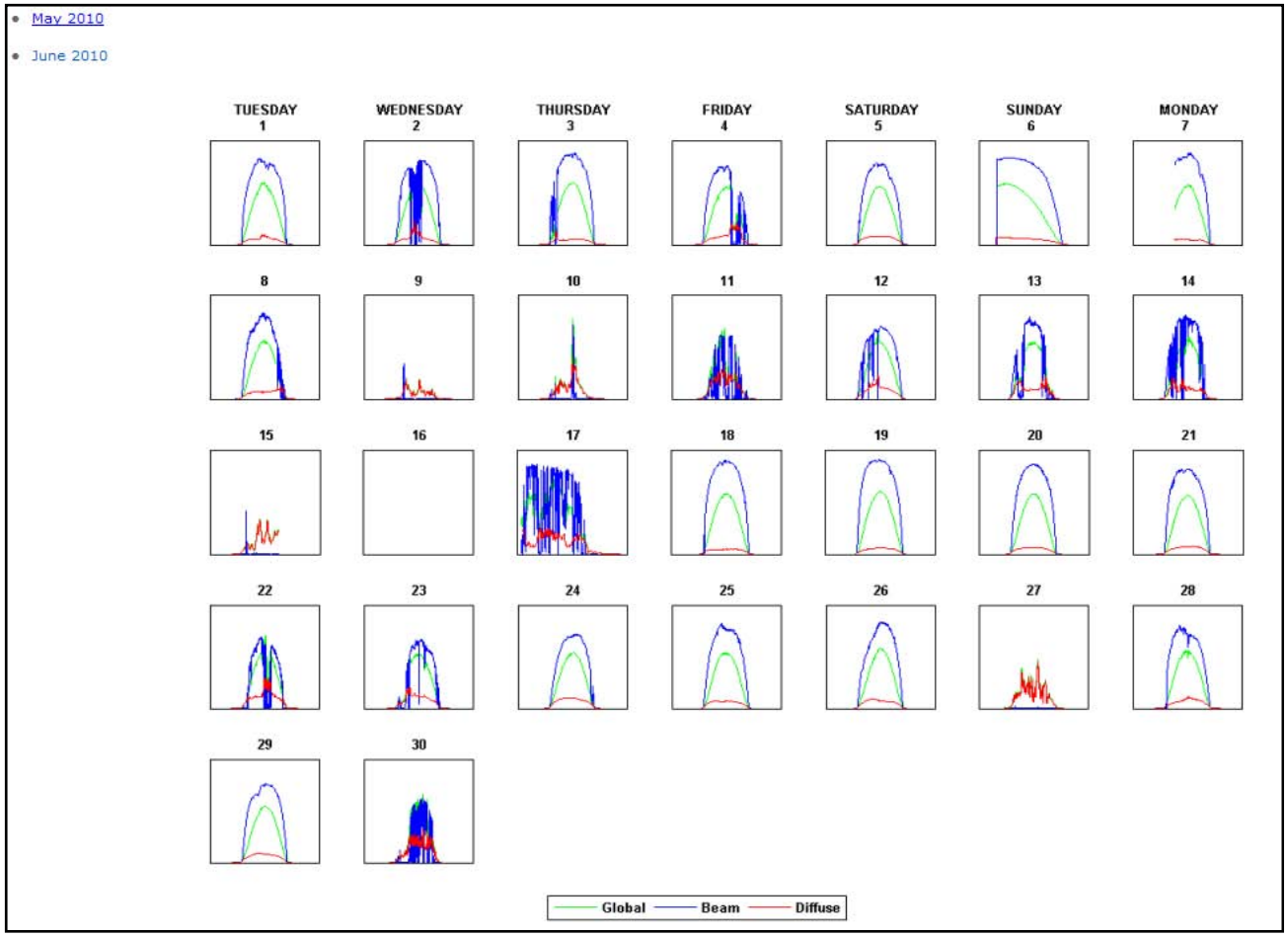

Fig. 3-8 A solar calendar of the month of June 2010 for the three separately measured components of radiation: GHI, DNI and DHI at the Howard College station.

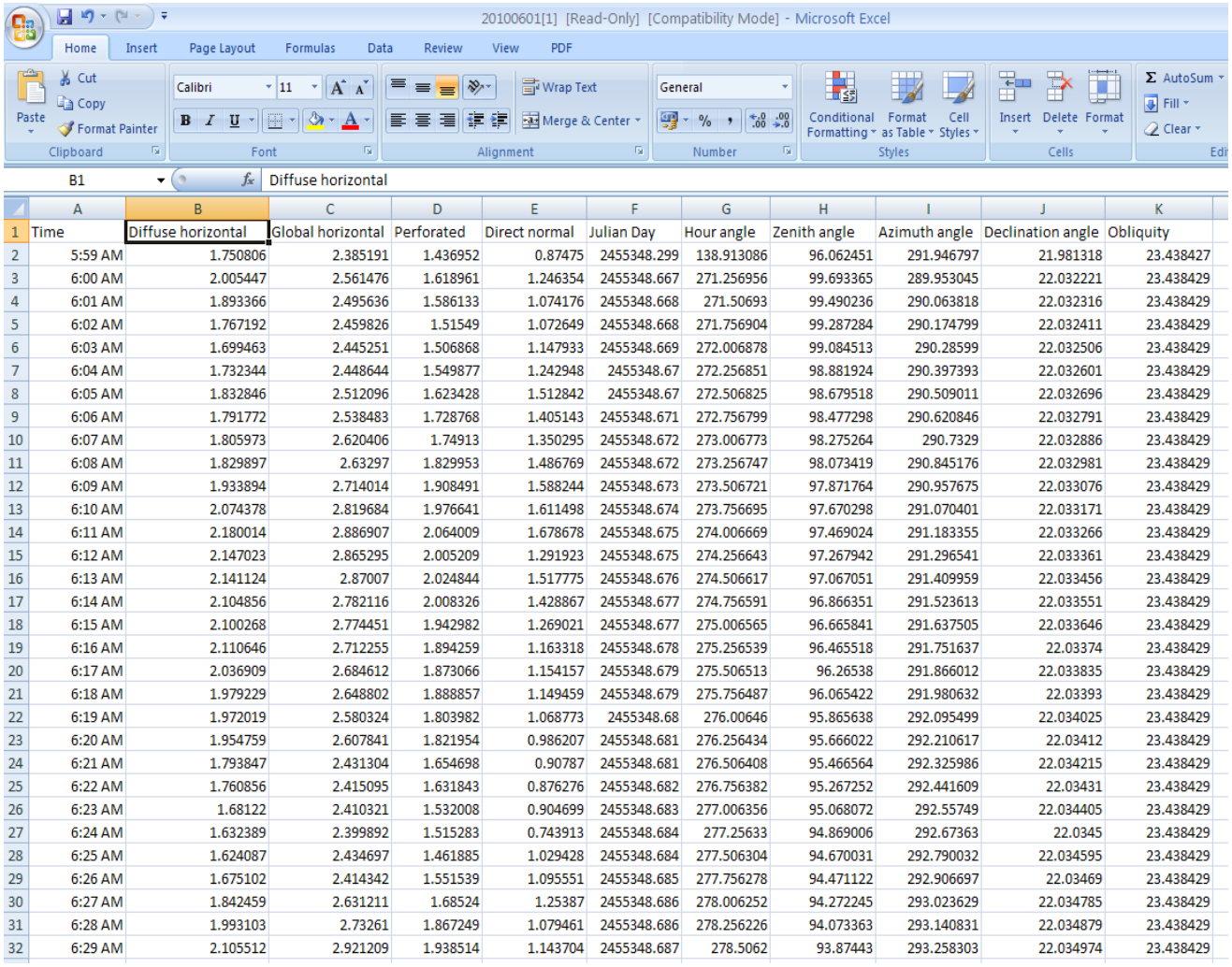

	A	B	C	D	E	F	G	H	I	J	K
1	Time	Diffuse horizontal	Global horizontal	Perforated	Direct normal	Julian Day	Hour angle	Zenith angle	Azimuth angle	Declination angle	Obliquity
2	5:59 AM	1.750806	2.385191	1.436952	0.87475	2455348.299	138.913086	96.062451	291.946797	21.981318	23.438427
3	6:00 AM	2.005447	2.561476	1.618961	1.246354	2455348.667	271.256956	99.693365	289.953045	22.032221	23.438429
4	6:01 AM	1.893366	2.495636	1.586133	1.074176	2455348.668	271.50693	99.490236	290.063818	22.032316	23.438429
5	6:02 AM	1.767192	2.459826	1.51549	1.072649	2455348.668	271.756904	99.287284	290.174799	22.032411	23.438429
6	6:03 AM	1.699463	2.445251	1.506868	1.147933	2455348.669	272.006878	99.084513	290.28599	22.032506	23.438429
7	6:04 AM	1.732344	2.448644	1.549877	1.242948	2455348.67	272.256851	98.881924	290.397393	22.032601	23.438429
8	6:05 AM	1.832846	2.512096	1.623428	1.512842	2455348.67	272.506825	98.679518	290.509011	22.032696	23.438429
9	6:06 AM	1.791772	2.538483	1.728768	1.405143	2455348.671	272.756799	98.477298	290.620846	22.032791	23.438429
10	6:07 AM	1.805973	2.620406	1.74913	1.350295	2455348.672	273.006773	98.275264	290.7329	22.032886	23.438429
11	6:08 AM	1.829897	2.63297	1.829953	1.486769	2455348.672	273.256747	98.073419	290.845176	22.032981	23.438429
12	6:09 AM	1.933894	2.714014	1.908491	1.588244	2455348.673	273.506721	97.871764	290.957675	22.033076	23.438429
13	6:10 AM	2.074378	2.819684	1.976641	1.611498	2455348.674	273.756695	97.670298	291.070401	22.033171	23.438429
14	6:11 AM	2.180014	2.886907	2.064009	1.678678	2455348.675	274.006669	97.469024	291.183355	22.033266	23.438429
15	6:12 AM	2.147023	2.865295	2.005209	1.291923	2455348.675	274.256643	97.267942	291.296541	22.033361	23.438429
16	6:13 AM	2.141124	2.87007	2.024844	1.517775	2455348.676	274.506617	97.067051	291.409959	22.033456	23.438429
17	6:14 AM	2.104856	2.782116	2.008326	1.428867	2455348.677	274.756591	96.866351	291.523613	22.033551	23.438429
18	6:15 AM	2.100268	2.774451	1.942982	1.269021	2455348.677	275.006565	96.665841	291.637505	22.033646	23.438429
19	6:16 AM	2.110646	2.712255	1.894259	1.163318	2455348.678	275.256539	96.465518	291.751637	22.03374	23.438429
20	6:17 AM	2.036909	2.684612	1.873066	1.154157	2455348.679	275.506513	96.26538	291.866012	22.033835	23.438429
21	6:18 AM	1.979229	2.648802	1.888857	1.149459	2455348.679	275.756487	96.065422	291.980632	22.03393	23.438429
22	6:19 AM	1.972019	2.580324	1.803982	1.068773	2455348.68	276.00646	95.865638	292.095499	22.034025	23.438429
23	6:20 AM	1.954759	2.607841	1.821954	0.986207	2455348.681	276.256434	95.666022	292.210617	22.03412	23.438429
24	6:21 AM	1.793847	2.431304	1.654698	0.90787	2455348.681	276.506408	95.466564	292.325986	22.034215	23.438429
25	6:22 AM	1.760856	2.415095	1.631843	0.876276	2455348.682	276.756382	95.267252	292.441609	22.03431	23.438429
26	6:23 AM	1.68122	2.410321	1.532008	0.904699	2455348.683	277.006356	95.068072	292.55749	22.034405	23.438429
27	6:24 AM	1.632389	2.399892	1.515283	0.743913	2455348.684	277.25633	94.869006	292.67363	22.0345	23.438429
28	6:25 AM	1.624087	2.434697	1.461885	1.029428	2455348.684	277.506304	94.670031	292.790032	22.034595	23.438429
29	6:26 AM	1.675102	2.414342	1.551539	1.095551	2455348.685	277.756278	94.471122	292.906697	22.03469	23.438429
30	6:27 AM	1.842459	2.631211	1.68524	1.25387	2455348.686	278.006252	94.272245	293.023629	22.034785	23.438429
31	6:28 AM	1.993103	2.73261	1.867249	1.079461	2455348.686	278.256226	94.073363	293.140831	22.034879	23.438429
32	6:29 AM	2.105512	2.921209	1.938514	1.143704	2455348.687	278.5062	93.87443	293.258303	22.034974	23.438429

Fig. 3-9 Sample of a downloaded spreadsheet file for 1 June 2010. The complete data file for 1 June 2010 is given in Appendix C.

CHAPTER 4: RESULTS AND DISCUSSION

The results of this study are reported in four separate sections:

4.2.1 This section is an analysis of the raw irradiance data gathered at the HC and MUT sites, including a comparison between the current data and measurements taken in 2007.

4.2.2 Comparison between measured diffuse data obtained from equation 1.1 and four shadow band correction models by Drummond [24], Le Baron et al. [25], Batlles et al. [26] and Muneer and Zhang [27].

4.2.3 Comparison between measured direct normal data and predicted values obtained from six radiometric models by Erbs et al. [29], Orgill and Hollands [30], Reindl et al. [31], Boland et al. [32] and Skartveit and Olseth [33].

4.2.4 The application of diffuse fraction models to the HC and MUT data so as to compare results from both sites.

Before any comparison of data can be performed between stations to quantify potential spatial variations in sun strength, the data must be „cleaned" by various filters to remove erroneous measurements. The various quality control schemes that were used to filter data from GRADRAD are discussed below.

4.1 Quality control filter schemes

Solar radiation data is susceptible to errors due to equipment failure and operational errors. In this study, the hourly data were checked for inconsistencies to eliminate outlying data points. Three quality control filter schemes were implemented.

Filter 1: Limiting the zenith angle, θ_z, to less than 75°

The breakdown of irradiance into its different components is relatively insignificant at high zenith angles due to the cosine error. Cosine correction factors vary amongst instrument manufacturers. Eppley instruments are known to have a large cosine error and their calibration factors are valid up to 75°. For that reason, Filter 1 removes data for all $\theta_z > 75°$ to eliminate the cosine error. As described in Chapter 1, Eppley instruments also experience thermal offset errors. Thermal offset is reduced by ventilation of the pyranometer or by correcting measurements using infrared data from a pyrgeometer. The latter proves costly as a new and expensive instrument has to be purchased.

Ventilation, which reduces thermal exchange between the internal and external atmospheres of the sensor was not available for instruments at either station of the network. For these reasons, all pyranometric measurements from the GRADRAD network, that is, global and diffuse irradiances carry an error associated with thermal offset. The error causes an underestimation of global and diffuse measurements by 15% and 1.5% respectively [20].

Filter 2: European Commission- Daylight 1, 1993

The hourly data set were checked against quality filters proposed by the European Commission-Daylight 1, 1993. The quality control check eliminates data when:

a) Horizontal diffuse irradiance is greater than the horizontal global irradiance, $0 < I_d < 1.1I_g$
b) Global data greater than corresponding extraterrestrial, $0 < I_g < 1.2I_o$
c) Diffuse data greater than corresponding extraterrestrial, $0 < I_d < 0.8I_o$
d) Global horizontal less than 5 W/m^2, $I_g < 5\ W/m^2$
e) Direct normal irradiance exceeds the corresponding extraterrestrial solar irradiance, $0 < I_b < I_o$

where I_o is the hourly horizontal extraterrestrial solar irradiation, given by:

$$I_o = I_{SC} E_0 (\sin\delta \sin\varphi + \cos\delta \cos\varphi \cos\omega_i) \quad (4.1)$$

and I_{sc}= 1367 W/m^2 is the solar constant. The parameters δ and φ are the solar declination and site latitude respectively. The hourly horizontal extraterrestrial solar irradiation is calculated at the middle of every hour from ω_i, the hour angle at the middle of the ith hour. The eccentricity correction factor is given by:

$$E_0 = 1 + 0.033\cos(\frac{2\pi n}{365}) \quad (4.2)$$

and is a reciprocal of the square of the radius vector of the earth, *n* is the day number of the year.

Filter 3: Outlier analysis

A further filter scheme was implemented to remove outliers (Fig. 4-1 and Fig. 4-2). These are data points that lie unusually far removed from the bulk of the data population [4]. Another definition of an outlier is that it lies three or four standard deviations from the mean of the data population [4]. They should be removed as they indicate measurement error. Their presence results in observed

high kurtosis in the population as the outliers will lie far from the mean thus skewing the distribution [52]. As a rule, an outlier should be carefully examined. In this work, they are removed as they are suspected to emanate from incidental systematic errors and mechanical faults from the equipment such as misalignment in the tracker. The method proposed to remove outliers is the box and whisker plot. Here, a 25th percentile outlier is removed when the measured value is less than three times the inter-quartile range. Similarly, a 75th percentile outlier is removed when the measured value is greater than three times the inter-quartile range. Using these criteria, 12 data points were removed from STARlab data and 25 data points were removed from Howard College. Figure 4-3 and Fig. 4-4 are box and whisker plots showing the outliers present in the diffuse horizontal irradiance measurement at both locations. They are 75th percentile outliers as they lie above the third quartile of the box and whisker plot. These outliers are marked as red crosses. The algorithm to remove outliers is shown in Appendix D. The circled points are deemed infeasible as they demonstrate peculiar behavior. Such are circled data points in the unfiltered data shown in Fig. 4-1 and Fig. 4-2.

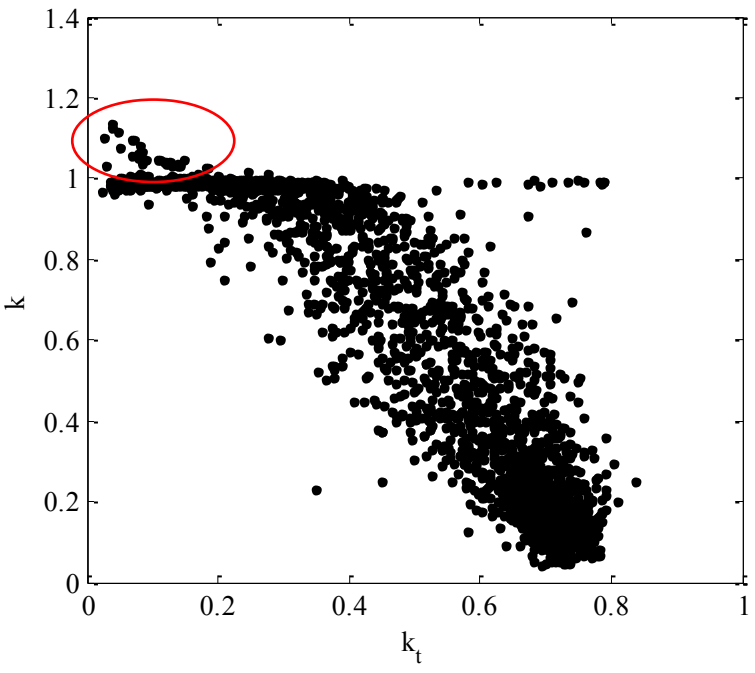

Fig. 4-1 Diffuse fraction, k vs. clearness index, k_t plot using data from Howard College. The circled points show outliers present in the data set that should be removed by filter 3.

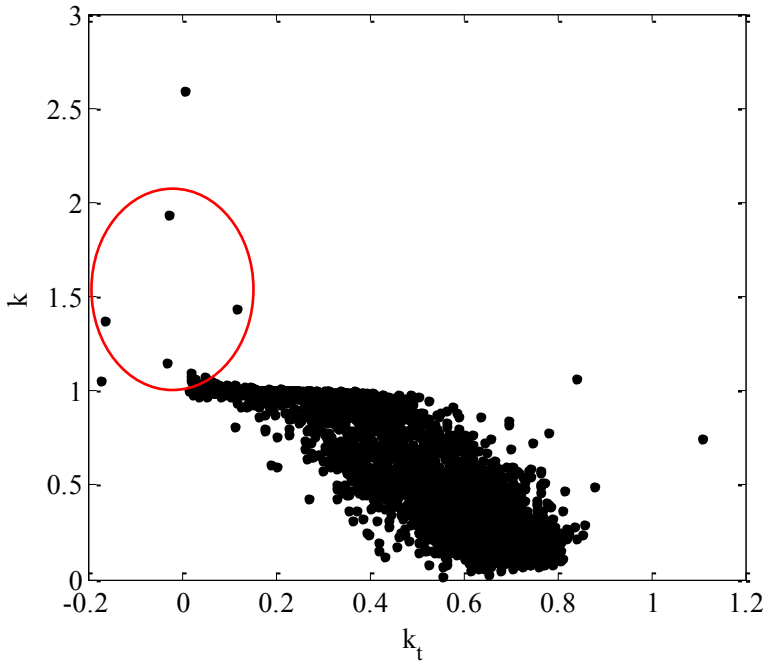

Fig. 4-2 Diffuse fraction, k vs. clearness index, k_t plot of unfiltered data from STARlab. The circled points show outliers present in the data set that should be removed.

Table 4-1 Quality control filter scheme indicating the removal of outlier data.

		Howard College		**STARlab**	
		Removed	**Remaining**	**Removed**	**Remaining**
Filter 1	$\theta_z > 75°$	476	2961	520	3360
Filter 2	$0 < I_d < 1.1I_g$	6	2955	0	3360
	$I_g < 5$	0	2955	0	336
	$0 < I_g < 1.2I_0$	0	2955	0	3360
	$0 < I_d < 0.8I_0$	0	2955	0	336
	$I_b > I_0$	469	2486	728	2632
Filter 3	Outliers	25	2461	12	2620

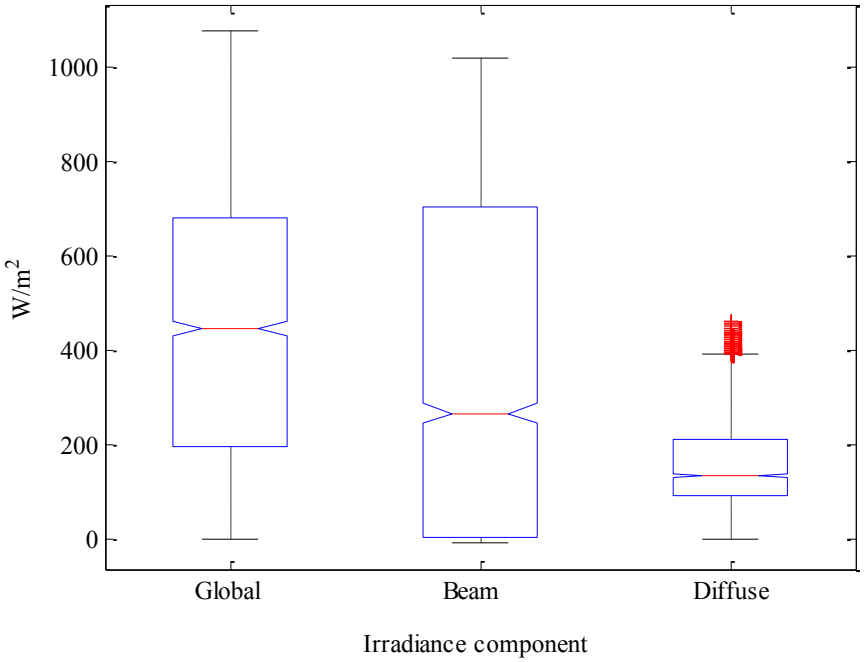

Fig. 4-3 Box and whisker plot of Howard College showing outliers (red crosses).

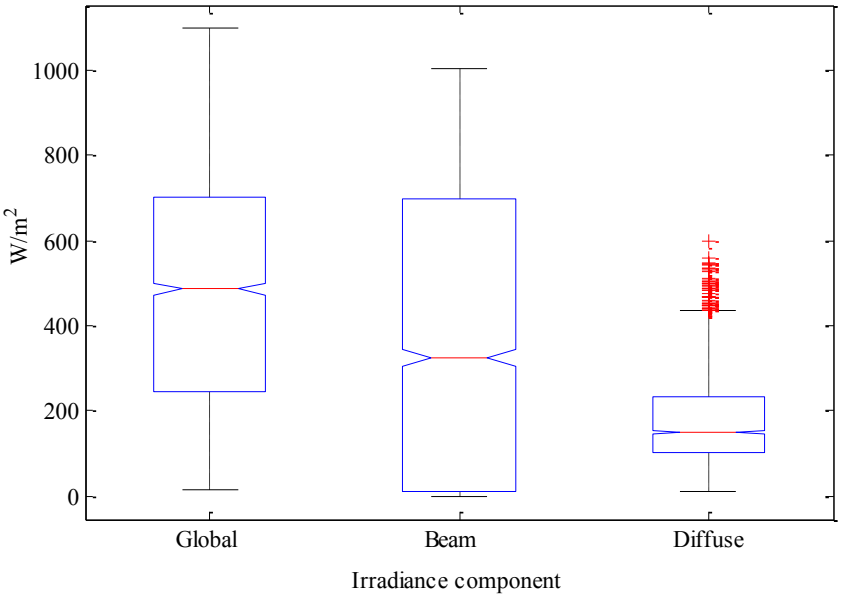

Fig. 4-4 Box and whisker plot of STARlab showing outliers (red crosses).

4.2 Solar resource assessment

Global horizontal radiation is one of the key inputs in the design and analysis of solar technologies. The efficiency of solar energy systems is evaluated over long periods of time. Even though various solar radiometric ground stations record irradiance values at short time intervals of less than a minute [13], [53] and [54], it is necessary to integrate these values over longer periods. Such integrations are hour intervals, daily, monthly and even yearly values to observe the performance of solar energy systems. General solar energy calculations require average values of solar radiation integrated over these time intervals [55]. Although averaging radiation values can lead to inaccuracies, it gives project managers and engineers a picture of the available radiation and efficiency of intended solar projects. More accurate methods such as probability density functions are used for improved solar radiation estimation [55]. This section describes an assessment of the solar resource of Durban. In this study, twelve months worth of solar radiation data was sampled at six-second intervals and integrated into average monthly values for Howard College and the STARlab station. The data were recorded between May 2010 and April 2011. The comparison is performed after a quality control scheme described in section 4.1. Results obtained from STARlab during the period May 2010 to April 2011 are also compared with data reported by Zawilska and Brooks [56] from 2007 to investigate any pattern in radiation over the years.

4.2.1 Analysis of radiometric data

4.2.1.1 Howard College and STARlab data for May 2010 to April 2011.

Figure 4-5 shows measured daily global radiation at STARlab over the period May 2010 to April 2011. The figure shows high values of global horizontal irradiance for summer months between September and March and low values for the winter period, April to August. The dip in the graph indicates the winter season during which high angles of incidence result in lower solar radiation intensities. Irregularities are present in the month of July when several days were removed and used for a calibration process described in Chapter 2.

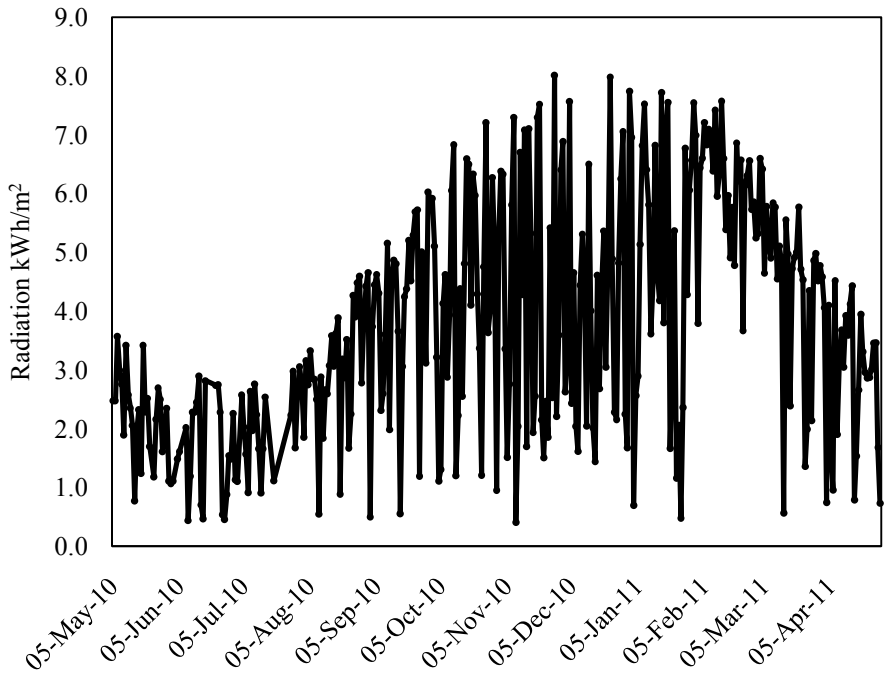

Fig. 4-5 Measured daily global horizontal radiation at STARlab for May 2010 to April 2011.

Following the work of [56] to enable comparison of data for different stations, six-second data were averaged into minute data. Average minute values were integrated for hourly periods and the average radiation for the day was calculated in kWh/m^2. Daily radiation values were integrated to give monthly averages. Table 4-2 shows a comparison of the average monthly radiation for the Howard College and MUT (STARlab) stations using the described methodology. The MBE and RMSE are given in Table 4-3. Figure 4-6 to Fig. 4-8 show comparisons of monthly average GHI, DNI and DHI between the HC and MUT stations.

The monthly average global radiation for winter and summer calculated at UKZN Howard College are 1.62 kWh/m^2 and 5.98 kWh/m^2 respectively. A maximum monthly average daily global radiation was recorded in February and a minimum recorded in June. In a similar way, the monthly average direct normal radiation for winter and summer recorded were 1.79 kWh/m^2 and 5.18 kWh/m^2, recorded in February and June respectively. Average monthly daily diffuse radiation recorded was a high of 2.49 kWh/m^2 in December and a low of 0.68 kWh/m^2 in July. Annual average values obtained for direct normal radiation, diffuse horizontal radiation and global horizontal are 2.85 kWh/m^2, 1.60 kWh/m^2 and 3.64 kWh/m^2 respectively.

Applying the same methodology to STARlab, the monthly average global radiation for winter and summer seasons recorded was a maximum of 1.64 kWh/m^2, measured in June and 6.18 kWh/m^2 recorded in February respectively. Similarly, the monthly average daily direct normal radiation for winter and summer were 1.78 kWh/m^2 and 4.89 kWh/m^2 respectively. The highest value for the monthly average daily direct normal radiation was recorded in February and the lowest in June. Average monthly daily diffuse radiation recorded were a high of 2.69 kWh/m^2 in January and a low of 0.73 kWh/m^2 in June. Annual average values obtained for global radiation, direct normal radiation and diffuse horizontal radiation are 3.66 kWh/m^2, 2.81 kWh/m^2 and 1.70 kWh/m^2 respectively.

The mean bias difference between the two stations is calculated as -0.02 kWh/m^2, 0.04 kWh/m^2 and -0.10 kWh/m^2 for GHI, DNI and DHI respectively with corresponding percentage root mean square differences of 6.42%, 7.94% and 12.9% (Table 4-3). A close similarity of all three components is present in the winter season, April to October. This is characteristic of the weather in Durban which is a summer rainfall region and where winters have more clear days. A larger deviation is observed during the summer season. Summers in Durban have changing unstable weather patterns accompanied by storms with parts of the sky clear and overcast at different times of the day. Figure 4-9 is a profile of a summer day, 4 December 2010, showing a partly overcast sky and Fig. 4-10 is a clear day (24 June 2010) in winter showing low intensity of irradiance of less than 800 W/m^2. Figure 4-11 is a profile of a clear day (7 February 2010) with high solar intensities of GHI of more than 1000 W/m^2.

Table 4-2 Comparison of measured monthly average daily radiation at Howard College and MUT, May 2010 to April 2011.

Month	HC I_g kWh/m^2	MUT I_g kWh/m^2	HC I_b kWh/m^2	MUT I_b kWh/m^2	HC I_d kWh/m^2	MUT I_d kWh/m^2
May	2.21	2.26	2.26	2.54	0.88	0.80
Jun	1.62	1.64	1.79	1.78	0.69	0.73
Jul	1.74	1.97	1.88	2.14	0.68	0.78
Aug	3.52	2.98	3.08	3.04	1.19	1.06
Sep	4.25	4.01	3.65	3.29	1.81	1.80
Oct	4.25	4.21	2.63	2.51	2.30	2.35
Nov	4.11	4.30	2.52	2.56	2.12	2.23
Dec	4.22	4.05	2.13	1.80	2.49	2.58
Jan	4.55	4.84	2.95	2.72	2.20	2.69
Feb	5.98	6.18	5.18	4.89	1.93	2.39
Mar	4.57	4.59	3.72	3.81	1.88	1.87
Apr	2.67	2.92	2.41	2.68	1.04	1.13
Annual	3.64	3.66	2.85	2.81	1.60	1.70

Table 4-3 Mean bias difference and root mean square difference for Howard College versus STARlab data (May 2010-April 2011), where difference is defined as HC data minus MUT data.

Solar radiation component	MBE (kWh/m^2)	MBE %	RMSE (kWh/m^2)	RMSE %
Global	-0.02	-0.68	0.23	6.42
Beam	0.04	1.34	0.23	7.94
Diffuse	-0.10	-6.27	0.21	12.9

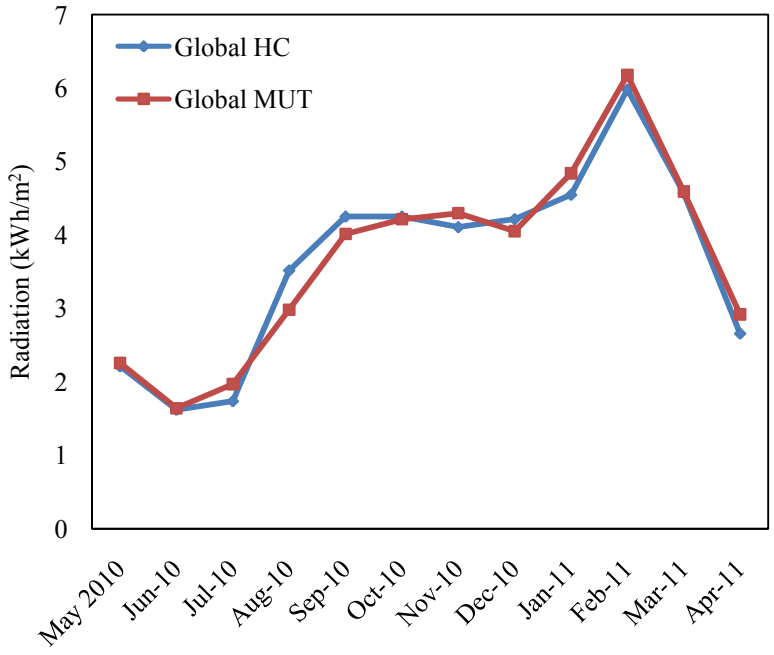

Fig. 4-6 Comparison of monthly average daily global horizontal radiation at Howard College and STARlab from May 2010-April 2011.

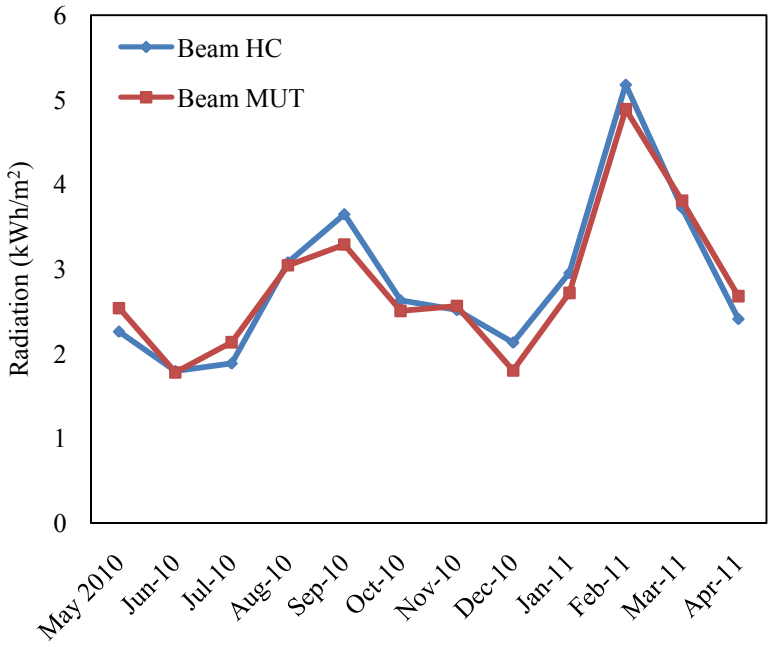

Fig. 4-7 Comparison of monthly average daily direct normal radiation at Howard College and STARlab from May 2010-April 2011.

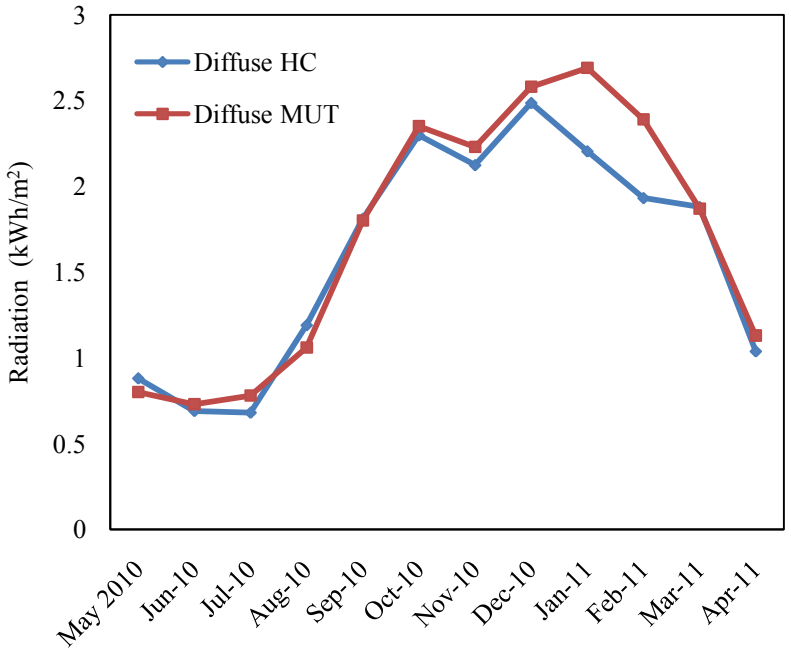

Fig. 4-8 Comparison of monthly average daily diffuse horizontal radiation at Howard College and STARlab from May 2010-April 2011.

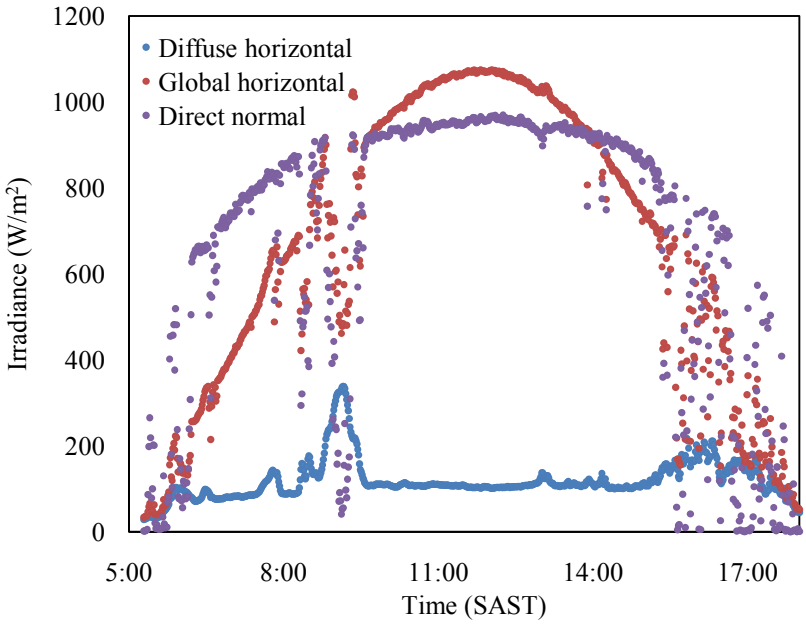

Fig. 4-9 Solar irradiance for a partly cloudy day, 4 December 2010 for Howard College.

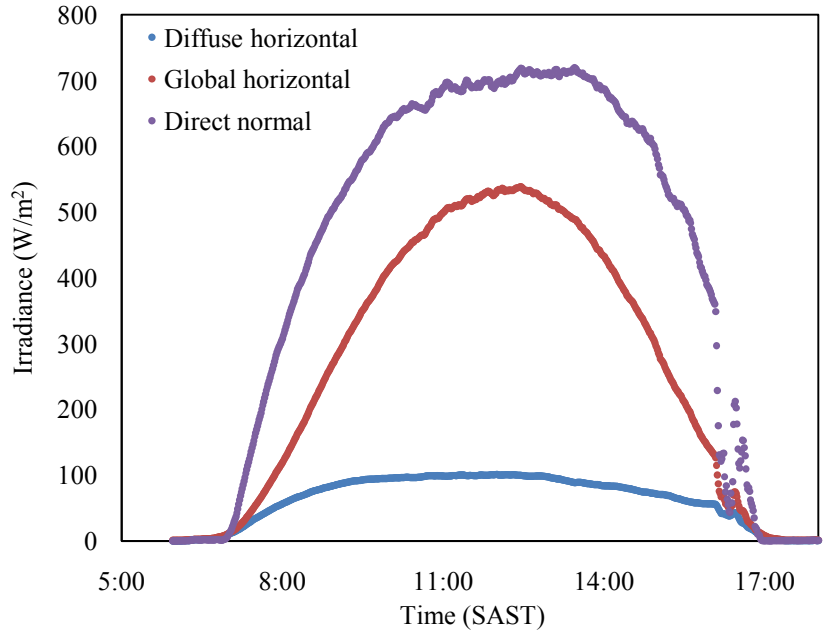

Fig. 4-10 Solar irradiance for a clear day in winter, 24 June 2010 for Howard College. Low irradiance intensities of less than 800 W/m^2 are observed.

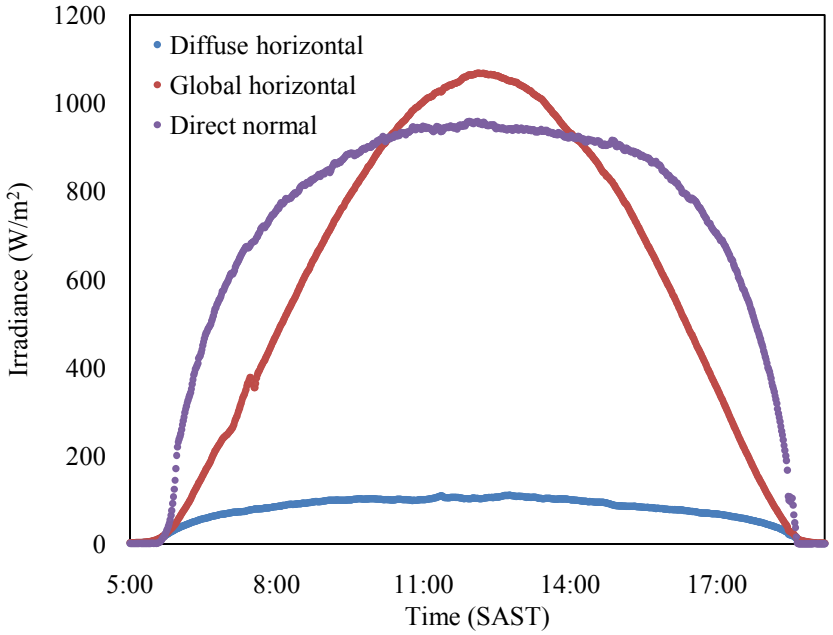

Fig. 4-11 Solar irradiance for a clear day in summer, 7 February 2010 for Howard College. High irradiance intensities of more than 1000 W/m^2 are recorded.

4.2.1.2 Analysis of radiometric data for 2007 and the period 2010-2011 of STARlab.

To accurately analyze the pattern of solar radiation, data should be recorded for many years [57]. A year‟s worth of data, even accurately measured, cannot quantify the solar pattern of an area. Data recorded at STARlab in 2007 were compared to that measured in the period May 2010 to April 2011 at the same location. It should be noted that results reported in [56] did not employ a data quality check. Data obtained for the period 2010-2011 were subject to a quality control filter. Comparing the results for different years (Table 4-4 and Table 4-5) it can be shown that data recorded in 2007 is quite markedly higher than those of the recent study. Mean bias errors are reported to be -0.77 kWh/m^2 (-21.1%), -2.25 kWh/m^2 (-80.1%) and -0.001 kWh/m^2 (-0.05%) with corresponding root mean square differences of 1.00 kWh/m^2 (27.4%), 2.39 kWh/m^2 (84.9%) and -0.17 kWh/m^2 (10.1%) for GHI, DNI and DHI respectively.

Figure 4-12 to Fig. 4-14 show quite markedly higher monthly averages of GHI, DNI and DHI for 2007 data. There is no way to determine whether the difference is due to quality filters not implemented on the 2007 data or if the difference is due to different weather patterns that applied during 2007 and the period 2010-2011. It is assumed that the large differences emanate from shadows and nearby artificial obstructions such as tall buildings. Another reason could be the change in cloud field over the years as STARlab is situated close to industrial activity that might pollute the air with aerosols, smoke and dust that cause increased attenuation of solar radiation that is incident on the sensors. Similar patterns though are observed for maximum and minimum radiation values for all three components of radiation obtained in the same months. Maximum monthly average daily global radiation is recorded in February with values of 6.18 kWh/m^2 in 2007 and 6.14 kWh/m^2 in 2011 and lows of 1.64 kWh/m^2 in 2007 and 2.81 kWh/m^2 in 2011 recorded in June. Similarly, the maximum monthly average daily direct normal radiation was 4.89 kWh/m^2 in 2007 and 5.90 kWh/m^2 in 2011 recorded in February and lows of 1.78 kWh/m^2 in 2007 recorded in June and 3.78 kWh/m^2 in 2011 recorded in October. Maximum monthly average daily diffuse radiation is recorded in June with values of 2.61 kWh/m^2 in 2007 and 2.69 kWh/m^2 in 2011 and a low of 0.73 kWh/m^2 for both periods.

An assessment of the local solar resource will aid in constructing a reliable record of solar radiometric data for solar energy technologies and urban planning. Durban has a considerable solar energy resource that remains to be exploited [56]. The findings from the current study can help

eThekwini refine its interest in solar energy technologies to reduce reliance on the national electricity grid.

Table 4-4 Comparison of monthly average daily radiation of MUT, 2007 data versus 2010-2011 data.

Month	MUT 2010 I_g kWh/m^2	MUT 2007 I_g kWh/m^2	MUT 2010 I_b kWh/m^2	MUT 2007 I_b kWh/m^2	MUT 2010 I_d kWh/m^2	MUT 2007 I_d kWh/m^2
May	2.26	3.64	2.54	5.65	0.80	0.81
Jun	1.64	2.81	1.78	4.94	0.73	0.73
Jul	1.97	3.17	2.14	5.18	0.78	0.81
Aug	2.98	3.71	3.04	5.15	1.06	1.00
Sep	4.01	4.10	3.29	5.19	1.80	1.68
Oct	4.21	4.07	2.51	3.78	2.35	2.46
Nov	4.30	4.85	2.56	4.64	2.23	2.56
Dec	4.05	5.93	1.80	4.92	2.58	2.26
Jan	4.84	6.39	2.72	5.76	2.69	2.61
Feb	6.18	6.14	4.89	5.90	2.39	2.16
Mar	4.59	4.77	3.81	4.99	1.87	2.03
Apr	2.92	3.64	2.68	4.71	1.13	1.29
Annual	3.64	4.45	2.89	5.07	1.59	1.70

Table 4-5. Mean bias error and root mean square error for STARlab data (May 2010-April 2011) versus STARlab 2007, where error is defined as STARlab data (May 2010-April 2011) minus STARlab 2007 data.

Solar radiation component	MBE (kWh/m^2)	MBE %	RMSE (kWh/m^2)	RMSE %
Global	-0.77	-21.1	1.00	27.4
Beam	-2.25	-80.1	2.39	84.9
Diffuse	-0.001	-0.05	0.17	10.1

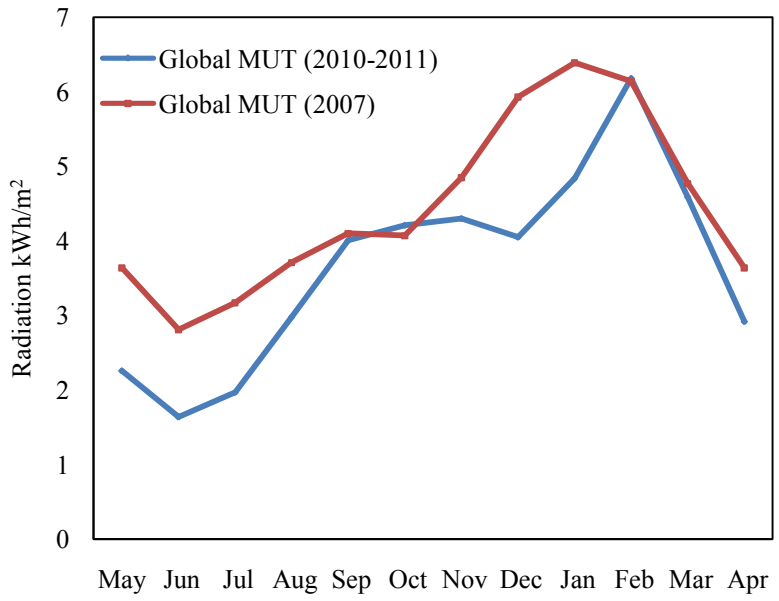

Fig. 4-12 A comparison of monthly average daily global horizontal radiation for STARlab using data from 2007 and the period May 2010-April 2011.

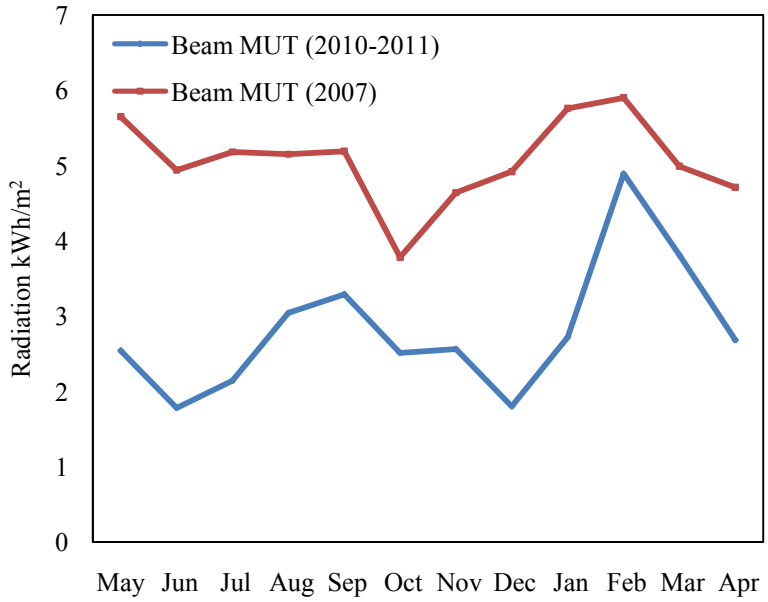

Fig. 4-13 A comparison of monthly average daily direct normal radiation for STARlab using data from 2007 and the period May 2010-April 2011.

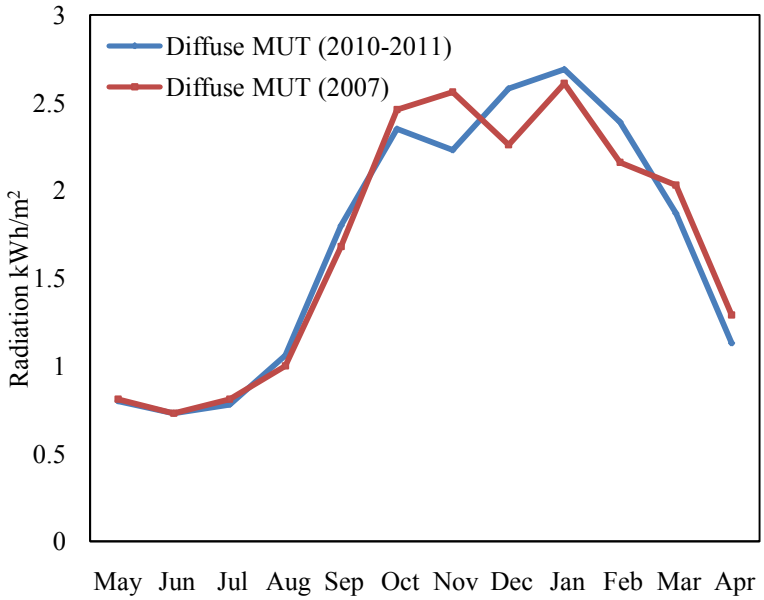

Fig. 4-14 A comparison of monthly average daily diffuse horizontal radiation comparison for STARlab using data from 2007 and the period May 2010-April 2011.

4.2.2 Comparison between measured diffuse data and shadow band correction models.

A shadow band correction model corrects the output from a pyranometer that has been shaded to measure diffuse radiation. This is necessary because the band creates a permanent shadow on the sensor by blocking off the DNI component of the global radiation, thus theoretically, giving the DHI component. Although the stationary band blocks off the intended DNI, it also shades a portion of the sky and blocks off the diffuse irradiance that is obscured by the band, thus measuring lower diffuse radiation values. Four models by Drummond [24], Le Baron et al. [25], Batlles et al. [26] and Muneer and Zhang [27] are investigated to correct the shadow band effect by comparing the model output with data from the collocated reference instruments via equation 1.1 to determine the accuracy of each model. Minute data from STARlab in uMlazi and UKZN Howard College integrated over hourly periods were used to generate the results presented in this work. A MATLAB code for the four models used to correct the shadow band effect is shown in Appendix F. A solar radiometric station can implement many possible combinations of instrumentation the most common of which utilize the following:

1) NIP + PSP(shaded)
2) NIP + PSP(unshaded)

3) PSP(shaded) + PSP(unshaded)

The above schemes provide no redundancy in the measured irradiance as the third component has to be calculated using equation 1.1. Stations that comprise the GRADRAD network are intended to measure all three components separately to ensure redundancy as a cross-check between measured and calculated values, shown later in this chapter. The proposed scheme given below is that intended for all GRADRAD stations such that all components are measured separately:
PSP (shaded) + PSP (unshaded) + NIP.

Irradiance measurements are acquired through the Normal Incidence Pyrheliometer (NIP) and a Precision Spectral Pyranometer (PSP), all produced by Eppley. Routine diffuse horizontal measurements are gathered by a PSP equipped with a shading band, mounted on a shadow band stand (SBS). The shadow band is aligned parallel to the earth‟s polar axis to track the sun in an east-west axis and is adjusted for changes in declination, particularly at high zenith angles where the instrument responds to the Lambertian response or cosine error [10].

Studies dating back to 1956 by Drummond [24] have been made in developing correction models for the diffuse measurement made with a shadow band. Drummond developed a model based on isotropic sky conditions. Selected models by Drummond [24], Le Baron et al. [25], Batlles et al. [26] and Muneer and Zhang [27] were used to correct the shadow band effect for data acquired at the two operational stations of GRADRAD. The results of the selected models are shown in Fig. 4-15 and Fig. 4-16 for the Howard College and STARlab respectively. The three models by Le Baron et al. [25], Batlles et al. [26] and Muneer and Zhang [27] were selected because they describe anisotropic sky conditions whereas the model by Drummond [24] assumes an isotropic sky, that is, uniformly overcast by clouds. Graphical and statistical analyses of data were investigated to obtain an understanding of the performance of the models and the effect of assuming an isotropic sky condition. The Batlles et al. [26] criterion defines a clear sky when $k_t > k_{tt}$ and $k^{true} < k_k$ where k^{true} is the ratio of the actual measured diffuse horizontal irradiance (calculated from equation 1.1) to measured global horizontal irradiance.

k_k and k_{tt} are defined as follows

$$k_{tt} = -0.3262 - 0.0032\alpha + 0.6843\log(\alpha) \quad (4.3)$$

$$k_k = 1.0827 - 0.3893\log(\alpha) \quad (4.4)$$

where α is the solar altitude (the complement of the zenith angle) measured in degrees. After the application of a quality control filter, described in section 4.1, 2461 data points remained for Howard College station. On application of Batlles" criterion [26], 788 records accounted for clear skies. This is representative of 32% of the data from Howard College and the remaining 68% corresponding to cloudy to partly cloudy sky conditions. Similarly, for STARlab, 2620 data points remained after applying a quality control filter scheme. Of these data points, 909 records constitute clear skies and 1711 represent cloudy-partly cloudy sky conditions. The results represent 34.7% and 65.7% for clear and cloudy to partly cloudy conditions respectively.

Diffuse measurements can be obtained by one of two methods:

1) Direct method, through the use of a shading band pyranometer or an occulting disk, then further application of a correction factor to compensate for the shadow band effect, or
2) Indirect method, which comprises the concurrent measurement of both the global horizontal irradiance (using an unshaded pyranometer) and the beam irradiance (using a normal incidence pyrheliometer). The former method is most common as it eliminates the use of the expensive cost of the pyrheliometer and the cumbersome tracking system required though at the cost of reduced accuracy from embedded instrument errors.

Drummond (1956)

The model by Drummond [24] is based purely on a geometric analysis. It assumes that the sky is uniformly overcast by clouds, which is not necessarily representative of a true sky. The portion of the hemispherical radiation blocked by the shadow band is given by the following expression,

$$f = \frac{2b}{\pi r}\cos^3\delta(\omega_s \sin\varphi \sin\delta + \cos\varphi \cos\delta \sin\omega_s) \tag{4.5}$$

where ω_s is the sunset hour angle in radians given by

$$\omega_s = \cos^{-1}(-tan\varphi tan\delta), \tag{4.6}$$

The symbol φ is the station latitude and δ is the declination angle obtained from the LabVIEW logging file. The parameters b and r in equation (4.5) are the width and radius of the shadow band (SBS model) respectively. For an Eppley SBS model, the shadow band has a diameter of 635 mm and a width of 76.3 mm [12]. For isotropic conditions, the correction factor applied is

$$C_D = \frac{1}{1-f} \tag{4.7}$$

The corrected diffuse horizontal irradiance by Drummond [24] is given by

$$I_{dD} = C_D I_{dUn} \tag{4.8}$$

where I_{dUn} is the uncorrected diffuse irradiance measured by a shaded pyranometer. This formula is applicable worldwide at any location [24]. A further 7% is added for cloudless skies and 3% for overcast skies. These additions are reported to be dependent on the size of the data and shadow band used [24].

Le Baron et al (1990)

Le Baron et al. [25] proposed a model encompassing both conditions: isotropic and anisotropic conditions using Drummond‟s correction factor as one of the four parameters in their model. The three other factors are solar zenith angle (θ_Z) which defines the position of the sun in the vertical plane, ε is a dimensionless parameter indicating the sky‟s clearness and a function of cloud conditions and a dimensionless parameter that defines the sky‟s brightness that is a function of cloud thickness, (Δ). The uncorrected direct normal irradiance is given by equation (4.9) and is calculated as the difference between the uncorrected diffuse horizontal irradiance (measured from a shaded Eppley PSP) and global radiation using an unshaded pyranometer.

$$I_b = \frac{I_g - I_{dUn}}{\cos\theta_Z} \tag{4.9}$$

Epsilon and delta are given by the following equations

$$\varepsilon = \frac{I_{dUn} + I_n}{I_d}, \tag{4.10}$$

and

$$\Delta = \frac{I_d}{I_o} A \tag{4.11}$$

where I_n is the normal beam component. The parameter A represents the air mass and is calculated by the Kasten formula [9] given by

$$A = 1/[\cos\theta_z + 0.15(93.885 - \theta_z)^{-1.125}] \tag{4.12}$$

The corrected diffuse measurement given by Le Baron et al. [25] using a shadow band is given by

$$I_{dL} = C_L I_{dUn} \tag{4.13}$$

The value C_L is obtained from lookup tables shown in Appendix E.

Batlles et al (1995)

In 1995, Batlles et al. [26] proposed a model that uses multiple linear regression and four parameters from the model of Le Baron et al. (1990). The correction factor, C_B, is calculated as follows:

$$C_B = 1.178C_D + 0.207log\Delta + \frac{0.1220}{\exp(4)} \quad for\ \varepsilon \leq 3.5 \tag{4.14}$$

$$C_B = 1.454C_D + 0.655log\Delta + \frac{0.4756}{\exp(4)} \quad for\ 3.5 \leq \varepsilon \leq 8 \tag{4.15}$$

$$C_B = 1.486C_D + 0.495log\Delta \quad for\ 8 \leq \varepsilon \leq 11 \tag{4.16}$$

$$C_B = 1.454C_D + 0.363log\Delta \quad for\ \varepsilon \geq 11 \tag{4.17}$$

The corrected diffuse horizontal irradiance is given by

$$I_{dB} = C_B I_d. \tag{4.18}$$

Muneer and Zhang (2002)

The diffuse irradiance I_d is calculated from parameters b_1 and b_2 for two sky conditions containing and opposing the sun respectively as shown.

$$I_d = \left(\frac{\pi L_Z}{6}\right)[(3 + 2b_1) + (1 + 2b_2)/(1 + b_2)] \tag{4.19}$$

where

$$b_1 = \left(\frac{3.6 - 10.4 + 2k_t}{-0.4 + 6.974k_t}\right) \tag{4.20}$$

and

$$b_2 = \left(\frac{1.565 + 0.990k_t}{0.957 - 0.660k_t}\right) \tag{4.21}$$

for values of $k_t > 0.2$

For $k_t \leq 0.2$, $b_1 = b_2 = 1.68$

The correction by Muneer and Zhang [27] is given by

$$C_M = \frac{1}{1-{}^{F}/_{I_d}} \tag{4.22}$$

where

$$F = WL_Z cos^3\delta \left[{}^{(I_1 + b_1 I_2)}/_{(1+b_1)} \right] \tag{4.23}$$

$$W = \left({}^{2b}/_{r} \right) \tag{4.24}$$

where the parameter W is the view angle of the shadow band,

$$I_1 = \cos\varphi \cos\delta \sin\omega_s + \omega_s \sin\varphi \sin\delta \tag{4.25}$$

and

$$I_2 = sin^2\varphi sin^2\delta + 2\sin\omega_s \sin\varphi \cos\varphi \sin\delta \cos\delta + cos^2\varphi cos^2\delta \left[{}^{\omega_s}/_{2} + {}^{\sin 2\omega_s}/_{4} \right] \tag{4.26}$$

The corrected diffuse horizontal irradiance by Muneer and Zhang [27] is

$$I_{dM} = C_M I_d \ . \tag{4.27}$$

The accuracy of these models in correcting the shadow band effect was investigated by plotting the diffuse horizontal irradiance calculated indirectly by equation 1.1 against the modelled diffuse irradiance using the mentioned shadow band correction models for the two operational GRADRAD stations. Figure 4-15 and Figure 4-16 show these plots. The plots show that all four models improve the uncorrected diffuse quantity as more points lie on the 45° line that indicates a best fit of the measured and modeled quantity. Statistical measures such as the MBE, RMSE and R^2 were examined to better quantify the performance of the shadow band correction models. Table 4-6 to Table 4-8 contains these results for the different sky conditions described by the criteria by Batlles et al. [26]. In addition to MBE and RMSE explained in Chapter 2, the coefficient of determination, R^2 (equation (4.33)) was also calculated. The indicator gives a proportion of variance between the measured and predicted values. It indicates how well future outcomes can be predicted. Ideally, it should be close to unity thus implying good correlation. The MBE and RMSE for this section are defined as

$$E_i = measured - model \tag{4.28}$$

where E_i is the error of the i[th] data point between the model (the shadow band correction model by either Drummond [24], Le Baron et al. [25], Batlles et al. [26] or Muneer and Zhang [27]) and the DHI calculated from equation 1.1.

$$MBE = \frac{\sum E_i}{N} \tag{4.29}$$

$$RMSE = \sqrt{\frac{\sum (E_i)^2}{N}} \tag{4.30}$$

$$SST = \sum [(measured - mean(measured)]^2 \tag{4.31}$$

$$SSE = \sum [(measured - modelled]^2 \tag{4.32}$$

$$R^2 = 1 - \frac{SSE}{SST} \tag{4.33}$$

where SSE is the sum of squares of residuals which measures the squared distances between the actual and predicted values. The statistical indicator measures the discrepancy between a model and the measured data. A low value close to zero signifies a tight fit of the model to the data. The total sum of squares (SST) is the sum of the squared distances between the actual values and their mean.

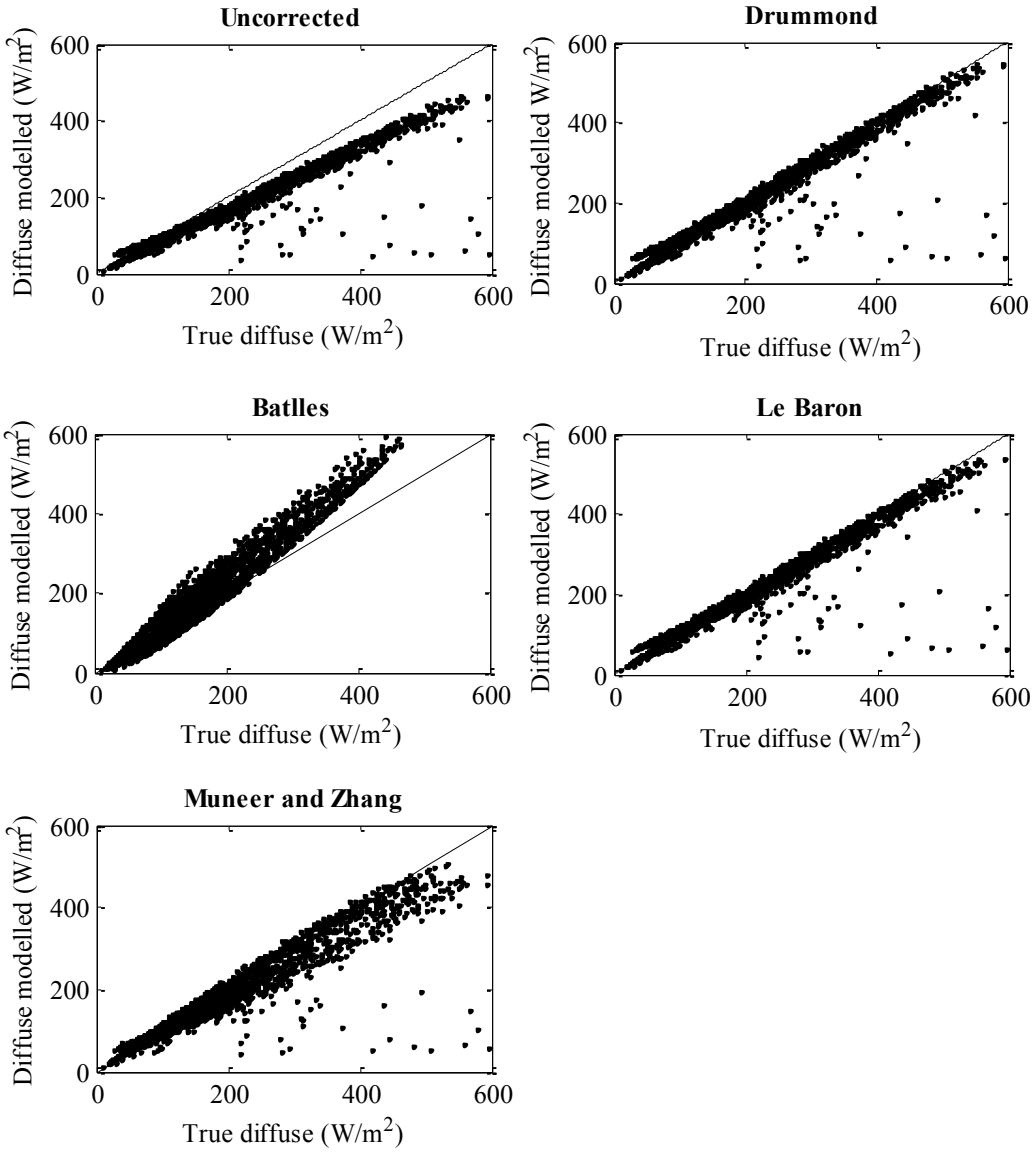

Fig. 4-15 Shadow band correction models implemented on data from Howard College. The plot of the uncorrected and filtered data shows a large deviation between the measured and modeled diffuse irradiance.

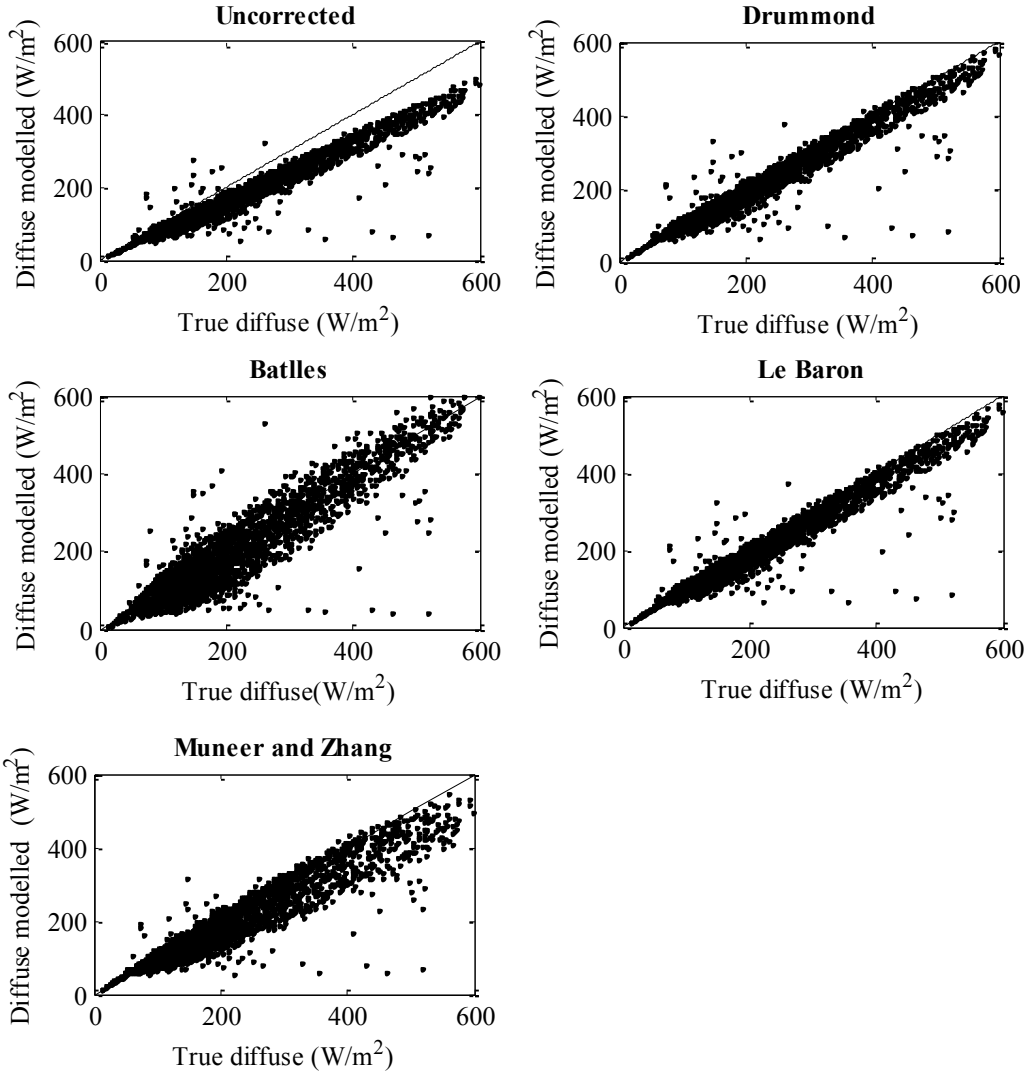

Fig. 4-16 Shadow band correction models implemented on data from Mangosuthu University of Technology data. The plot of the uncorrected and filtered data shows a distinct deviation between the measured and modeled diffuse irradiance.

The results from Table 4-6 (all sky conditions) show an improvement from the uncorrected diffuse irradiance as there is a reduction in MBE and RMSE. The coefficient of variation increases signifying better correlation when the models are used. We would expect the three models by Batlles et al. [26], Le Baron et al. [25] and Muneer and Zhang [27] to perform better for all sky conditions as they represent anisotropic skies. However, the model by Drummond [24] performs better at both the STARlab and Howard College stations. Lower MBE and RMSE of 3.16 W/m^2 (1.61%) and 49.7 W/m^2 (25.4%) respectively are reported for Howard College and similarly for

STARlab, MBE and RMSE are calculated to be 12.1 W/m^2 (5.50%) and 35.3 W/m^2 (16.1%) respectively . The high performance of an isotropic model (Drummond [24]) could be that of the data collected from the two stations during the period May 2010 to April 2011, a higher percentage represents overcast to cloudy and partly cloudy conditions (65.7% for STARlab and 68.0% for Howard College respectively). From the statement mentioned, an isotropic model would perform better for these conditions. Of the three anisotropic models, the model by Le Baron et al. [25] performs the best with an MBE of 5.76 W/m^2 (2.94%) and a corresponding RMSE of 50.0 W/m^2 (25.5%) for the Howard College station. The model by Le Baron et al. [25] model has the highest coefficient of determination value of 0.837 that signifies better correlation between measured and modeled values as compared to the models by Batlles et al. [26] and Muneer and Zhang [27] with reported values of 0.779 and 0.795 respectively. Similarly, for the MUT station, the model by Le Baron et al. [25] is the better performer of the anisotropic models. The MBE is calculated as 14.9 W/m^2 (6.78%) with an RMSE of 36.5 W/m^2 (16.6%). The coefficient of determination calculated for the Le Baron et al. [25] model was 0.912 compared to values of 0.824 and 0.833 reported for the models by Batlles et al. [26] and Muneer and Zhang [27] respectively.

Table 4-6 Model performance for all sky conditions using shadow band correction models

Station	Model	R^2	MBE (W/m^2)	MBE %	RMSE (W/m^2)	RMSE %
HC	Uncorrected	0.766	32.3	16.5	61.9	31.6
	Drummond	0.839	3.16	1.61	49.7	25.4
	Batlles	0.779	6.02	3.07	58.2	29.7
	Le Baron	0.837	5.76	2.94	50.0	25.5
	Muneer	0.795	13.9	7.14	56.1	28.6
MUT	Uncorrected	0.801	43.4	19.8	58.3	26.6
	Drummond	0.918	12.1	5.50	35.3	16.1
	Batlles	0.824	12.6	5.75	51.8	23.6
	Le Baron	0.912	14.9	6.78	36.5	16.6
	Muneer	0.833	24.5	11.2	50.4	23.0

From Table 4-7 (cloudy and partly cloudy sky conditions) we would expect the model by Drummond [24] to perform better as diffuse radiation is known to be isotropic for cloudy-partly cloudy conditions. An isotropic sky is assumed to be uniformly cast by clouds, a principle on which

the model by Drummond [24] was founded. However the model only performs well for STARlab. This could be due to the fact that STARlab is located close to industrial activity which could cause filtration of the air. The anisotropic nature of the other three models have a minor effect on the calculated MBE and RMSE. However, again the model by Le Baron et al. [25] gives the best results followed by the models by Drummond [24], Muneer and Zhang [27] and Batlles et al. [26] in order of decreasing performance for the Howard College station.

Table 4-7 Model performance for cloudy and partly cloudy conditions as defined by the Batlles criterion [26], when $k_t < k_{tt}$ and $k^{true} > k_k$.

Station	Model	R^2	MBE (W/m^2)	MBE %	RMSE (W/m^2)	RMSE %
HC	Uncorrected	0.731	40.3	17.8	72.7	32.1
	Drummond	0.809	7.27	3.21	58.7	25.9
	Batlles	0.749	2.01	0.89	67.2	29.6
	Le Baron	0.810	4.25	1.88	58.5	25.8
	Muneer	0.762	14.3	6.33	65.4	28.9
MUT	Uncorrected	0.804	45.6	18.1	63.3	25.2
	Drummond	0.923	8.99	3.57	37.7	15.0
	Batlles	-0.338	-121	-47.9	157	62.3
	Le Baron	0.916	13.5	5.34	39.4	15.7
	Muneer	0.852	17.9	7.12	5.22	20.7

Table 4-8 (clear skies) shows the anisotropic model by Le Baron et al. [25] as the top performer at Howard College whist that by Drummond performs well at STARlab. The differences between the performances of models at the two locations can be assumed to emanate from the immediate human activity nearby the stations, shading and the cloud field distribution over the radiometric stations. Reported values of MBE at Howard College are -3.65 W/m^2 (-2.78%) with an RMSE of 19.9 W/m^2 (15.2%) from the Le Baron et al. model. Similarly for STARlab, reported values of MBE and RMSE at Howard College are 6.60 W/m^2 (4.17%) and 18.4 W/m^2 (11.6%) respectively from the Drummond [24] model. Based on the variance between the measured and modeled data (R^2), the models by Muneer and Zhang [27] and Batlles et al. [26] do not improve the uncorrected data as lower R^2 values of 0.380 and 0.164 are reported for Muneer and Zhang [27] and Batlles et al. [26] respectively. In this sky category, anisotropic models are expected to perform better than isotropic

models as clear skies are typically anisotropic. On this note, the model by Drummond [24] is expected to be the worst performer. However, the model by Batlles et al. [26] is the worst performer at both stations with an MBE of 16.5 W/m^2 (12.6) and RMSE of 31.5 W/m^2 (24.0%) for the Howard College station and similarly, MBE of 38.9 W/m^2 (24.6) and RMSE were calculated as 54.4 W/m^2 (34.4%) for the MUT station. Similar trends are observed for models by Batlles et al. [26] and Muneer and Zhang [27] for both STARlab and Howard College. For this work, all DHI measurements are corrected for the shadowband effect with the model by Le Baron et al. [25].

Table 4-8 Model performance for clear sky conditions as defined by the Batlles criterion [26], when $k_t > k_{tt}$ and $k^{true} < k_k$.

Station	Model	R^2	MBE (W/m^2)	MBE %	RMSE (W/m^2)	RMSE %
HC	Uncorrected	0.793	15.1	11.5	27.3	20.9
	Drummond	0.881	-5.55	-4.24	20.1	15.3
	Batlles	0.707	16.5	12.6	31.5	24.0
	Le Baron	0.883	-3.65	-2.78	19.9	15.2
	Muneer	0.785	13.2	10.0	27.0	20.6
MUT	Uncorrected	0.555	14.5	9.13	28.9	18.3
	Drummond	0.741	6.60	4.17	18.4	11.6
	Batlles	0.164	38.9	24.6	54.4	34.4
	Le Baron	0.719	19.8	12.5	31.6	20.0
	Muneer	0.380	36.8	23.3	46.9	29.7

Stations comprising the GRADRAD network are intended to measure all three components of solar radiation separately. This allows for redundancy in the measured quantities. Figure 4-17 and Fig. 4-18 illustrate this property for all three irradiance components. It should be noted that from this point onwards, all diffuse horizontal irradiances are subject to correction by the model of Le Baron et al. [25]. After correcting the measured DHI (measured by a shaded pyranometer) by the model of Le Baron et al. [25], better agreement is observed for the measured and calculated irradiance values.

Table 4-9 is a statistical analysis to quantify the difference between the model-corrected component and the direct measured values for all three components (GHI, DNI and DHI). The table shows that GHI measurements can be estimated with a percentage of 96.9 and 98.1 for Howard College and STARlab respectively. Higher MBE and RMSE are however observed for the diffuse irradiance

component for both stations. This is largely due to the fact that this component relies heavily on a correction factor by existing models. The magnitude of DHI depends on the sky condition. For clear skies, DNI is the dominant factor contributing to the total radiation (GHI).

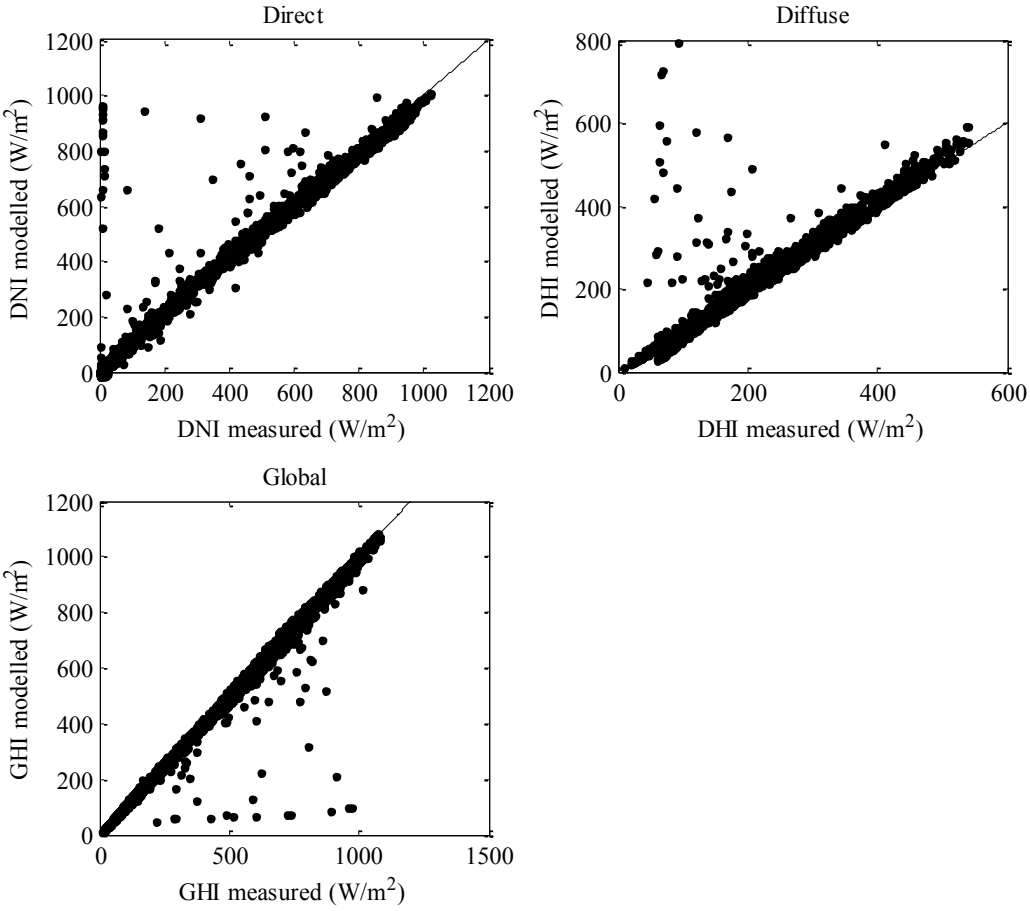

Fig. 4-17 A crosscheck of GHI, DHI and DNI for Howard College data. Measured values from the instruments are compared with calculated values using equation (1.1) after correction of the shadow band effect using the model by Le Baron et al. [25].

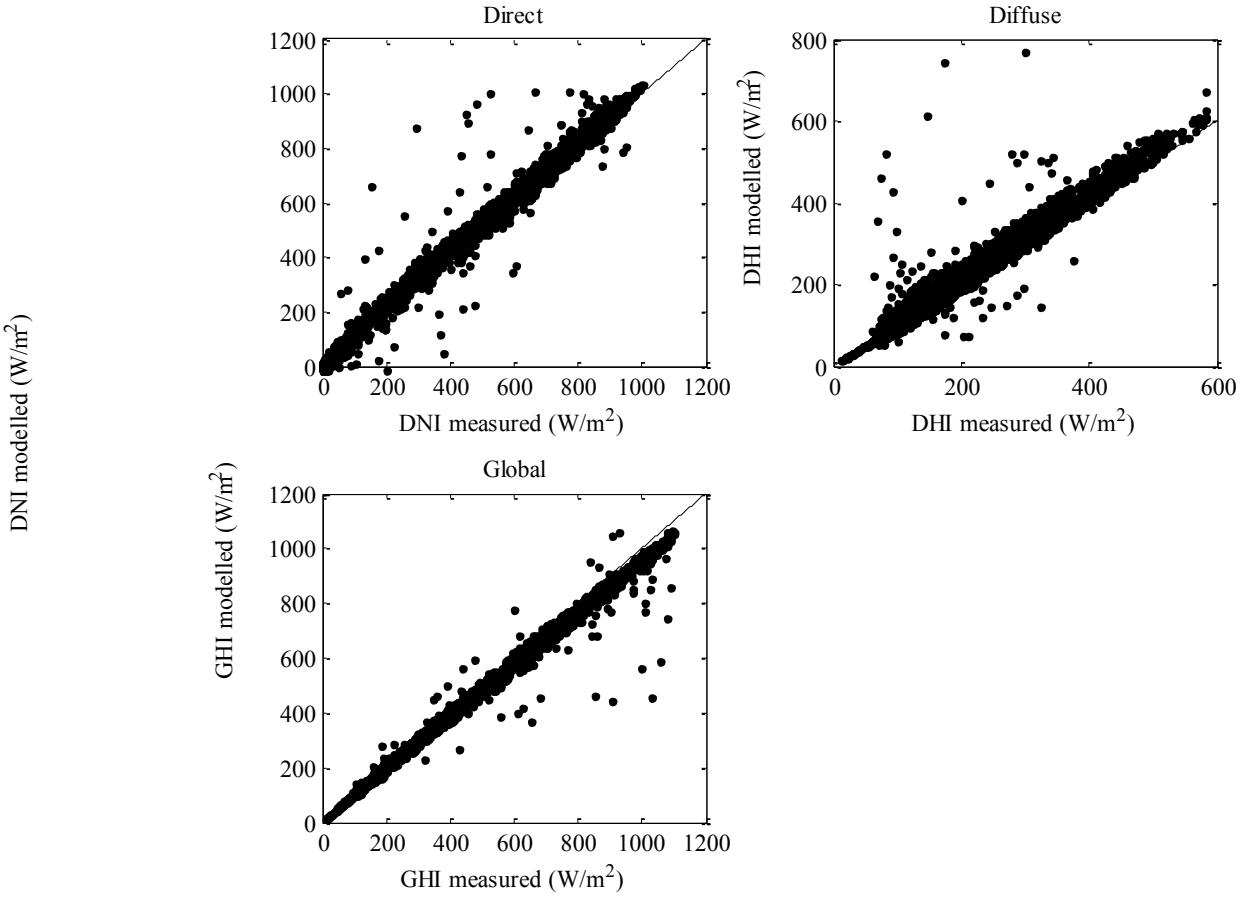

Fig. 4-18 A crosscheck of GHI, DHI and DNI for STARlab data. Measured values from the instruments are compared with calculated values using equation (1.1) after correction of the shadow band effect using the model by Le Baron et al. [25] for STARlab.

Table 4-9 Statistical analysis of direct measured irradiance values against model-corrected values.

Station	Model	R^2	MBE (W/m^2)	MBE %	RMSE (W/m^2)	RMSE %
HC	Global (GHI)	0.969	5.76	1.25	20.0	10.8
	Beam (DNI)	0.957	-7.85	-2.17	71.7	19.8
	Diffuse (DHI)	0.796	-5.76	-3.03	50.0	26.3
MUT	Global (GHI)	0.983	14.9	3..4	36.5	7.47
	Beam (DNI)	0.981	-17.8	-4.81	45.9	12.4
	Diffuse (DHI)	0.897	-14.9	-7.27	36.5	17.9

4.2.3 Comparison between measured direct normal data and predictive models

Due to the high cost of radiometric instruments, various mathematical models have been developed to estimate the missing component of irradiance as calculated from equation 1.1. Examples are those linking the diffuse fraction, k and the clearness index, k_t. Orgill and Hollands, Skartveit and Olseth, Reindl et al. and Boland et al. [29, 33, 31, and 32] established hourly correlations between the diffuse fraction, k and clearness index, k_t under diverse climatic conditions. In [29], [31] and [33], the data were split into regions defined for different values of the clearness index before attempting any regression. Boland et al. [32] constructed a continuous model for the whole range of the clearness index, that is, from zero (fully overcast) to unity (clear sky). They showed that this empirical relationship does not require splitting the clearness interval into three sub intervals as done by the other authors (Fig. 4-19). This allows for greater flexibility for altering the relationship to cater for location differences [60]. Using this proposed model, they showed that it can be adopted for 15 minute data as well as hourly data as experimental validation showed similarity. Figure 4-19 is an illustration of the clearness index split into three different regions that describe the condition of the sky: overcast, partly cloudy and clear.

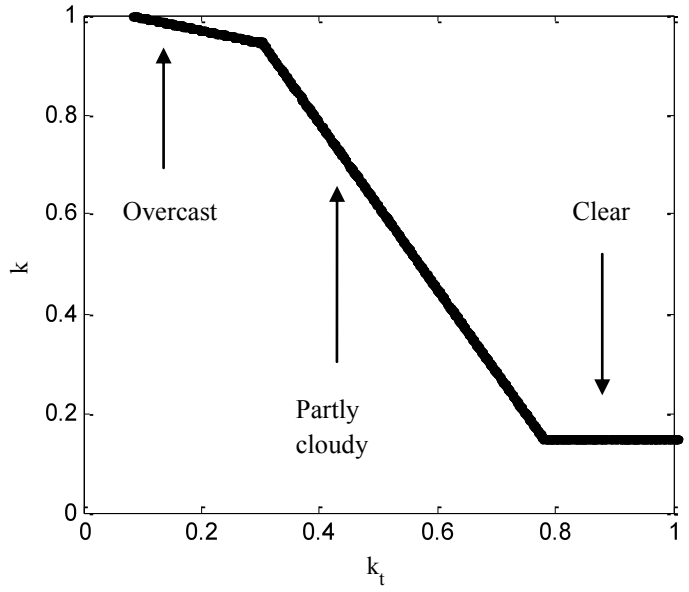

Fig. 4-19 Splitting the clearness index into three sub-regions: overcast, partly cloudy and clear skies using a correlation between diffuse fraction and clearness index.

Measurement of the direct normal irradiance is relatively accurate especially when measured through a single instrument [16] as this method eliminates embedded errors associated with the other instruments measuring the global and diffuse components. When the direct irradiance is estimated as the „missing" component, the closure equation 1.1 can be used for stations that have the radiometric scheme of PSP (shaded) + PSP (unshaded).

A review on how the beam irradiance is calculated is given below: As shown by Myers [5], beam irradiance can be estimated in two ways:

1) Modelling from first principles. Atmospheric data such as ozone, aerosol depth and water vapour are used as inputs in the models. Such an approach is highly specialised and complex and will not be reviewed in this work. An example is the fast atmospheric signature code (FASCODE) [28].
2) Modelling from conversion models to convert existing hemispherical data to direct irradiance. In other words, GHI or DHI is used to generate DNI through a mathematical model. This is achieved by developing relationships between the clearness index, k_t and the diffuse fraction, k. Parameters such as temperature, humidity, cloud cover, and solar altitude are used to augment the k-k_t correlation. These models are generally known as decomposition models. They are mainly used when atmospheric data such as water vapour, ozone, nitrogen, and weather data are not readily available. They are, however, quite often inaccurate as compared to spectral models that have atmospheric data as inputs. In this study, decomposition models have been implemented on data acquired at Howard College and STARlab to estimate the direct normal irradiance. DNI is obtainable from two measured components in the following way:

i) Measure GHI from an unshaded PSP
ii) Calculate the clearness index, k_t from equation 4.34
iii) Calculate the diffuse fraction, k from the model equations 4.37 to 4.60
iv) Calculate the DNI or I_b from equation 4.36

The models differ in the way the diffuse fraction is calculated in that some functions only use the clearness index as the determining parameter to obtain polynomial functions of various degree whilst others use the solar altitude to augment the clearness index. The modelled values are then compared with the directly measured DNI to quantify their accuracy. The estimation of the direct normal irradiance is derived below. Figure 4-20, Fig. 4-21 and Table 4-10 show these results. A

MATLAB codes is found in Appendix G for computation of the direct normal irradiance using models in Table 4-10.

The equation to estimate the direct normal irradiance is derived below from equation 1.1,

$$k_t = \frac{I_g}{I_0} \tag{4. 34}$$

where I_o is the extraterrestrial radiation for one hour given in equation 4.1. The diffuse fraction, k is defined as the ratio of the measured diffuse horizontal to the global horizontal irradiance,

$$k = \frac{I_g - I_b \cos\theta_Z}{I_g} \rightarrow I_g = \frac{I_d}{k} \tag{4.35}$$

Therefore, from equation 1.1, the beam irradiance, is given as

$$I_b = \frac{I_g(1-k)}{\cos\theta_z} \tag{4.36}$$

The selected models are listed in Table 4-10. The models proposed by Orgill and Hollands [30], Erbs et al. [29] and Reindl et al. [31] estimate the direct and diffuse irradiances by splitting the clearness index into different regimes. The second model developed by Reindl et al. [31] introduces the solar altitude as a new variable in the model. The model proposed by Skartveit and Olseth [33] estimate the irradiance from both the clearness index and solar elevation but the equations are more complex than Reindl [31]. The model by Boland et al. [32] is an empirical model that comprises a continuous function. A sample calculation is shown in Appendix H on how a data point is calculated using the model by Erbs et al. [29].

4.2.3.1 Orgill and Hollands (1977)

This correlation was developed from four years of data obtained at Toronto, Canada on a site located at high altitude, 43° West 48° North. The correlation is given below as:

$$k = 1.0 - 0.249k_t \quad when \;\; k_t < 0.35 \tag{4.37}$$

$$k = 1.577 - 1.84k_t \quad when \;\; 0.35 \leq k_t \leq 0.75 \tag{4.38}$$

$$k = 0.177 \quad when \;\; k_t > 0.75 \tag{4.39}$$

4.2.3.2 Erbs et al. (1982)

Erbs et al. [29] revised Orgill and Hollands' correlation [30] by using data at lower altitudes ranging from 31° to 42° North. By [29], altitude does have an influence on the mean daily diffuse radiation as high altitude locations exhibit dry air conditions and it is known that dry air is denser than moist air. As elevation increases, the average air mass increases with the air becoming denser. Air masses are determined by factors such as latitude, altitude, ocean currents, and sunshine hours to name a few. The database consisted of hourly pyrheliometer and global measurements of five United States stations from which the diffuse fraction was calculated as the difference of the two quantities. The correlation is given below as:

$$k = 1.0 - 0.098k_t \quad when \;\; k_t < 0.35 \qquad (4.40)$$

$$k = 0.9511 - 0.1604k_t + 4.388{k_t}^2 - 16.638{k_t}^3 + 12.336{k_t}^4 \quad when \;\; 0.35 \leq k_t \leq 0.75 \qquad (4.41)$$

$$k = 0.165 \quad when \;\; k_t > 0.75 \qquad (4.42)$$

4.2.3.3 Reindl-A (1990)

Two models using measurements from five stations in the United States and Europe of global and diffuse measurements on a horizontal surface were derived. The first model (referred to in the text as Reindl-A) estimates the diffuse fraction with the clearness index as the only input parameter whilst the second model (Reindl-B) has the clearness index and solar altitude as inputs. Reindl-A correlation is given as:

$$k = 1.020 - 0.248k_t \quad when \;\; k_t < 0.30 \qquad (4.43)$$

$$k = 1.450 - 1.670k_t \quad when \;\; 0.30 \leq k_t \leq 0.75 \qquad (4.44)$$

$$k = 0.147 \quad when \;\; k_t > 0.75 \qquad (4.45)$$

4.2.3.4 Reindl-B et al. (1990)

Reindl-B [31] correlation is given by the following equations where the solar altitude, α, is used to augment the clearness index:

$$k = 1.020 - 0.254k_t + 0.0123\sin(\alpha) \quad when \;\; k_t < 0.30 \; (4.53) \qquad (4.46)$$

$$k = 1.400 - 1.749k_t + 0.177\sin(\alpha) \quad when \;\; 0.30 \leq k_t \leq 0.78 \qquad (4.47)$$

$$k = 0.486k_t - 0.182\sin(\alpha) \quad when \;\; k_t > 0.75 \qquad (4.48)$$

4.2.3.5 Boland et al (2001)

Boland et al [32] constructed a simple exponential correlation using data from a location in Victoria, Australia.

$$k = \frac{1}{1+e^{7.997(k_t-0.586)}} \tag{4.49}$$

4.2.3.6 Skartveit and Olseth (1987)

The authors estimated direct irradiance from the solar elevation and the global irradiance using the equation:

$$I_b = I_g(1-\varphi)/\sin(\alpha) \tag{4.50}$$

If $k_t < k_0$

φ =1;

where

$k_0 = 0.2$

If $k_0 \le k_t \le 1.09k_1$

$$\varphi = 1-(1-d_1)(ak^{\frac{1}{2}} + (1-a)k^2) \tag{4.51}$$

where

$$k_1 = 0.87 - 0.56\exp(-0.06\alpha) \tag{4.52}$$

$$d_1 = 0.15 + 0.43\exp(-0.06\alpha) \tag{4.53}$$

and α is the solar altitude in degrees

a = 0.27

$$k = 0.5(1+\sin\left[\pi\left(\frac{a'}{b'}-0.5\right)\right]) \tag{4.54}$$

where

$$a' = k_t - k_0 \tag{4.55}$$

$$b' = k_1 - k_0 \tag{4.56}$$

If $k_t > 1.09k_t$

$$\varphi = 1-(1.09k_t(1-\xi)/k_t) \tag{4.57}$$

where

$$\xi = 1 - (1 - d_1)(ak'^{\frac{1}{2}} + (1 - a)k'^{2}) \quad (4.58)$$

where

$$k' = 0.5(1 + \sin\left[\pi\left(\frac{a''}{b'} - 0.5\right)\right]) \quad (4.59)$$

where

$$a'' = 1.09k_1 - k_0 \quad (4.60)$$

The graphical plots of Fig. 4-20 and Fig. 4-21 show that all six models slightly underestimate the direct beam irradiance as most of the data points lie below the 45° line for both Howard College and STARlab. It is likely that better results would have been achieved by using spectral models, where detailed information of the atmosphere is used as an input in determining the direct irradiance.

Statistical indicators such as the RMSE, MBE and R^2 were used to validate the performance of the selected six models by comparing model data with readings obtained at the ground stations. From Table 4-10, the models by Erbs et al. [29] and Reindl-A overestimate the DNI as negative values of MBE are reported for STARlab, where the error is defined as measured data minus model (the six prediction models) data. The estimation of DNI using equation 1.1 gives better results than the six implemented models. Better correlation between measured and modelled data is observed with a high R^2 value of 0.950 for the MUT station. Correspondingly, MBE values of -59.4 W/m^2 (-16.1%) with RMSE values of 74.3 W/m^2 (20.1%) account for DNI modeled from equation 1.1. However, for the Howard College station, none of the models seem to overestimate the DNI. Again, the DNI modelled from equation 1.1 gives better results. Calculated MBE values of -47.3 W/m^2 (-12.8%) with RMSE values of 88.1 W/m^2 (2.9%) are reported. The poor results of the models are seemingly due to the location dependence of the models to some extent. The location in which the models were derived is different from that of Durban. Different atmospheric conditions, seasons and radiation levels apply which could contribute to the results obtained. Further, no adjustments of regression constants in the models were performed to cater for location. The dependency is due to geographical location and the local atmospheric condition under which they were derived [61]. A better correlation would have been observed if a model of a site of similar geographical location and climate to that of Durban was used.

A new model was derived for both stations that better interprets the climatic conditions and solar radiation for Durban. This was achieved by using the Curve Fitting Toolbox in MATLAB (the results shown in section 4.2.4). A yearly equation was derived for STARlab and UKZN Howard College stations to better show correlation between the stations as they experience similar climate. The new model has the clearness index as the only defining parameter in estimating the diffuse fraction. By plotting the diffuse fraction against the clearness index for the filtered data from both stations, various polynomial curves were fit on the data set and the best was chosen. The model was refined by splitting the clearness index into three regions. These regions divide the sky into overcast, partly cloudy and clear conditions as done by other authors (Fig. 4-19). Detailed derivation of the model is found in section 4.2.4.

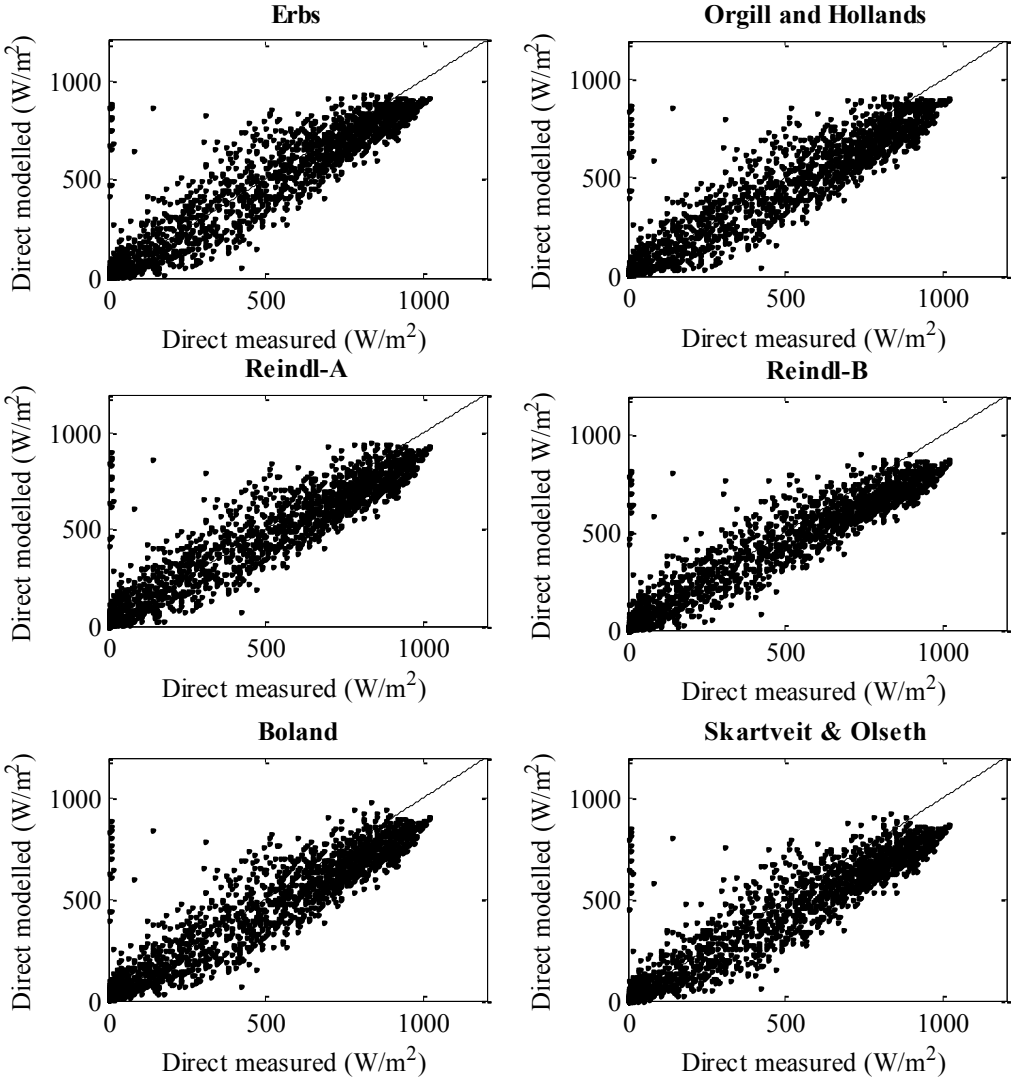

Fig. 4-20 Direct normal irradiance estimation using data from Howard College applying existing models by Erbs et al. [29], Orgill and Hollands [30], Reindl et al. [31], Boland et al. [32], and Skartveit and Olseth [33].

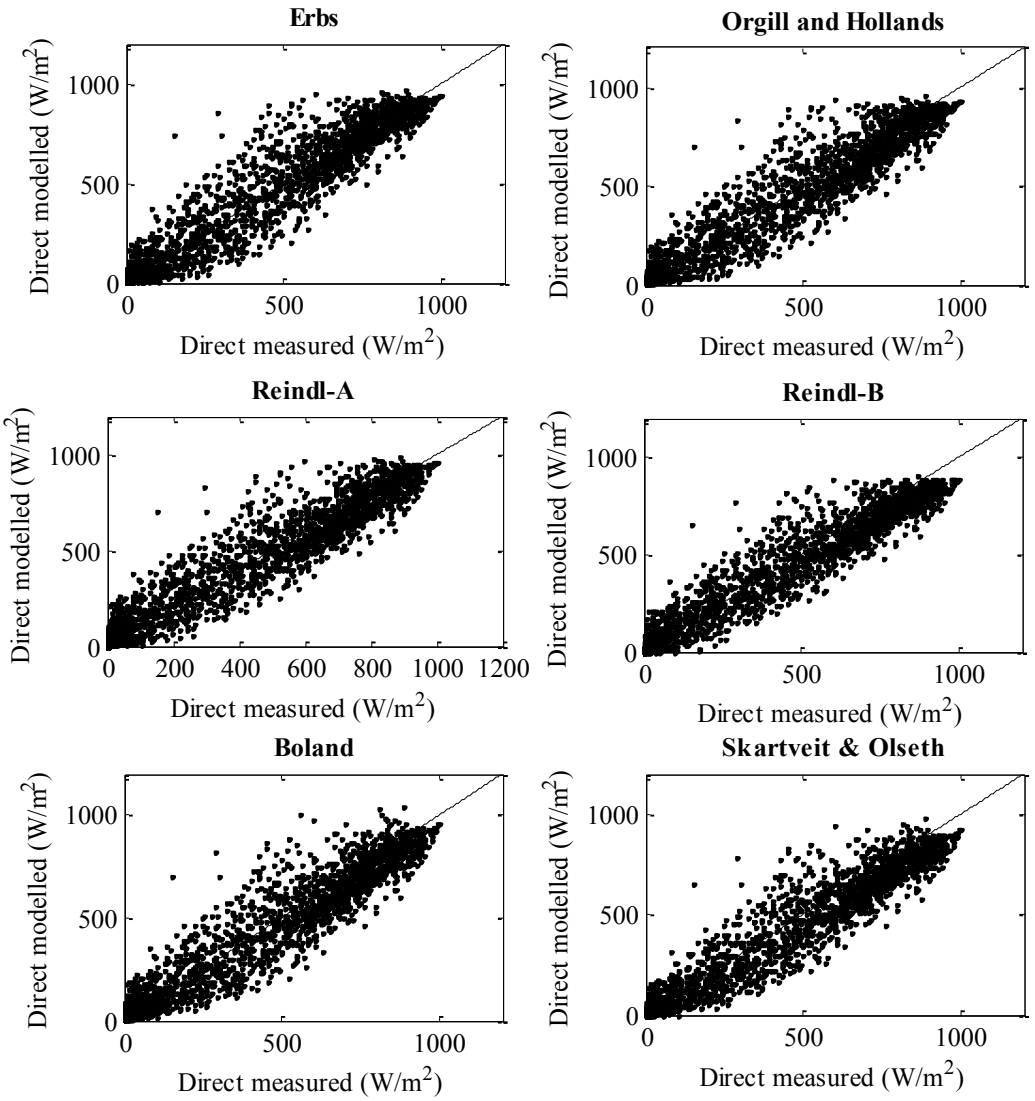

Fig. 4-21 Direct normal irradiance estimation using data from MUT applying existing models by Erbs et al. [29], Orgill and Hollands [30], Reindl et al. [31], Boland et al. [32], and Skartveit and Olseth [33].

Table 4-10 Beam estimation performance for all sky conditions, ranked in descending order of accuracy based on MBE and RMSE.

Station	Model	R^2	MBE (W/m^2)	MBE %	RMSE (W/m^2)	RMSE %
HC	Equation (1.1)	0.932	-47.3	-12.8	88.1	23.9
	Erbs	0.898	11.2	3.11	105	28.9
	Reindl-A	0.881	14.4	3.98	108	29.8
	Boland	0.872	23.4	6.45	110	30.4
	Orgill & Hollands	0.875	24.3	6.71	110	30.4
	Reindl-B	0.866	31.6	8.73	110	30.4
	Skartveit	0.854	41.7	11.5	115	31.8
MUT	Equation (1.1)	0.950	-59.4	-16.1	74.3	20.1
	Reindl-A	0.925	-4.87	-1.32	91.0	24.6
	Erbs	0.925	-6.08	-1.64	91.0	24.6
	Reindl-B	0.936	13.7	3.71	84.4	22.8
	Boland	0.924	5.22	1.41	91.5	24.7
	Skartveit	0.928	24.5	6.61	89.6	24.2
	Orgill & Hollands	0.925	6.21	1.68	91.3	24.7

4.2.4 Comparison of station data

This section contains an analysis of differences in recorded data between the UKZN HC and MUT stations for the period May 2010 to April 2011. The aim of this analysis is to establish possible differences in spatial variations due to climate effects which are known to exist for stations located a short distance apart [1]. In order to quantify possible differences in sun strength between UKZN Howard College and STARlab, data were analyzed using the radiometric models described in 4.2.3 and a direct comparison of measured radiation for each site was undertaken, as follows:

1. The models proposed by Erbs et al. [29], Orgill and Hollands [30], Reindl et al. [31], Boland et al. [32], and Skartveit and Olseth [33], were used to establish the profile for each station separately.

2. By summing the measured irradiance data at each station, a comparison of solar radiation data was obtained. To ensure the validity of the analysis, all days in which measurements were missing were excluded. This eliminates days for example, at Howard College, where there is no consistency in measured data due to the lack of an uninterruptible power supply. A total of 2183 hourly irradiance values satisfied this condition. Total irradiation gathered at the stations was calculated for all three components of solar radiation. These were given as $\sum I_g$, $\sum I_d$, $\sum I_b$ and measured in kJ/m^{2}h for GHI, DHI and DNI respectively. As discussed in Chapter 1, the instrument difference on measuring GHI was calculated to be 1.36% for a clear day 23 July 2010. Therefore, only a comparison of total irradiation can be made between stations on the above-identified number of days. A summary of the results is given in Table 4-11.

The results reported in section 4.2.3 showed that the predictive models by Erbs et al. [29], Orgill and Hollands [30], Reindl et al. [31], Boland et al. [32], and Skartveit and Olseth [33] are location dependent to some extent when applied to HC and MUT. This is because no alterations were made for regression constants obtained where the models were derived. An investigation was carried out to derive models for HC and MUT that better suit Durban. Upon plotting the diffuse fraction, k versus the clearness index, the curve fitting toolbox in MATLAB was used to fit a polynomial function on the cleaned data. Figure 4-22 and Fig. 4-23 show the resulting relationship between diffuse fraction, k and the clearness index, k_t of filtered data on both stations. Low clearness index values have corresponding high diffuse fraction values. This means that, for example, a cloudy sky (characteristic of a low clearness index) has a high diffuse fraction (a ratio of DHI to GHI) as the sky is predominantly diffuse and covered by clouds. Similarly, for clear skies, the dominating factor is DNI when high clearness indices persist. Other factors such as cloud cover and solar altitude can be used to augment the clearness index. Following this ideology, the solar altitude angle (complement of the solar zenith angle) was used.

Figure 4-24 is a plot of the solar altitude versus the clearness index. The figure shows that no relationship seems to exist between the two parameters. The result is similar to the work by Boland et al. [32]. The results show that the solar altitude cannot be used as the sole variable linking k and k_t. Other parameters such as cloud cover, temperature and humidity should be used in conjunction with the solar altitude in augmenting the clearness index.

In deriving yearly equations for either station, polynomial functions of second, third and fourth degrees were fitted to observe which best fits the data from either station (Fig. 4-25 to Fig. 4-30 for Howard College and STARlab respectively). Table 4-11 is a summary of the statistics of the various polynomial orders investigated. This aids in selecting the best polynomial based on both graphical and statistical performance. The fourth degree polynomial function best fits the datasets for both HC and MUT with observed lower values of the coefficient of determination R^2 signifying better correlation between measured and modeled values. The equations of the fourth degree polynomial are given by equations (4.61) and (4.62) for HC and MUT respectively.

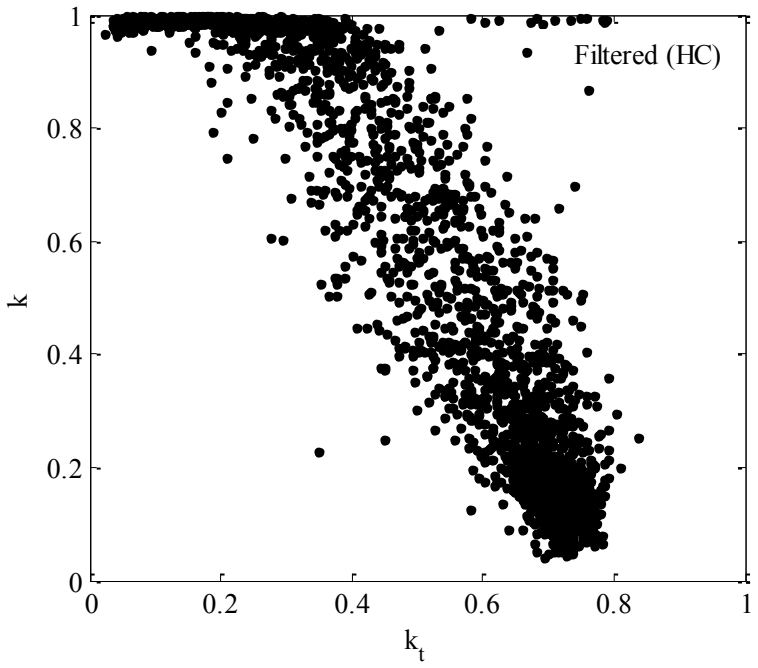

Fig. 4-22 Filtered data from UKZN Howard College station after the removal of outliers.

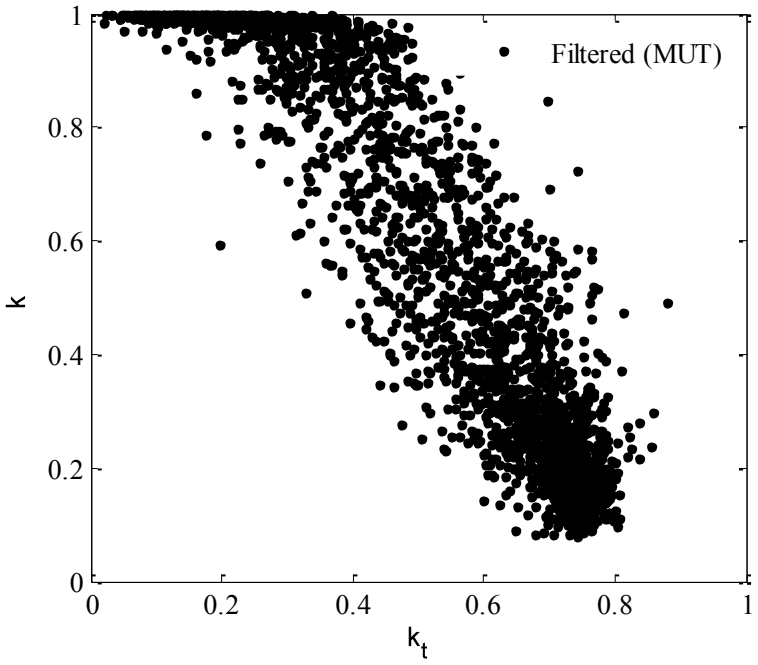

Fig. 4-23 Filtered data from STARlab after the removal of outliers.

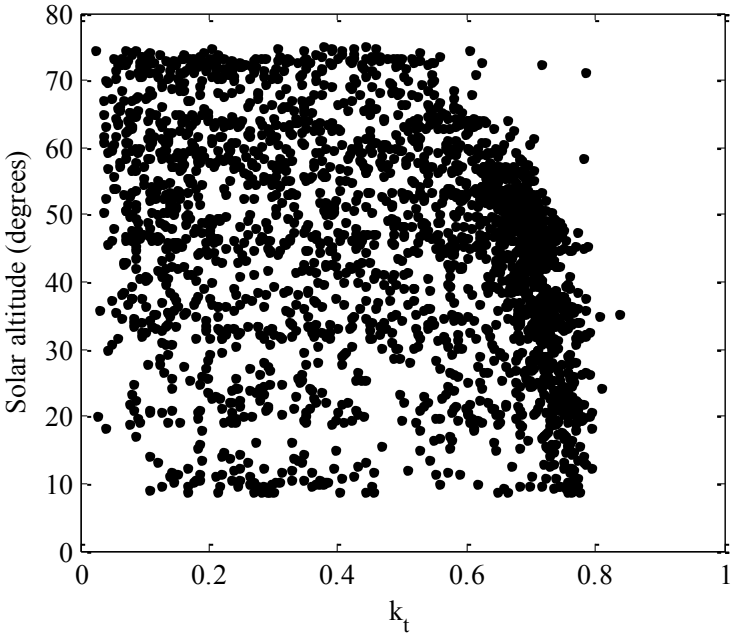

Fig. 4-24 Solar altitude versus clearness index.

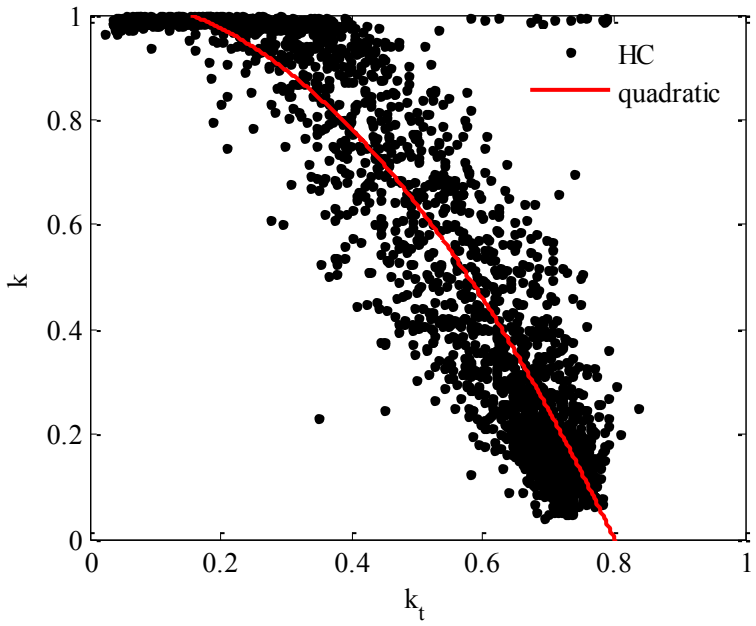

Fig. 4-25 A quadratic fit onto UKZN Howard College data using the curve fitting tool in MATLAB.

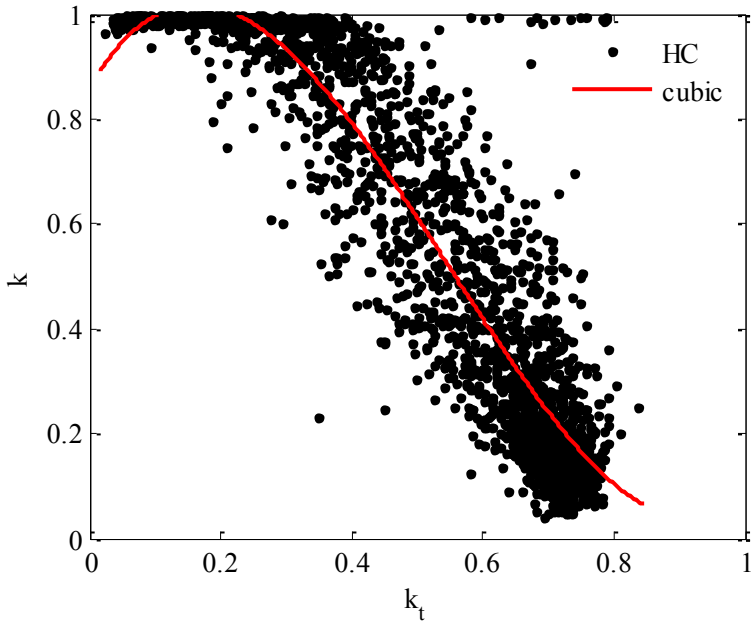

Fig. 4-26 A cubic fit onto UKZN Howard College data using the curve fitting tool in MATLAB.

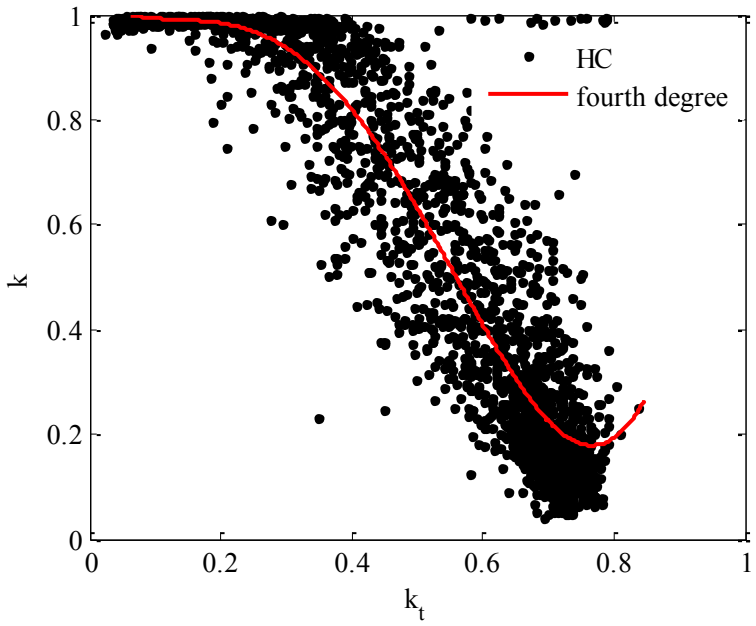

Fig. 4-27 A fourth degree polynomial fit onto HC data using the curve fitting tool in MATLAB.

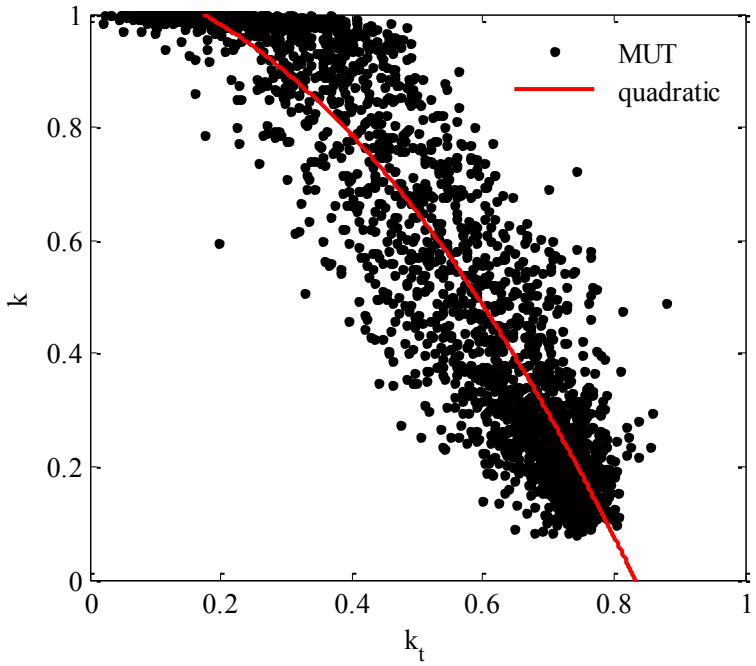

Fig. 4-28 A quadratic fit onto STARlab data using the curve fitting tool in MATLAB.

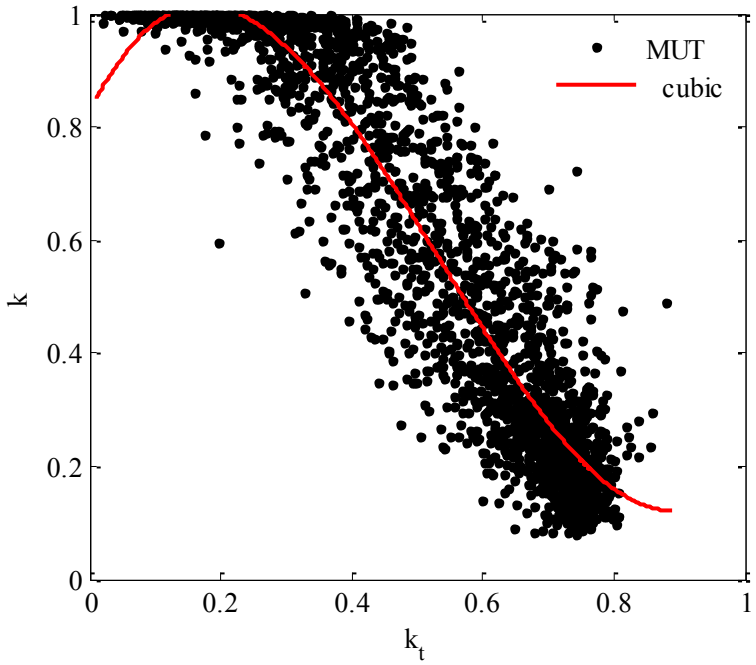

Fig. 4-29 A cubic fit onto STARlab data using the curve fitting tool in MATLAB.

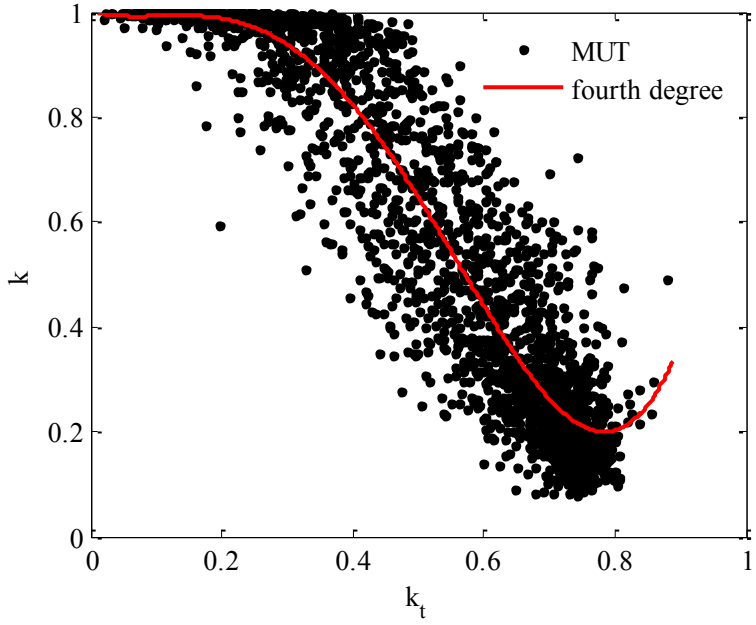

Fig. 4-30 A fourth degree polynomial fit onto STARlab data using the curve fitting tool in MATLAB.

Table 4-11 Statistical analysis of various polynomial degrees for HC and MUT.

Polynomial	Howard College		STARlab	
	SSE (W/m^2)	R^2	SSE (W/m^2)	R^2
2nd	41.1	0.863	37.0	0.869
3rd	38.4	0.872	33.3	0.882
4th	37.2	0.876	32.5	0.884

From the above statistical analysis and graphical display of the plots, equations 4.61 and 4.62 were obtained for each station. Both equations are fourth degree functions predicted within a 95% confidence interval in MATLAB using the Curve Fitting Toolbox. The fourth degree polynomial equations give a better fit between the diffuse fraction, k and the clearness index, k_t for both the Howard College and MUT station.

The following equation was obtained for Howard College,

$$k = 14.99{k_t}^4 - 20.77{k_t}^3 + 6.852{k_t}^2 - 0.9157k_t + 1.036 \qquad (4.61)$$

and that for STARlab is given by:

$$k = 11.33{k_t}^4 - 15.05{k_t}^3 + 3.684{k_t}^2 - 0.3575k_t + 1.003 \qquad (4.62)$$

Assuming a single fitting equation for the whole range of the clearness index poses overestimations or underestimations of the diffuse fraction on certain intervals. A new approach was performed which is similar to the work of Erbs et al. [29], Orgill and Hollands [30] and Reindl et al. [31]. In these cases, the clearness index intervals are divided into three regions (Fig. 4-19).

Based on the dataset of each station, the clearness index was divided into three regions, that is, overcast, partly cloudy and clear skies based on the changing gradient of the fourth degree polynomial obtained along the region of the clearness index. The point at which there is a gradient change marks the end of a sky category and the progression into a new sky condition. For example, for the Howard College station, a gradient change occurred at 0.2 and 0.75 along the axis of the clearness index. The two values obtained divide the clearness index into three regions, given by

$0 < k_t < 0.20$ representing overcast skies,

$0.15 \leq k_t \leq 0.75$ representing partly cloudy skies, and

$k_t > 0.75$ representing clear skies.

Upon determining the three categories above, the data set for the Howard College station was further divided into these divisions of the clearness index. All hourly irradiance values for clearness indices less than 0.20 were grouped together. The same applied for hourly irradiance values for regions representing partly cloudy skies and clear skies. Again, polynomial functions of various orders were applied to the data set for each of the three sky conditions using the Curve fitting toolbox in MATLAB, and the best fit polynomial was chosen for each category. The same methodology was applied to the MUT dataset. The models obtained are shown in equations 4.63 to 4.68. Implementing the new approach that defines an equation for each sub-interval, the yearly curve was modified and presented as follows: the correlation for Howard College is

$$k = 0.982 \qquad when \;\; k_t < 0.2 \tag{4.63}$$

$$k = 0.8081 + 1.653k_t - 3.247{k_t}^2 - 4.364{k_t}^3 + 5.613{k_t}^4 \qquad when \;\; 0.20 \leq k_t \leq 0.75 \tag{4.64}$$

$$k = 0.156 \qquad when \;\; k_t > 0.75 \tag{4.65}$$

and the correlation for STARlab is given as:

$$k = 0.982 \qquad when \;\; k_t < 0.20 \tag{4.66}$$

$$k = 0.7433 + 2.266 - 5.266 - 1.449{k_t}^3 + 4.22{k_t}^4 \qquad when \;\; 0.20 \leq k_t \leq 0.76 \tag{4.67}$$

$$k = 0.196 \qquad when \;\; k_t > 0.79 \tag{4.68}$$

With the current emphasis on determining spatial variations in sun strength, data from each station were categorized into two seasons: winter and summer that best describe the weather of the KwaZulu-Natal province. The cold season is defined from April to October whilst the warm season is defined from November to March. This division of data was performed to establish whether the variation in sun strength is seasonally dependent [32] and [7] .The equations derived for the summer season at Howard College are

$$k = 0.981 \qquad when \;\; k_t < 0.20 \tag{4.69}$$

$$k = 0.651 + 2.348k_t - 7.273{k_t}^2 + 4.311{k_t}^3 \qquad when \;\; 0.20 \leq k_t \leq 0.76 \tag{4.70}$$

$$k = 0.15 \qquad when \;\; k_t > 0.76 \tag{4.71}$$

and for STARlab

$$k = 0.85 \quad when \quad k_t < 0.20 \tag{4.72}$$

$$k = 0.7117 + 2.886k_t - 8.476{k_t}^2 + 5.033{k_t}^3 \quad when \quad 0.20 \leq k_t \leq 0.80 \tag{4.73}$$

$$k = 0.175 \quad when \quad k_t > 0.80 \tag{4.74}$$

Similarly, for the winter season equations derived for Howard College are,

$$k = 0.9865 \quad when \quad k_t < 0.20 \tag{4.75}$$

$$k = 0.7732 + 2.364k_t - 6.917{k_t}^2 + 1.824{k_t}^3 + 3.292{k_t}^4 \quad when \quad 0.20 \leq k_t \leq 0.77 \tag{4.76}$$

$$k = 0.132 \quad when \quad k_t > 0.77 \tag{4.77}$$

And for STARlab,

$$k = 0.98 \quad when \quad k_t < 0.2 \tag{4.78}$$

$$k = 0.8984 + 0.6657k_t + 0.2863{k_t}^2 - 9.785{k_t}^3 + 8.712{k_t}^4 \quad when \quad 0.20 \leq k_t \leq 0.77 \tag{4.79}$$

$$k = 0.175 \quad when \quad k_t > 0.77 \tag{4.80}$$

For comparison purposes, the derived yearly curves for each station (representing different sky conditions) were drawn together with the experimental seasonal curves obtained for summer and winter (Fig. 4-31 and Fig. 4-32). The yearly curve lies in between the seasonal curves strengthening the assertion of seasonal dependence as shown in earlier work by Jacovides et al. [7] and De Miguel et al. [62]. This implies that the use of a yearly equation for a dataset of a location could underestimate irradiance in winter months for low values of the clearness index as clouds are the regulating factor for diffuse skies. Similarly, for high clearness indices (summer months with high solar intensities), the use of one yearly equation can underestimate radiation for the summer period. Figure 4-31 and Fig. 4-32 suggests that using separate equations to estimate irradiance patterns for summer and winter can give better results as the figure illustrates seasonal dependence of solar irradiance.

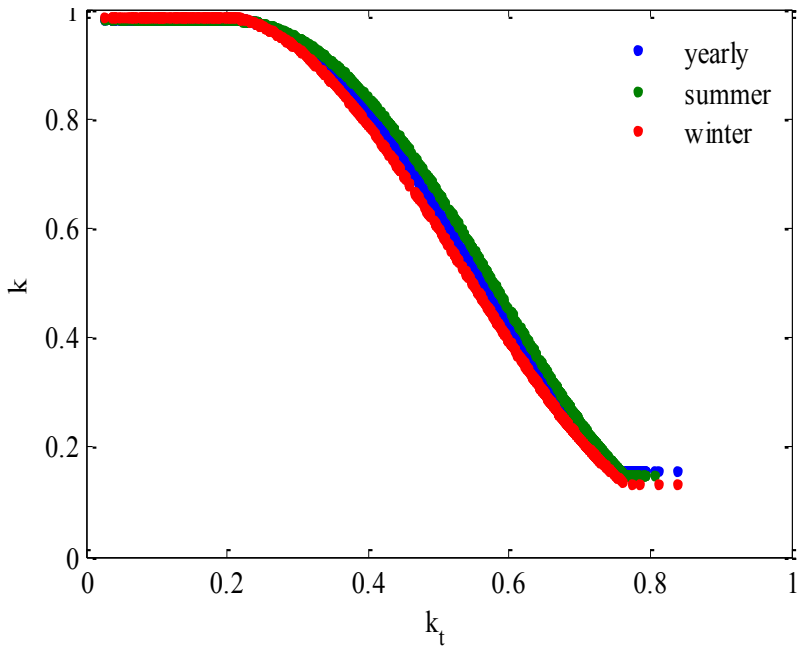

Fig. 4-31 Seasonal dependence of solar radiation at the Howard College station.

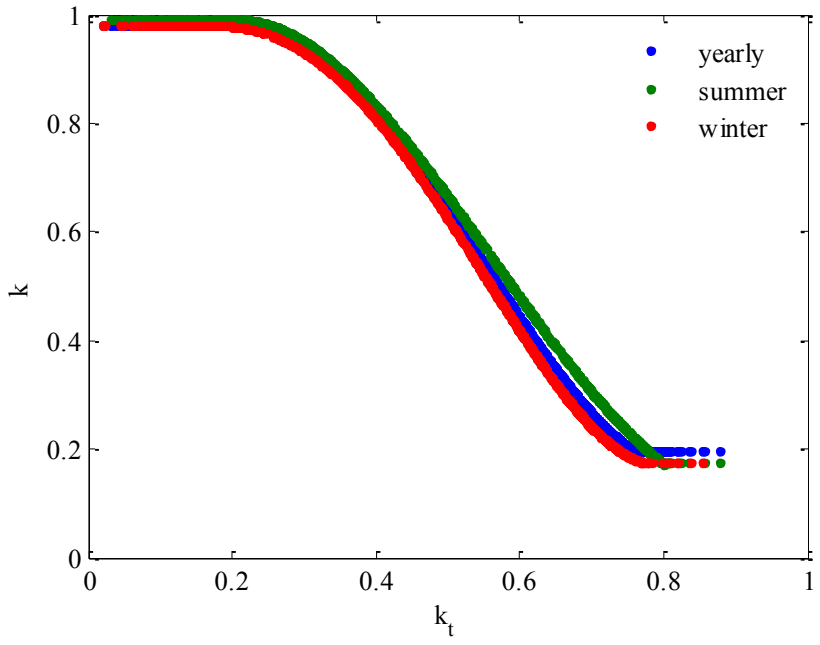

Fig. 4-32 Seasonal dependence of solar radiation at the STARlab station.

The attempt to quantify spatial variations due to micro-climate effects between Howard College and STARlab are illustrated in Fig. 4-33 to Fig. 4-38 and Table 4-12. Hourly filtered data for twelve months were used for each station. The diffuse fraction for each of the six selected models was calculated from equation 4.37 to equation 4.60, as described in section 4.2.3. The diffuse fraction was plotted against the clearness index to observe the relationship of the two parameters. By displaying similar plots for either station, a comparison can be made for any differences between the Howard College and MUT stations to quantify any spatial variations in sun strength. Figure 4-33 to Fig. 4-38 show similar trends of smooth profiles of the dataset between plots of the clearness index and diffuse for each the six models investigated. However, scattering is observed in the Reindl-B [31] and the Skartveit and Olseth [33] models. The scatter is assumed to emanate from the use of the solar altitude in an attempt to augment the clearness index thus improving the accuracy in the calculation of the diffuse fraction. The use of a moving average is suggested to be used to obtain a smooth profile and clearly distinguish the relation between the clearness index and the diffuse fraction. On comparing the two models by Reindl et al. [31] (Reindl-A and Reindl-B), the second model is observed to perform better. Table 4-10 verifies the improvement of results for the MUT station when the solar altitude (the complement to the solar zenith angle) is used to augment the clearness index. The Reindl-B model is reported with an increased R^2 value of 0.936 compared to 0.925 obtained from Reindl-A. Reduced root mean square differences of 84.4 W/m^2 (22.8%) as compared to the former model (Reindl-A) where calculated RMSE was 91.0 W/m^2 (24.6%).

Table 4-12 is a quantitative approach to establish spatial differences between MUT and HC. As earlier shown in Chapter 2, the percentage difference between instruments of HC and MUT was reported to be 1.36% based on measurements of GHI. What is to be established is whether the difference increases when instruments are run separately at different locations. When the instruments were run separately at both station, a difference of 0.72% in the GHI was calculated (Table 4-12). No comparison of the DNI and DHI can be made to very potential microclimate effects between HC and MUT as instruments measuring these components were not run at one location.

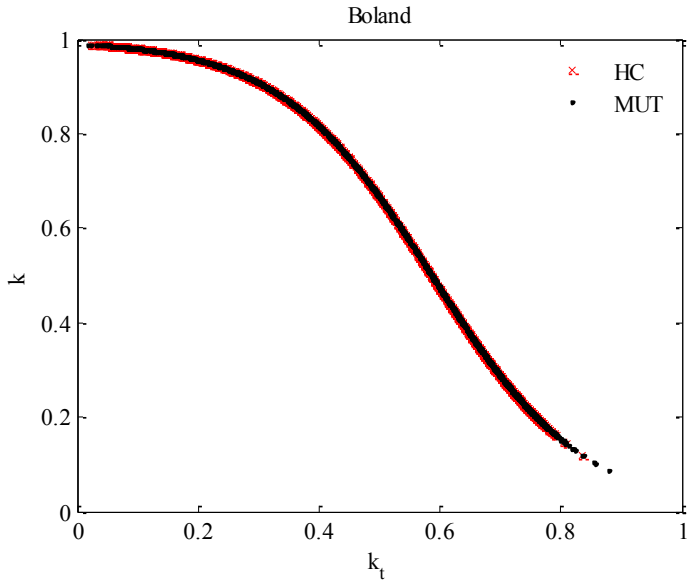

Fig. 4-33 An inter-comparison of the relationship of the diffuse fraction versus the clearness index between Howard College station and the STARlab station to verify spatial variations using the model by Boland et al. [32].

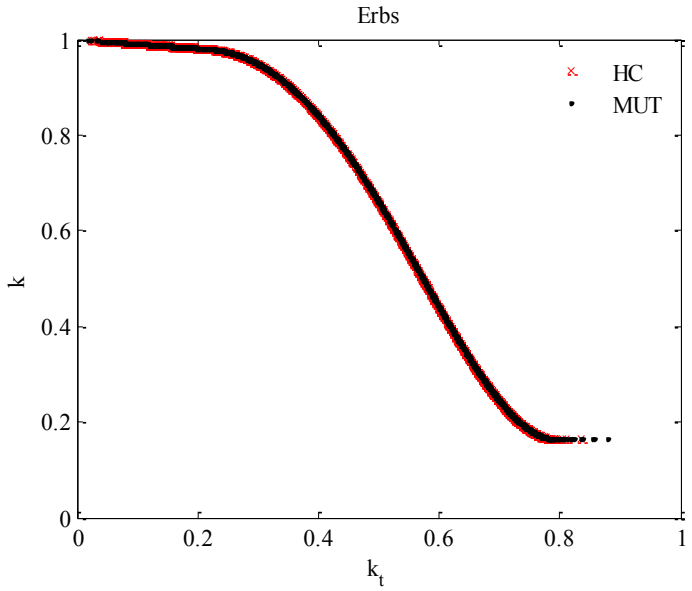

Fig. 4-34 An inter-comparison of the relationship of the diffuse fraction versus the clearness index between Howard College station and the STARlab station to verify spatial variations using the model by Erbs et al. [29].

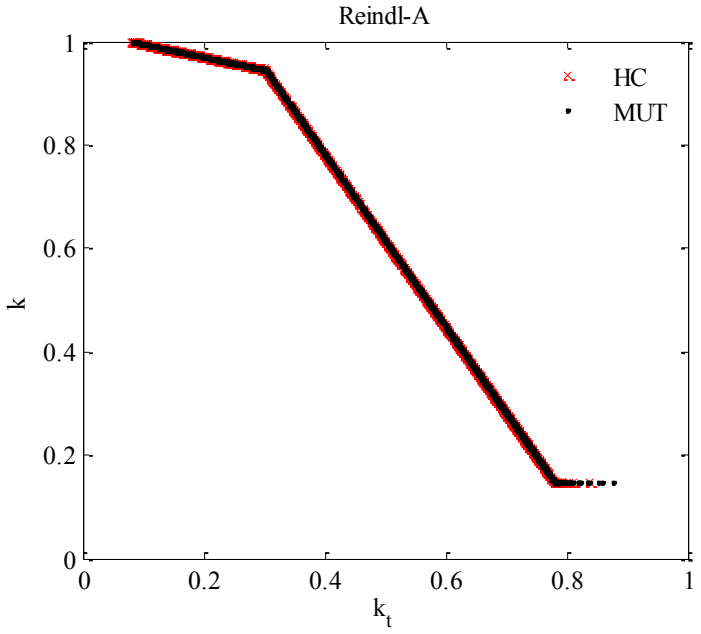

Fig. 4-35 An inter-comparison of the relationship of the diffuse fraction versus the clearness index between Howard College station and the STARlab station to verify spatial variations using the Reindl-A model [31].

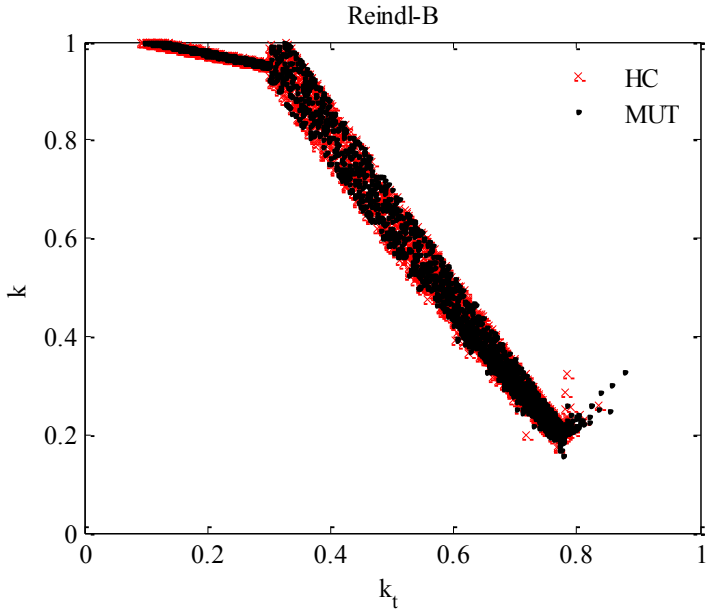

Fig. 4-36 An inter-comparison of the diffuse fraction versus the clearness index between Howard College station and the STARlab station using the Reindl-B model [31].

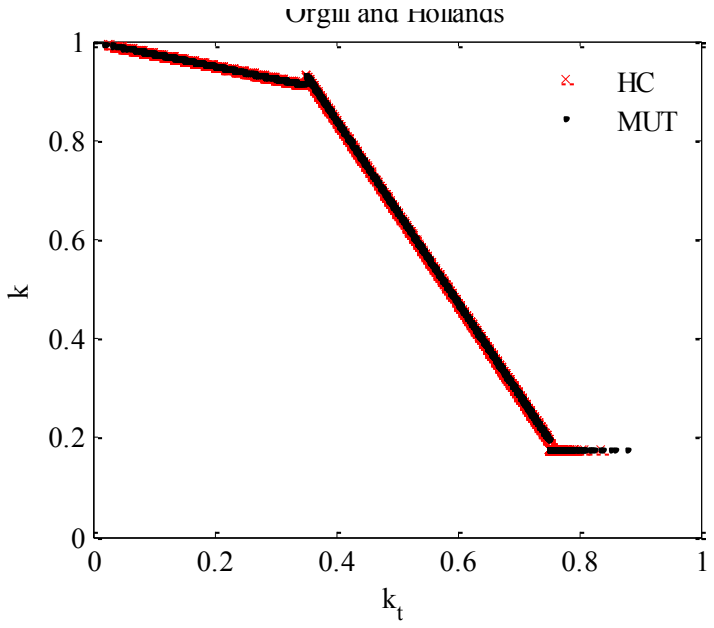

Fig. 4-37 An inter-comparison of the diffuse fraction versus the clearness index between Howard College station and the STARlab station using the Orgill and Hollands model [30].

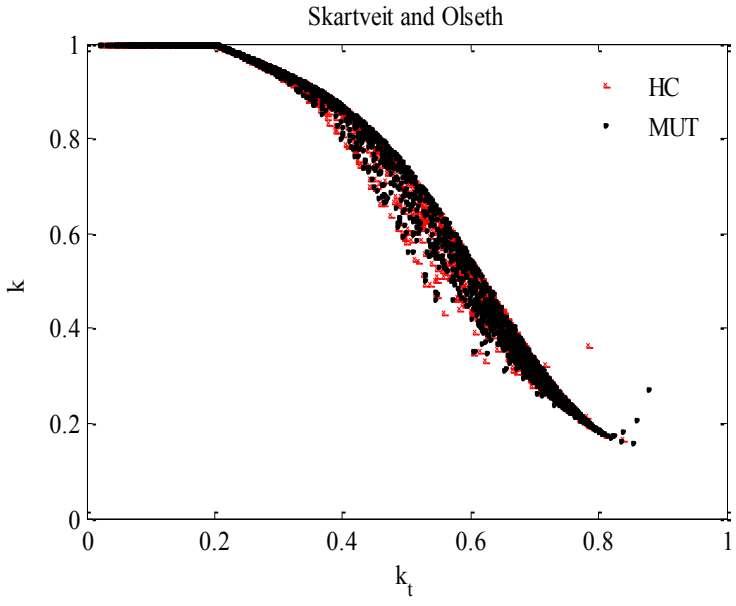

Fig. 4-38 An inter-comparison of the relationship of the diffuse fraction versus the clearness index between Howard College station and the STARlab using the Skartveit and Olseth model [33].

Table 4-12 Comparison of solar irradiation values between Howard College and MUT using data from May 2010 to April 2011.

Average	Howard College (kJ/m^2h)	MUT (kJ/m^2h)	% difference
Irradiation $(\sum I_g)$/N	1783	1796	0.72
Irradiation $(\sum I_d)$/N	620	635	2.36
Irradiation $(\sum I_b)$/N	1410	1362	-3.52

Only a comparison of the global irradiation was calculated when instruments from both stations measuring GHI were run at STARlab. From the above table, a difference of 0.72% in the global irradiance is obtained. A sample calculation is shown below:

$$\%\, difference = \frac{\sum I_{gMUT} - \sum I_{gHC}}{\sum I_{gMUT}} * 100$$

$$\%\, difference = \frac{1796 - 1783}{1796} * 100$$

$$= 0.72$$

where the total global irradiation calculated for the MUT station is denoted as $\sum I_{gMUT}$ and $\sum I_{gHC}$ is the total global irradiation calculated for the Howard College station. The difference of 0.72% calculated above is less than the calculated instrument difference of 1.36% obtained in Chapter 1 when both pyranometers were run at STARlab to measure the global horizontal irradiance. The results obtained are within the instrument uncertainty of 3-4% (Table 1-2) reported by the manufacturers. Therefore, no spatial variation was detectable between STARlab and Howard College. It can be assumed that for the annualized period during which data were recorded, the measurements at the Howard College station can be used as an estimate of the MUT data, and vice versa.

The yearly equation derived for each station was plotted along with the six proposed models to observe its performance. Figure 4-39 and Fig. 4-40 show plots of the yearly equation from Howard College and STARlab respectively against existing models described in Chapter 1. The models tend

to overestimate solar radiation incident on the whole region of the clearness index at either location (Fig. 4-39 and Fig. 4-40). The plots show that mathematical models generally donot perform well when implemented on locations other than those for which they were developed.

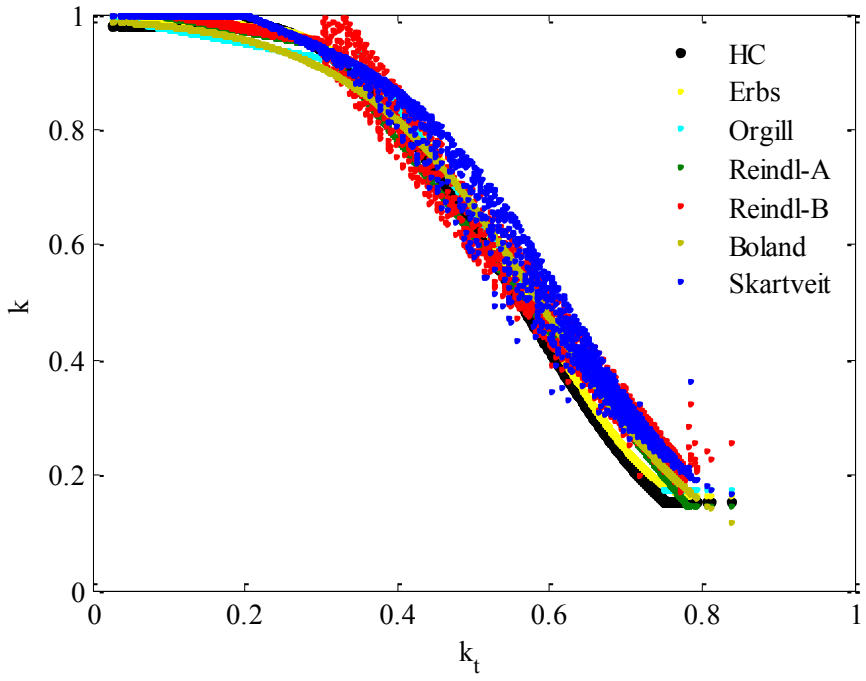

Fig. 4-39 A comparison between the yearly equation derived for HC (in black) with decomposition models.

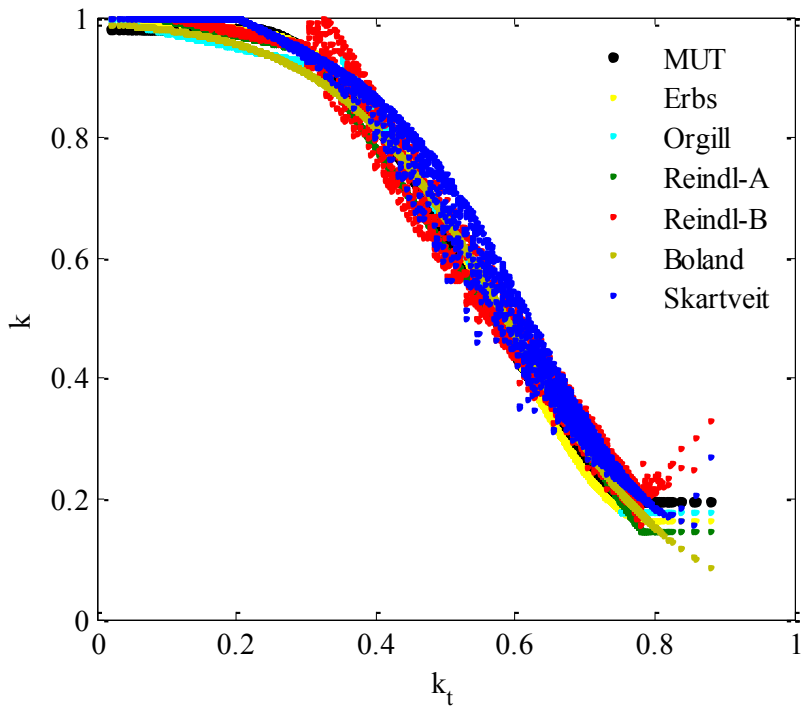

Fig. 4-40 A comparison between the yearly equation derived for STARlab (in black) with decomposition models.

CHAPTER 5: CONCLUSION

Solar radiation data is a vital input in assessing solar energy projects. GRADRAD is an initiative aimed at gathering solar radiation data. Even though the current focus is on Durban, Kwa-Zulu Natal province, it is expected to expand to cover the whole country by establishing similar radiometric stations of similar equipment. This has potential for further research studies to be undertaken in establishing a solar radiation map of South Africa with the establishment of numerous ground stations throughout the country. Collaboration can result with personnel from existing stations and different ideas and research ventures can be achieved. Sponsors and investors can benefit from the data gathered from these stations as they can give an idea on the available solar radiation incident at a location, a defining parameter in their work. All data acquired across the network can be posted on the same website for convenience for the global research community.

Findings of the study show that no potential spatial variations exist for stations located less than 20km apart as the findings of 1.36% (when pyranometers from both stations were run at STARlab) lie within the known instrument uncertainty of 3-4%. When instruments were run at separate locations, a difference of 0.72% was reported. Since the difference lies within the instrument accuracy range (3-4%), it can be concluded that no measurable spatial variations exist between the Howard College and STARlab stations. For the period in which the data was collected from both stations, data from STARlab can be used to estimate irradiance patterns for the Howard College station and vice versa. Measured monthly average daily global horizontal radiation for the summer months were 6.18 kWh/m^2 for STARlab and 5.96 kWh/m^2 for Howard College respectively. Based on the comparison of data for 2007 and the period May 2010-April 2011, the results obtained were maximum monthly average daily global radiation recorded in February with values of 6.18 kWh/m^2 in 2007 and 6.14 kWh/m^2 in 2010 to 2011 and lows of 1.64 kWh/m^2 in 2007 and 2.81 kWh/m^2 in 2010 to 2011 recorded in June.

The study shows that of the various radiometric schemes available, one that measures each radiation component separately is the best. In this way, measured values can be compared with values calculated from the closure equation. Direct measured values estimate solar irradiance well provided the instruments are regularly maintained. For schemes that provide no redundancy in the measured irradiance, existing solar radiometric models have to be used to estimate the missing quantity. Correction factors have to be implemented in correcting the shadow band effect. For the

various models available, the best estimator should be selected to give more accurate results. Of the four selected shadow band correction models, the Le Baron et al. model performs better for Howard College whilst the Drummond model works best on STARlab data. The difference of model performance at the two locations can be ascribed to industrial activity closer to STARlab that pollutes the air and increases scattering of radiation. Further, it was shown that for all sky conditions, an isotropic model (Drummond) performs better for GRADRAD stations on data gathered during the period May 2010 to April 2011. The data set from both locations constitute a higher percentage of overcast to cloudy and partly cloudy skies that are described as isotropic.

Similarly, estimation of the direct normal irradiance is achieved through two methods: spectral and decomposition models. The former gives better estimates as it takes into account atmospheric constituents that attenuate the direct normal irradiance. Due to their complex nature and the unavailability of atmospheric data, spectral models were not treated in this work. Decomposition models by Erbs et al. [29], Orgill and Hollands [30], Reindl et al. [31], Boland et al. [32] and Skartveit and Olseth [33] were implemented on data available at GRADRAD. Plots of the modelled DNI versus the measured DN were drawn. Better results are likely if spectral models are used. Calculating the DNI from the closure equation 1.1 gave better results as compared to the use of the decomposition models. The use of the closure equation gave better fit between the measured DNI (from a NIP) and the modeled values (equation 1.1). An R^2 value of 0.932 and 0.951 for Howard College and STARlab respectively were reported which was higher than any of the decomposition models used. The coefficient of determination indicates how well a regression line approximates real data points. The higher the value, the better is the fit. Implementation of the selected decomposition models show that they are location dependant. To better estimate DNI at stations in Durban, a curve fitting toolbox available in MATLAB was used to generate polynomials that best describe the irradiance in Durban. The models derived for Howard College from this method is given by

$$k = 0.982 \qquad when \;\; k_t < 0.2$$

$$k = 0.8081 + 1.653k_t - 3.247{k_t}^2 - 4.364{k_t}^3 + 5.613{k_t}^4 \qquad when \;\; 0.20 \leq k_t \leq 0.75$$

$$k = 0.156 \qquad when \;\; k_t > 0.75$$

and the correlation for STARlab is given as:

$$k = 0.982 \qquad when \;\; k_t < 0.20$$

$$k = 0.7433 + 2.266 - 5.266 - 1.449{k_t}^3 + 4.22{k_t}^4 \qquad when \;\; 0.20 \leq k_t \leq 0.76$$

$k = 0.196$ $when \;\; k_t > 0.79$

It is evident that more ground stations are required to better correlate ground-based measurements with model estimates. The existence of more ground stations would promote the development of new and more accurate models that give close reading to the true ground-based measurements. It is highly recommended that solar radiometric stations implement radiometric schemes that provide redundancy in the measurement of each of the irradiance quantities.

CHAPTER 6: REFERENCES

[1] Davidson, M., "Influence of direct beam solar radiation on hillslope morphology (microclimate)", Michigan: Ann Abor, 1992.

[2] Bayer, H. G., Constanzo, C. and Heinamann, D., "Modifications of the heliosat procedure for irradiance estimates from satellite images", Solar Energy (56), pp 207-212, 1996.

[3] Zelenka, A., Perez, R., Seals, R. and Renne, D., "Effective accuracy of satellite-derived hourly irradiances", Theor. Appl. Climatol. (62), pp 199-207, 1999.

[4] Muneer, T., "Solar radiation and daylight models", Great Britain: Elsevier Butterworth-Heinemann, 2004.

[5] Myers, D. R., "Solar radiation modeling and measurements for renewable energy applications: data and model quality", Energy (30), pp 1517-1531, 2005.

[6] Batlles, F. J., Rubio, M. A., Tovar, J., Olmo, F. L. and Alados-Arboledas, L., "Empirical modelling of hourly direct irradiance by means of hourly global irradiance", Energy (25), pp 675–688, 2000.

[7] Jacovides, C. P., Tymvios, F. S., Assimakopoulos, V. D. and Kaltsounides, N. A., "Comparative study of various correlations in estimating hourly diffuse fraction of global solar radiation", Renewable Energy (31), pp 2492-2504, 2006.

[8] Stewart, A. L. and Dellar, P. J., "The role of the complete Coriolis force in cross-equatorial flow of abyssal ocean currents", Ocean Modelling (38), pp 187-202, 2011.

[9] Twidell, J. and Weir, T., "Renewable Energy Resources", New York: Taylor and Francis, 2006.

[10] Iqbal, M., "An introduction to solar radiation", New York: Academic Press, 1983.

[11] Duffie, J. A. and Beckman, W. A, "Solar engineering of thermal processes", New York: Wiley, 2006.

[12] http://www.eppleylab.com/ Accessed on 9 December 2009.

[13] http://www.nrel.gov/midc/srrl_bms/instruments.html Accessed on 9 December 2009.

[14] http://www.kippzonen.com/ Accessed on 6 July 2011.

[15] Reda I., "Method to calculate uncertainties in measuring shortwave solar irradiance using thermopile and semiconductor solar radiometers", NREL/TP-3B10-52194, 2011.

[16] Gueymard, C. and Myers, D. R., "Evaluation of conventional and high-performance routine solar radiation measurements for improved solar resource, climatological trends, and radiative modeling", Solar Energy (83), pp 171–185, 2008.

[17] Michalsky, J., Harrison, J. L. and Berkheiser, W., "Cosine response characteristics of some radiometric and photometric sensors", Solar Energy (54), pp 397- 402, 1995.
[18] Wilcox, S. M. and Myers D. R., "Evaluation of Radiometers in Full-Time Use at the National Renewable Energy Laboratory Solar Radiation Research Laboratory", Technical Report, NREL/TP-550-44627, 2008.
[19] Gueymard, C. and Myers, D. R., "Evaluation of conventional and high-performance routine solar radiation measurements for improved solar resource, climatological trends, and radiative modeling", Solar Energy (83), pp 171–185, 2009.
[20] Lester, A. and Myers, D. R., "A method for improving global pyranometer measurements by modelling responsivity functions", Solar Energy (80), pp 322–331, 2006.
[21] Stoffel T., "Solar Infrared Radiation Station (SIRS) Handbook", ARM TR-025, 2004.
[22] Dutton, E. G., Michalsky, J. J., Stoffel, T., Forgan, B. W., Hickey, J., Nelson, D. W., Alberta, T. L. and Reda I., "Measurement of broadband diffuse solar irradiance using current commercial instrumentation with a correction for thermal offset errors", Journal of atmospheric and oceanic technology (18), pp 300-314, 2001.
[23] Reda, I. and Andreas, A., "Solar Position Algorithm for Solar Radiation Applications", Solar Energy (76), pp 577-589, 2004.
[24] Drummond, A. J., "On the measurement of sky radiation", Radiation Service, South African Weather Bureau, Pretoria, 1956.
[25] Batlles, F. J., Olmo, F. L. and Alados-Arboledas, L., "On shadow band correction methods for diffuse irradiance measurements", Solar Energy (54), pp 105–114, 1995.
[26] Le Baron, B. A., Michalsky, J. J. and Perez, R., "A simple procedure for correcting shadow band data for all sky conditions", Solar Energy (44), pp 249-256, 1990.
[27] Muneer, T. and Zhang, X., "A new method for correcting shadow band diffuse irradiance data", Solar Energy (124), pp 34-43, 2002.
[28] Snell, H. E., Moncet, J. L., Chetwynd, J. H., Miller, S. and Wang, J., "FASCODE for the environment (FASE)", In proceedings of SPI Optic and Photonics, Orlando, USA, 1995.
[29] Erbs, D. G., Klein, S. A. and Duffie, J. A., "Estimation of the diffuse radiation fraction for hourly, daily and monthly-average global radiation", Solar Energy (28), pp 293-302, 1982.
[30] Orgill, J. F. and Hollands, K. G., "Correlation equation for hourly diffuse radiation on a horizontal surface", Solar Energy (19), pp 357-359, 1977.
[31] Reindl, D. T., Beckman, W. A. and Duffie, J. A., "Diffuse fraction correlations", Solar Energy (45), pp 1-7, 1990.

[32] Boland, J., Scott, L. and Luther, M., "Modelling the diffuse fraction of global solar radiation on a horizontal surface", Environmetrics (12), pp 103-116, 2001.

[33] Skartveit, A. and Olseth, J. A., "A model for the diffuse fraction of hourly global radiation", Solar Energy (38), pp 271-274, 1987.

[34] Kunene, K., Brooks, M., Roberts, L, and Zawilska, E., "Introducing GRADRAD: The Greater Durban Radiometric Network", In proceedings of World Renewable Energy Congress XI, Abu Dhabi, UAE, 2010.

[35] http://www.wordtravels.com/Cities/South+Africa/Durban/Climate Assessed on 9 December 2009.

[36] Brooks, M. and Roberts, L., "Establishment of a broadband radiometric ground station on the South African east coast", In proceedings of SPIE Optics and Photonics, San Diego, USA, 2009.

[37] Brooks, M., "The development and impact of an outdoor solar thermal test facility", Journal of Energy in Southern Africa (16), 2005.

[38] Brooks, M., "The development and impact of an outdoor solar thermal test facility". University of Stellenbosch, MSc thesis, 2005.

[39] Lysko, M., "Measurement and models of solar irradiance", Norwegian University of Science and Technology, PhD Thesis, 2006.

[40] Hirata, K., Kurokawa, K., Miyake, Y., Nakamura, K. and Kato, T., "Development of a reliable, long life pyranometer composed of multiple photosensors", In proceedings of the 15th International Photovoltaic Science and Engineering Conference, Shangai, China, 2005.

[41] Fröhlich, C., "History of solar radiometry and the world radiometric reference", Metrologia (28), pp 111-115, 1991.

[42] Myers, D. R., Stoffel, T. L., Andreas, A., Wilcox, S. and Reda I., "Improved radiometric calibrations and measurements for evaluating photovoltaic devices" NREL/TP-520-28941, 2000.

[43] Reda, I., Stoffel, T. and Myers, D., "A method to calibrate a solar pyranometer for measuring reference diffuse irradiance", Solar Energy (74), pp 103-112, 2003.

[44] Peppler, R. A., Long, C. N., Sisterson, D. L., Turner, D. D., Bahrmann, C. P., Christensen S. S., Doty, K. J., Eagan, R. C., Halter, T. D., Ivey, M. D., Keck, N. N., Kechoe, K. E., Liljegren, J. C., Macduff, M. C., Mather, J. H., McCord R. A., Monroe, J. W., Moore, S. T., Nitschke, K. L., Orr, B. W., Perez, R. C., Perkins, B. D., Richardson, S. J., Sonntag, K. L., Voyles, J. W. and Wagener, R., "An overview of ARM program climate research facility data quality assurance", The Open Atmospheric Science Journal (2), pp 192-216, 2008.

[45] Reda, I., Stoffel, T. and Myers, D., "A method to calibrate a solar pyranometer for measuring diffuse irradiance", Solar Energy (74), pp 103-112, 2003.

[46] Blanco-Muriel, M., Alarcon-Padilla, D. C., Lopez-Moratalla, T. and Lara-Coira, M., "Computing the solar vector" Solar Energy (70), pp 431-441, 2001.

[47] Michalsky J. J., "The astronomical almanac"s algorithm for approximate solar position (1950-2050)", Solar Energy (40), pp 227-235, 1988.

[48] Walraven R., "Calculating the position of the sun", Solar Energy (22), pp 393-397, 1978.

[49] Grena, R., "An algorithm for the computation of the solar position", Solar Energy (82), pp 462-470, 2008.

[50] Cooper P. I., "The absorption of solar radiation in solar stills", Solar Energy (12), pp 333-346, 1972.

[51] http://www.nrel.gov/ Accessed on 20 August 2010.

[52] Jackson, S., "Research methods and statistics: a critical thinking approach", USA: Wadswoth, 2009.

[53] http://gradrad.ukzn.ac.za Accessed on 25 September 2010.

[54] http://solardat.uoregon.edu Accessed on 10 July 2011.

[55] Coskun, C., Oktay, Z. and Dincer, I., "Estimation of monthly solar radiation distribution for solar energy system analysis", Energy (36), pp 1319-1323, 2011.

[56] Zawilska, E. and Brooks, M. J., "An assessment of the solar resource for Durban, South Africa", Renewable Energy, pp 1-6, 2011.

[57] Gueymard, C. A. and Wilcox, S. M., "Assessment of spatial and temporal variability in the US solar resource from radiometric measurements and predictions from models using ground-based or satellite data", Solar Energy (85), pp 1068-1084, 2011.

[58] Lopez, G., Muneer, T. and Claywell, R., "Comparative study of four shadow band diffuse irradiance correction algorithms for Almeria, Spain", Solar Energy (126), pp 696-671, 2004.

[59] Lopez G., Muneer, T. and Claywell, R., "Assessment of four shadow band correction models using beam normal irradiance data from the United Kingdom and Israel", Energy Conservation and Management (45), pp 1963-1979, 2004.

[60] Boland, J., Ridley, B. and Brown B., "Models of diffuse solar radiation", Renewable Energy (33), pp 575-584, 2008.

[61] Oliveira, A. P , Escobedo, J. F., Machado, A. J. and Soares, J., "Correlation models of diffuse solar radiation applied to the city of Sao Paulo, Brazil", Applied Energy (71), pp 59–73, 2002.

[62] De Miguel, A., Bilbao, J., Agular, R., Kambezidis, H. and Negro, E., “Diffuse solar irradiation model evaluation in the north Mediterranean belt area”, Solar Energy (70), pp 143-153, 2001.

Appendix A: LabVIEW front panel and block diagram

LabVIEW front panel

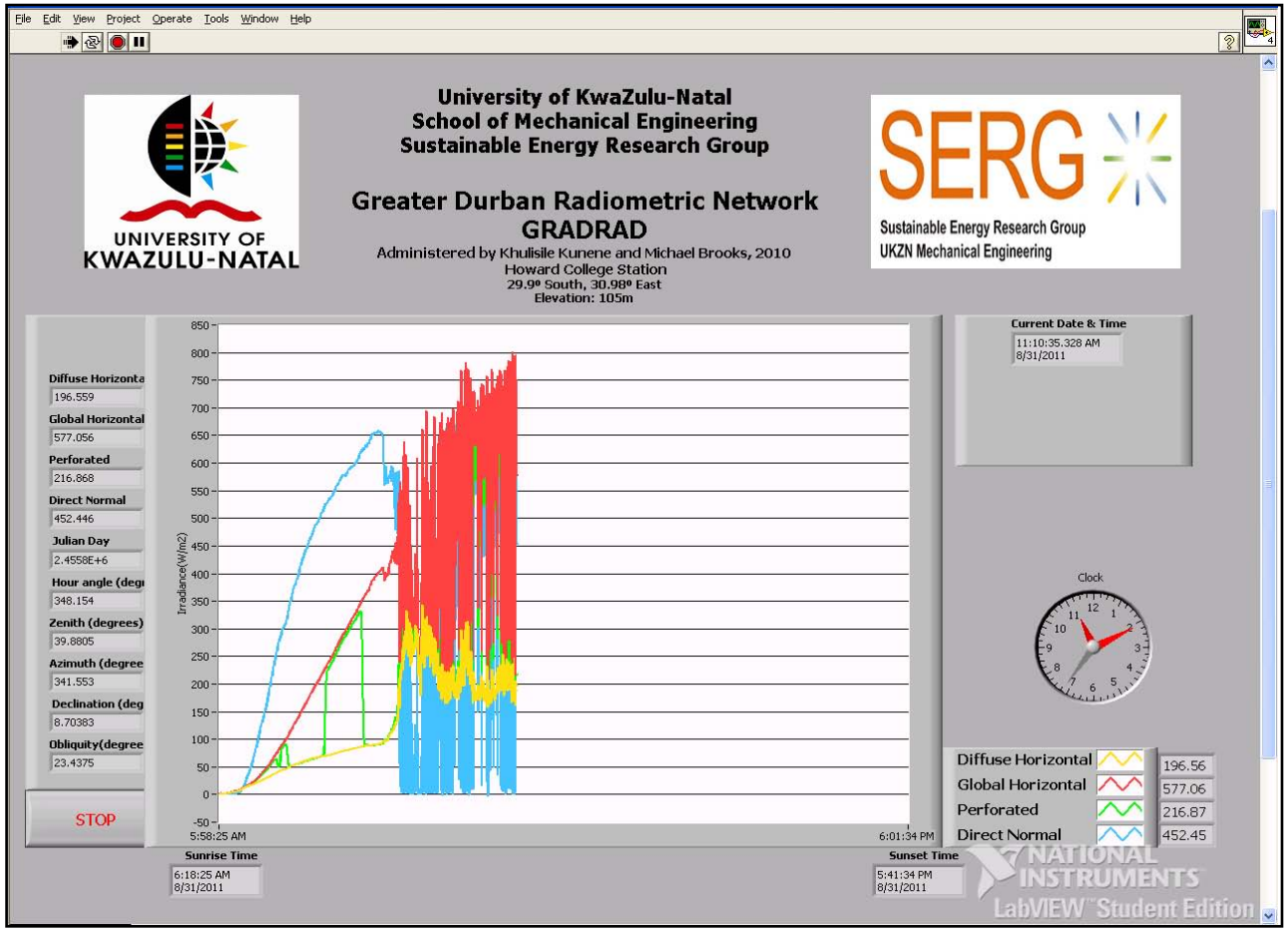

Appendix B: Solar Position Algorithm [23]

```
% SPA Algorithm
% Calculation of the Julian Day
  function result = SPA2(Y, M, D)
% Time zone = -2hrs
% Local time(lst) 12:30:30 pm
% Calculation for D(day number)
% where D = (lst-time zone)/24hrs + day number
% D = ((12+30/60+30/3600)-7)/24 + 17
%   = 17.812847222
A = fix(Y/100);
B = 2 - A + fix(A/4);
if M > 2
    Y = Y  ;
else  Y = Y-1 ;
end

if M > 2
   M = M;
else M = M+12;
end
JD = fix(365.25*(Y + 4716)) + fix(30.6001*(M + 1))+D-1524.5+B;
X = fprintf('%f\n',JD);

% Declaration of constants
sigma = 30.1786; %longitude
phi = -25.52*(pi/180);      % latitude
P = 820; %pressure
T = 25; %temperature
E = 151.3; %elevation
delT = 67;

% Calculation of the Julian Epheremis Day
JDE = JD + delT/86400;
% Calculation of the Julian century
JC = (JD-2451545)/36525;
% Calculation of the Julian Epheremis century
JCE = (JDE-2451545)/36525;
% Calculation of the Julian Epheremis Millenium
JME = JCE/10;

%Earth heliocentric longitude,latitude,radius vector(L,B and R)
A = xlsread('earth.xlsx',1,'c2:c65');
B = xlsread('earth.xlsx',1,'d2:d65');
C = xlsread('earth.xlsx',1,'e2:e65');
A1 = xlsread('earth.xlsx',1,'c67:c100');
B1 = xlsread('earth.xlsx',1,'d67:d100');
C1 = xlsread('earth.xlsx',1,'e67:e100');
A2 = xlsread('earth.xlsx',1,'c102:c121');
B2= xlsread('earth.xlsx',1,'d102:d121');
C2 = xlsread('earth.xlsx',1,'e0102:e121');
A3 = xlsread('earth.xlsx',1,'c123:c129');
B3 = xlsread('earth.xlsx',1,'d123:d129');
C3 = xlsread('earth.xlsx',1,'e123:e129');
A4 = xlsread('earth.xlsx',1,'c131:c133');
```

```
B4 = xlsread('earth.xlsx',1,'d131:d133');
C4 = xlsread('earth.xlsx',1,'e131:e133');
A5 = xlsread('earth.xlsx',1,'c135');
B5 = xlsread('earth.xlsx',1,'d135');
C5 = xlsread('earth.xlsx',1,'e135');
Lo = A.*cos(B+C.*JME);
Lo = sum(Lo);
L1 = A1.*cos(B1+C1.*JME);
L1 = sum(L1);
L2 = A2.*cos(B2+C2.*JME);
L2 = sum(L2);
L3 = A3.*cos(B3+C3.*JME);
L3 = sum(L3);
L4 = A4.*cos(B4+C4.*JME);
L4 = sum(L4);
L5 = A5.*cos(B5+C5.*JME);
L5 = sum(L5);
L = (Lo+ L1*JME+L2*JME^2 + L3*JME^3+L4*JME^4+L5*JME^5)/10^8;

L = L*(180/pi);
a = L/360;
F = a - fix(a);
if  L>0
    L = 360*F;
else L = 360-360*F;
end
fprintf('%f\n',L);

bA = xlsread('earth.xlsx',1,'i2:i6');
bB = xlsread('earth.xlsx',1,'j2:j6');
bC = xlsread('earth.xlsx',1,'k2:k6');
bA1 = xlsread('earth.xlsx',1,'i8:i9');
bB1 = xlsread('earth.xlsx',1,'j8:j9');
bC1 = xlsread('earth.xlsx',1,'k8:k9');
Bo = bA.*cos(bB+bC.*JME);
Bo = sum(Bo);
B1 = bA1.*cos(bB1+bC1.*JME);
B1 = sum(B1);
B = (Bo+ B1*JME)/10^8;
format long
B = B*(180/pi);


rA = xlsread('earth.xlsx',1,'o2:o41');
rB = xlsread('earth.xlsx',1,'p2:p41');
rC = xlsread('earth.xlsx',1,'q2:q41');
rA1 = xlsread('earth.xlsx',1,'o43:o52');
rB1 = xlsread('earth.xlsx',1,'p43:p52');
rC1 = xlsread('earth.xlsx',1,'q43:q52');
rA2 = xlsread('earth.xlsx',1,'O54:O59');
rB2 = xlsread('earth.xlsx',1,'p54:p59');
rC2 = xlsread('earth.xlsx',1,'q54:q59');
rA3 = xlsread('earth.xlsx',1,'o61:o62');
rB3 = xlsread('earth.xlsx',1,'p61:p62');
```

```
rC3 = xlsread('earth.xlsx',1,'q61:q62');
rA4 = xlsread('earth.xlsx',1,'o64');
rB4 = xlsread('earth.xlsx',1,'p64');
rC4 = xlsread('earth.xlsx',1,'q64');

Ro = rA.*cos(rB+rC.*JME);
Ro = sum(Ro);
R1 = rA1.*cos(rB1+rC1.*JME);
R1 = sum(R1);
R2 = rA2.*cos(rB2+rC2.*JME);
R2 = sum(R2);
R3 = rA3.*cos(rB3+rC3.*JME);
R3 = sum(R3);
R4 = rA4.*cos(rB4+rC4.*JME);
R4 = sum(R4);
%X = [fprintf('%f\n',Lo)  fprintf('%f\n',L1) fprintf ('%f\n',L2)
fprintf('%f\n',L3) fprintf('%f\n',L4) fprintf('%f\n',L5)]
R = (Ro+ R1*JME+R2*JME^2 + R3*JME^3+R4*JME^4)/10^8;
X = fprintf('%f\n',R);

% Calculation of the geocentric longitude and latitude (theta and beta)
theta = L+180;
a = theta/360;
F = a - fix(a);
if  F>0
    theta = 360*F;
else theta = 360-360*F;
end
beta = -B;

% Calculation of the nutation in longitude and obliquity (delSi and
delEps)
Xo = 297.85036 + 445267.111480*JCE-0.0019142*JCE^2 + (JCE^3/189474);
X1 = 357.52772+35999.050340*JCE-0.0001603*JCE^2-(JCE^3/300000);
X2 = 134.96298+477198.867398*JCE+0.0086972*JCE^2+(JCE^3/56250);
X3 = 93.27191+483202.017538*JCE-0.0036825*JCE^2+(JCE^3/327270);
X4 = 125.04452-1934.136261*JCE+0.0020708*JCE^2+(JCE^3/450000);

a = xlsread('earth.xlsx',1,'x2:x64');
b = xlsread('earth.xlsx',1,'y2:y64');
c = xlsread('earth.xlsx',1,'z2:z64');
d = xlsread('earth.xlsx',1,'aa2:aa64');
Yo = xlsread('earth.xlsx',1,'s2:s64');
Y1 = xlsread('earth.xlsx',1,'t2:t64');
Y2 = xlsread('earth.xlsx',1,'u2:u64');
Y3 = xlsread('earth.xlsx',1,'v2:v64');
Y4 = xlsread('earth.xlsx',1,'w2:w64');
X = Xo*Yo+X1*Y1+X2*Y2+X3*Y3+X4*Y4;
delSi = (a+b.*JCE).*sin(X*(pi/180));
delEps = (c+d.*JCE).*cos(X*(pi/180));
delSi = sum(delSi)/36000000;     %  in degrees
delEps = sum(delEps)/36000000;   % in degrees
```

```
% Calculation of the true obliquity of the ecliptic,Eo(in degrees)
U = JME/10;
Eo = 84381.448-4680.93*U-1.55*U^2+1999.25*U^3-51.38*U^4-249.67*U^5 -
39.05*U^6+7.12*U^7+27.87*U^8+5.79*U^9+2.45*U^10;
eps = (Eo/3600)+delEps;         %  in degrees
fprintf('%.6f\n',eps);
% Calculation of the aberration correction,delTau(in degrees)
delTau = -20.4898/(3600*R);
% Calculation of the apparent sun longitude,(in degrees)
lambda = theta+delSi+delTau;
% Calculation of the apparent sidereal time at Greenwich at any given
time ,vo(in degrees)
vo = 280.46061837+360.98564736629*(JD-2451545)+0.000387933*JC^2-
(JC^3/38710000);
a = vo/360;
F = a - fix(a);
if  vo>0
    vo = 360*F;
else vo = 360-360*F;
end
v = vo+delSi.*cos(eps*(pi/180));
% Calculation of the sun right ascension,alpha(in radians)
ra1 = sin(lambda*(pi/180))*cos(eps*(pi/180))-
tan(beta*(pi/180))*sin(eps*(pi/180));
ra2 =(cos(lambda*(pi/180)));
alpha = atan2(ra1,ra2);
alpha = alpha*(180/pi);
a = alpha/360;
F = abs(a - fix(a));
if  alpha >0
    alpha = 360*F;
else alpha = 360-360*F;
end
decl =
asin(sin(beta*(pi/180)).*cos(eps*(pi/180))+cos(beta*(pi/180)).*sin(eps*(p
i/180)).*sin(lambda*(pi/180)));
decl = decl*(180/pi);
hangl = v+sigma-alpha;
a = hangl/360;
F = abs(a - fix(a));
if  hangl >0
    hangl = 360*F
else hangl = 360-360*F;
end

zeta =  8.794/(3600*R);
u = atan(0.99664719*tan(phi));
x = cos(u)+ (E/6378140)*cos(phi);
y = 0.99664719*sin(u)+ (E/6378140)*sin(phi);
w1 = (-x*sin(zeta*(pi/180))*sin(hangl*(pi/180)));
w2 = cos(decl*(pi/180))-sin(zeta*(pi/180))*cos(hangl*(pi/180));
delalpha = atan2(w1,w2);
delalpha = delalpha*(180/pi);
alphaP = alpha+delalpha;
```

```
w3 = sin(decl*(pi/180))-y*sin(zeta*(pi/180))*cos(delalpha*(pi/180));
w4 = cos(decl*(pi/180))-x*sin(zeta*(pi/180))*cos(hangl*(pi/180));
declP = atan2(w3,w4);
declP = declP*(180/pi);
hanglP = hangl-delalpha;
eo =
asin((sin(phi)*sin(declP*(pi/180))+cos(phi)*cos(declP*(pi/180))*cos(hangl
P*(pi/180))));
eo = eo*(180/pi);
dele =
(P/1010)*(283/(273+T))*(1.02/(60*tan(eo*(pi/180)+(10.3/(eo*(180/pi)+5.11)
))));
e = eo+dele;
thetaZ = 90-e;
k1 = sin(hanglP*(pi/180));
k2 =(sin(phi)*cos(hanglP*(pi/180))-(tan(declP*(pi/180))*cos(phi)));
t = atan2(k1,k2);
tt = t*(180/pi);
a = tt/360;
F = a - fix(a);
if  F>0
    tt = 360*F;
else tt = 360-360*F;
end
az = tt +180;

output = [fprintf('%.6f\n',JD) fprintf('%.6f\n',Lo) fprintf('%.6f\n',L1)
fprintf('%.6f\n',L2) fprintf('%.6f\n',L3) fprintf('%.6f\n',L4)
fprintf('%.6f\n',L5) fprintf('%.10f\n',L)
    fprintf('%.6f\n',Bo) fprintf('%.6f\n',B1) fprintf('%.10f\n',B)
fprintf('%.6f\n',Ro) fprintf('%.6f\n',R1) fprintf('%.6f\n',R2)
fprintf('%.6f\n',R3) fprintf('%.6f\n',R4)
    fprintf('%.10f\n',R) fprintf('%.10f\n',theta) fprintf('%.8f\n',delSi)
fprintf('%.6f\n',eps) fprintf('%.5f\n',alpha) fprintf('%.4f\n',hangl)
fprintf('%.5f\n',alphaP) fprintf('%.5f\n',thetaZ)
    fprintf('%.10f\n',beta) fprintf('%.8f\n',delEps)
fprintf('%.10f\n',lambda) fprintf('%.5f\n',decl) fprintf('%.5f\n',hanglP)
fprintf('%.6f\n',declP) fprintf('%.5f\n',az)]';
```

Appendix C: Sample of an excel data file for 1 June 2010, Howard College, available at http://gradrad.ukzn.ac.za

Time	DHI	GHI	Perforated	DNI	Julian Day	Hour angle	Zenith	Azimuth angle	Declination angle	Obliquity
5:59 AM	1.750806	2.385191	1.436952	0.87475	2455348	138.91	96.062451	291.95	21.9813	23.438427
6:00 AM	2.005447	2.561476	1.618961	1.246354	2455349	271.26	99.693365	289.95	22.0322	23.438429
6:01 AM	1.893366	2.495636	1.586133	1.074176	2455349	271.51	99.490236	290.06	22.0323	23.438429
6:02 AM	1.767192	2.459826	1.51549	1.072649	2455349	271.76	99.287284	290.17	22.0324	23.438429
6:03 AM	1.699463	2.445251	1.506868	1.147933	2455349	272.01	99.084513	290.29	22.0325	23.438429
6:04 AM	1.732344	2.448644	1.549877	1.242948	2455349	272.26	98.881924	290.4	22.0326	23.438429
6:05 AM	1.832846	2.512096	1.623428	1.512842	2455349	272.51	98.679518	290.51	22.0327	23.438429
6:06 AM	1.791772	2.538483	1.728768	1.405143	2455349	272.76	98.477298	290.62	22.0328	23.438429
6:07 AM	1.805973	2.620406	1.74913	1.350295	2455349	273.01	98.275264	290.73	22.0329	23.438429
6:08 AM	1.829897	2.63297	1.829953	1.486769	2455349	273.26	98.073419	290.85	22.033	23.438429
6:09 AM	1.933894	2.714014	1.908491	1.588244	2455349	273.51	97.871764	290.96	22.0331	23.438429
6:10 AM	2.074378	2.819684	1.976641	1.611498	2455349	273.76	97.670298	291.07	22.0332	23.438429
6:11 AM	2.180014	2.886907	2.064009	1.678678	2455349	274.01	97.469024	291.18	22.0333	23.438429
6:12 AM	2.147023	2.865295	2.005209	1.291923	2455349	274.26	97.267942	291.3	22.0334	23.438429
6:13 AM	2.141124	2.87007	2.024844	1.517775	2455349	274.51	97.067051	291.41	22.0335	23.438429
6:14 AM	2.104856	2.782116	2.008326	1.428867	2455349	274.76	96.866351	291.52	22.0336	23.438429
6:15 AM	2.100268	2.774451	1.942982	1.269021	2455349	275.01	96.665841	291.64	22.0336	23.438429
6:16 AM	2.110646	2.712255	1.894259	1.163318	2455349	275.26	96.465518	291.75	22.0337	23.438429
6:17 AM	2.036909	2.684612	1.873066	1.154157	2455349	275.51	96.26538	291.87	22.0338	23.438429
6:18 AM	1.979229	2.648802	1.888857	1.149459	2455349	275.76	96.065422	291.98	22.0339	23.438429
6:19 AM	1.972019	2.580324	1.803982	1.068773	2455349	276.01	95.865638	292.1	22.034	23.438429
6:20 AM	1.954759	2.607841	1.821954	0.986207	2455349	276.26	95.666022	292.21	22.0341	23.438429
6:21 AM	1.793847	2.431304	1.654698	0.90787	2455349	276.51	95.466564	292.33	22.0342	23.438429
6:22 AM	1.760856	2.415095	1.631843	0.876276	2455349	276.76	95.267252	292.44	22.0343	23.438429
6:23 AM	1.68122	2.410321	1.532008	0.904699	2455349	277.01	95.068072	292.56	22.0344	23.438429
6:24 AM	1.632389	2.399892	1.515283	0.743913	2455349	277.26	94.869006	292.67	22.0345	23.438429
6:25 AM	1.624087	2.434697	1.461885	1.029428	2455349	277.51	94.670031	292.79	22.0346	23.438429
6:26 AM	1.675102	2.414342	1.551539	1.095551	2455349	277.76	94.471122	292.91	22.0347	23.438429
6:27 AM	1.842459	2.631211	1.68524	1.25387	2455349	278.01	94.272245	293.02	22.0348	23.438429
6:28 AM	1.993103	2.73261	1.867249	1.079461	2455349	278.26	94.073363	293.14	22.0349	23.438429
6:29 AM	2.105512	2.921209	1.938514	1.143704	2455349	278.51	93.87443	293.26	22.035	23.438429
6:30 AM	2.256374	2.943323	2.054971	1.222277	2455349	278.76	93.675393	293.38	22.0351	23.438429
6:31 AM	2.438369	3.177784	2.185348	1.217462	2455349	279.01	93.476189	293.49	22.0352	23.438429
6:32 AM	2.66133	3.36211	2.392497	1.394338	2455349	279.26	93.276747	293.61	22.0353	23.438429
6:33 AM	2.792638	3.560007	2.49524	1.202546	2455349	279.51	93.076984	293.73	22.0354	23.438429
6:34 AM	2.935744	3.719707	2.711427	1.333852	2455349	279.76	92.876811	293.85	22.0354	23.438429
6:35 AM	3.102664	3.933687	2.924497	1.135248	2455349	280.01	92.676126	293.97	22.0355	23.438429
6:36 AM	3.180225	4.118767	3.085313	1.037649	2455349	280.26	92.474823	294.09	22.0356	23.438429
6:37 AM	3.367574	4.322947	3.289034	1.117161	2455349	280.51	92.272791	294.21	22.0357	23.438429
6:38 AM	3.637727	4.499358	3.476548	1.082749	2455349	280.76	92.069921	294.33	22.0358	23.438429

6:39 AM	3.86615	4.838861	3.767949	1.14899	2455349	281.01	91.866112	294.45	22.0359	23.438429
6:40 AM	4.180873	5.163537	4.127291	1.167194	2455349	281.26	91.661279	294.57	22.036	23.438429
6:41 AM	4.46916	5.520003	4.404251	1.116692	2455349	281.51	91.455363	294.69	22.0361	23.438429
6:42 AM	4.686659	5.774944	4.689938	1.077934	2455349	281.76	91.248337	294.81	22.0362	23.438429
6:43 AM	5.083641	6.19637	5.086263	1.272427	2455349	282.01	91.040219	294.93	22.0363	23.438429
6:44 AM	5.47243	6.581232	5.477498	1.328684	2455349	282.26	90.831058	295.05	22.0364	23.438429
6:45 AM	5.848219	6.983937	5.808687	1.10248	2455349	282.51	90.620892	295.18	22.0365	23.438429
6:46 AM	6.095213	7.188367	6.027887	1.190918	2455349	282.76	90.409448	295.3	22.0366	23.438429
6:47 AM	6.458003	7.588182	6.385359	1.265967	2455349	283.01	90.209972	295.42	22.0367	23.438429
6:48 AM	6.937353	8.071804	6.765374	1.452474	2455349	283.26	90.000161	295.55	22.0368	23.438429
6:49 AM	7.386333	8.484435	7.215512	1.499806	2455349	283.51	89.783756	295.67	22.0369	23.438429
6:50 AM	7.909926	8.923451	7.730995	1.566986	2455349	283.76	89.572843	295.79	22.037	23.438429
6:51 AM	8.36994	9.553329	8.234012	1.703577	2455349	284.01	89.363619	295.92	22.0371	23.438429
6:52 AM	8.949791	10.13358	8.817124	1.829246	2455349	284.26	89.155761	296.04	22.0372	23.438429
6:53 AM	9.449132	10.62134	9.26612	1.664584	2455349	284.51	88.949314	296.17	22.0373	23.438429
6:54 AM	9.88271	11.17294	9.739944	2.064728	2455349	284.76	88.744343	296.29	22.0373	23.438429
6:55 AM	10.56426	11.89555	10.48574	2.186052	2455349	285.01	88.540876	296.42	22.0374	23.438429
6:56 AM	11.34436	12.86757	11.35018	2.185934	2455349	285.26	88.338903	296.54	22.0375	23.438429
6:57 AM	12.20485	13.8034	12.20298	2.113234	2455349	285.51	88.138372	296.67	22.0376	23.438429
6:58 AM	13.03563	14.86199	13.11572	2.557891	2455349	285.76	87.939207	296.79	22.0377	23.438429
6:59 AM	13.92091	16.11094	14.27769	8.196079	2455349	286.01	87.74131	296.92	22.0378	23.438429
7:00 AM	14.95641	18.66425	16.57482	42.88128	2455349	286.26	87.544574	297.05	22.0379	23.438429
7:01 AM	15.79746	20.97141	18.76744	76.13727	2455349	286.51	87.348889	297.18	22.038	23.438429
7:02 AM	16.82651	25.45846	22.90179	149.0373	2455349	286.76	87.154148	297.3	22.0381	23.438429
7:03 AM	17.71835	28.97549	26.11935	194.574	2455349	287.01	86.960249	297.43	22.0382	23.438429
7:04 AM	18.47954	30.94189	27.61833	205.9724	2455349	287.26	86.7671	297.56	22.0383	23.438429
7:05 AM	19.18065	32.87437	27.14118	215.6707	2455349	287.51	86.574616	297.69	22.0384	23.438429
7:06 AM	19.77929	34.89719	23.81173	226.5153	2455349	287.76	86.382724	297.82	22.0385	23.438429
7:07 AM	20.36876	37.04026	21.15079	238.6817	2455349	288.01	86.191359	297.95	22.0386	23.438429
7:08 AM	20.91748	39.10781	20.90676	247.7918	2455349	288.26	86.000467	298.08	22.0387	23.438429
7:09 AM	21.53851	41.10852	21.36625	255.6023	2455349	288.51	85.81	298.21	22.0388	23.438429
7:10 AM	22.04932	43.20823	21.83125	264.0937	2455349	288.76	85.619918	298.34	22.0389	23.438429
7:11 AM	22.54298	44.90097	22.28637	267.0037	2455349	289.01	85.430188	298.47	22.039	23.438429
7:12 AM	23.05685	47.10988	22.77755	276.2571	2455349	289.26	85.240782	298.6	22.0391	23.43843
7:13 AM	23.60109	49.44607	23.22862	285.5415	2455349	289.51	85.051679	298.73	22.0391	23.43843
7:14 AM	24.27991	51.62846	23.7573	292.3094	2455349	289.76	84.862858	298.87	22.0392	23.43843
7:15 AM	24.75577	53.84478	24.29511	299.3862	2455349	290	84.674306	299	22.0393	23.43843
7:16 AM	25.20071	56.19944	24.79055	307.6253	2455349	290.25	84.48601	299.13	22.0394	23.43843
7:17 AM	25.62369	58.41475	25.17451	315.9457	2455349	290.5	84.297962	299.27	22.0395	23.43843
7:18 AM	26.17699	60.95286	25.70495	325.0234	2455349	290.75	84.110152	299.4	22.0396	23.43843
7:19 AM	26.80349	63.59085	26.3264	334.0409	2455349	291	83.922577	299.53	22.0397	23.43843

7:20 AM	27.4916	66.03761	27.00623	339.9078	2455349	291.25	83.735233	299.67	22.0398	23.43843
7:21 AM	28.10248	68.38511	27.60659	345.0603	2455349	291.5	83.548116	299.8	22.0399	23.43843
7:22 AM	28.60193	70.91919	28.06597	351.2725	2455349	291.75	83.361224	299.94	22.04	23.43843
7:23 AM	29.03419	73.32323	28.43175	358.0735	2455349	292	83.174558	300.07	22.0401	23.43843
7:24 AM	29.35973	75.7098	28.80065	364.4261	2455349	292.25	82.988116	300.21	22.0402	23.43843
7:25 AM	29.87546	78.2998	29.26835	370.4888	2455349	292.5	82.8019	300.35	22.0403	23.43843
7:26 AM	30.36737	80.76315	29.68857	376.3189	2455349	292.75	82.615911	300.48	22.0404	23.43843
7:27 AM	30.82149	83.41685	30.12988	383.1159	2455349	293	82.430149	300.62	22.0405	23.43843
7:28 AM	31.29417	85.89113	30.65564	388.0854	2455349	293.25	82.244616	300.76	22.0406	23.43843
7:29 AM	31.74752	88.50135	31.11482	393.2741	2455349	293.5	82.059315	300.9	22.0407	23.43843
7:30 AM	32.15466	90.90049	31.52164	398.1256	2455349	293.75	81.874248	301.04	22.0408	23.43843
7:31 AM	32.58333	93.46486	31.98237	402.3873	2455349	294	81.689416	301.18	22.0409	23.43843
7:32 AM	32.96829	96.1932	32.47199	407.823	2455349	294.25	81.504823	301.32	22.0409	23.43843
7:33 AM	33.43945	98.83848	32.91288	412.908	2455349	294.5	81.320471	301.46	22.041	23.43843
7:34 AM	33.83687	101.4532	33.33341	418.0679	2455349	294.75	81.136363	301.6	22.0411	23.43843
7:35 AM	34.21681	103.9369	33.81056	422.6215	2455349	295	80.952502	301.74	22.0412	23.43843
7:36 AM	34.6801	106.6244	34.31503	427.6826	2455349	295.25	80.76889	301.88	22.0413	23.43843
7:37 AM	35.08451	109.3935	34.72382	433.6116	2455349	295.5	80.585531	302.02	22.0414	23.43843
7:38 AM	35.36329	111.9126	35.03008	438.4406	2455349	295.75	80.402427	302.16	22.0415	23.43843
7:39 AM	35.70008	114.36	35.46567	441.6806	2455349	296	80.219582	302.31	22.0416	23.43843
7:40 AM	36.13191	117.0097	35.97222	445.8512	2455349	296.25	80.036997	302.45	22.0417	23.43843
7:41 AM	36.49754	119.7731	36.49404	449.8578	2455349	296.5	79.854677	302.6	22.0418	23.43843
7:42 AM	36.89037	122.513	37.05378	454.3016	2455349	296.75	79.672625	302.74	22.0419	23.43843
7:43 AM	37.28943	125.2414	37.8135	458.2298	2455349	297	79.490842	302.88	22.042	23.43843
7:44 AM	37.69777	127.9547	41.16642	462.7349	2455349	297.25	79.309333	303.03	22.0421	23.43843
7:45 AM	38.06045	130.5855	58.82218	466.1465	2455349	297.5	79.1281	303.18	22.0422	23.43843
7:46 AM	38.4889	133.2245	96.58155	471.2896	2455349	297.75	78.947146	303.32	22.0423	23.43843
7:47 AM	38.84328	135.8218	125.0954	475.4653	2455349	298	78.766475	303.47	22.0424	23.43843
7:48 AM	39.15188	138.6468	132.9792	480.3903	2455349	298.25	78.586089	303.62	22.0425	23.43843
7:49 AM	39.53193	141.4058	135.8887	484.3569	2455349	298.5	78.40599	303.76	22.0426	23.43843
7:50 AM	39.86282	144.4296	138.9948	490.379	2455349	298.75	78.226183	303.91	22.0427	23.43843
7:51 AM	40.14652	147.3359	142.0401	494.8281	2455349	299	78.04667	304.06	22.0427	23.43843
7:52 AM	40.43262	150.5524	145.3231	500.9829	2455349	299.25	77.867454	304.21	22.0428	23.43843
7:53 AM	40.82458	153.6774	148.4603	504.9587	2455349	299.5	77.688537	304.36	22.0429	23.43843
7:54 AM	41.1795	156.8383	151.6776	509.8531	2455349	299.75	77.509924	304.51	22.043	23.43843
7:55 AM	41.67306	159.5662	154.5189	511.9802	2455349	300	77.331616	304.66	22.0431	23.43843
7:56 AM	42.04174	162.5665	157.6165	516.5408	2455349	300.25	77.153617	304.81	22.0432	23.43843
7:57 AM	42.4219	165.2738	160.2772	518.719	2455349	300.5	76.97593	304.96	22.0433	23.43843
7:58 AM	42.73783	168.0276	163.0598	521.8836	2455349	300.75	76.798557	305.11	22.0434	23.43843
7:59 AM	43.03464	170.6833	165.7282	524.4133	2455349	301	76.621501	305.27	22.0435	23.43843
8:00 AM	43.35712	172.9184	168.0962	525.9966	2455349	301.25	76.444766	305.42	22.0436	23.43843

8:01 AM	43.57713	175.3849	170.469	527.3821	2455349	301.5	76.268354	305.57	22.0437	23.43843
8:02 AM	43.8499	178.01	173.263	530.8541	2455349	301.75	76.092268	305.73	22.0438	23.43843
8:03 AM	43.97728	180.6165	175.9697	535.9391	2455349	302	75.916511	305.88	22.0439	23.43843
8:04 AM	44.13087	183.3627	178.8692	538.9217	2455349	302.25	75.741086	306.04	22.044	23.43843
8:05 AM	44.36727	185.9828	181.4621	541.4235	2455349	302.5	75.565996	306.19	22.0441	23.43843
8:06 AM	44.71586	188.8758	184.2976	543.823	2455349	302.75	75.391244	306.35	22.0442	23.43843
8:07 AM	45.02457	191.9748	187.2365	548.3584	2455349	303	75.216832	306.51	22.0443	23.43843
8:08 AM	45.26141	194.9994	190.1798	552.3587	2455349	303.25	75.042764	306.67	22.0444	23.43843
8:09 AM	45.53746	198.2203	193.2502	555.7954	2455349	303.5	74.869043	306.82	22.0444	23.43843
8:10 AM	45.86758	201.004	195.8434	557.9631	2455349	303.75	74.695671	306.98	22.0445	23.43843
8:11 AM	46.07132	204.0134	198.7002	564.2637	2455349	304	74.522651	307.14	22.0446	23.43843
8:12 AM	46.0959	206.9389	201.5901	567.0154	2455349	304.25	74.349986	307.3	22.0447	23.43843
8:13 AM	46.36463	209.7534	204.3225	569.467	2455349	304.5	74.17768	307.46	22.0448	23.43843
8:14 AM	46.69585	212.8242	207.3155	572.2688	2455349	304.75	74.005735	307.62	22.0449	23.43843
8:15 AM	46.87446	216.0283	210.4641	577.6123	2455349	305	73.834155	307.78	22.045	23.43843
8:16 AM	47.08158	219.3138	213.6007	582.9093	2455349	305.25	73.662941	307.95	22.0451	23.43843
8:17 AM	47.28684	222.2578	216.3175	584.5026	2455349	305.5	73.492098	308.11	22.0452	23.43843
8:18 AM	47.52422	225.5141	219.3133	587.5697	2455349	305.75	73.321627	308.27	22.0453	23.43843
8:19 AM	47.81164	228.3194	221.8018	590.6935	2455349	306	73.151533	308.44	22.0454	23.43843
8:20 AM	48.0311	231.0238	224.2339	591.9432	2455349	306.25	72.981818	308.6	22.0455	23.43843
8:21 AM	48.23768	234.1239	226.9288	594.4648	2455349	306.5	72.812485	308.77	22.0456	23.43843
8:22 AM	48.60866	236.9285	229.2586	596.6074	2455349	306.75	72.643537	308.93	22.0457	23.43843
8:23 AM	48.86265	239.7356	229.6707	598.8411	2455349	307	72.474978	309.1	22.0458	23.43843
8:24 AM	48.97888	242.3634	212.9538	600.7123	2455349	307.25	72.306809	309.26	22.0459	23.43843
8:25 AM	49.16055	244.9043	152.3532	602.814	2455349	307.5	72.139035	309.43	22.046	23.43843
8:26 AM	49.46194	247.8034	80.69477	604.5724	2455349	307.75	71.971659	309.6	22.0461	23.43843
8:27 AM	49.67529	250.897	53.72729	609.3398	2455349	308	71.804683	309.77	22.0462	23.43843
8:28 AM	49.8161	253.7065	51.19288	612.4056	2455349	308.25	71.63811	309.94	22.0462	23.43843
8:29 AM	49.99132	256.5525	50.96787	614.1055	2455349	308.5	71.471945	310.11	22.0463	23.43843
8:30 AM	50.1589	259.3392	50.96704	615.9719	2455349	308.75	71.306189	310.28	22.0464	23.43843
8:31 AM	50.36974	261.9322	50.8752	617.313	2455349	309	71.140846	310.45	22.0465	23.43843
8:32 AM	50.54638	264.8317	50.79116	619.2752	2455349	309.25	70.975919	310.62	22.0466	23.43843
8:33 AM	50.78977	267.6608	50.96589	621.3995	2455349	309.5	70.811412	310.79	22.0467	23.43843
8:34 AM	50.94478	270.4659	50.98324	622.8884	2455349	309.75	70.647327	310.97	22.0468	23.43843
8:35 AM	51.27633	273.0998	51.31454	625.0783	2455349	310	70.483668	311.14	22.0469	23.43843
8:36 AM	51.57182	275.7106	51.48616	626.8787	2455349	310.25	70.320439	311.31	22.047	23.43843
8:37 AM	51.70138	277.6334	51.50652	627.7356	2455349	310.5	70.157641	311.49	22.0471	23.43843
8:38 AM	51.87879	280.2762	51.70993	629.5594	2455349	310.75	69.995278	311.66	22.0472	23.43843
8:39 AM	52.06439	283.0529	51.78909	633.2884	2455349	311	69.833355	311.84	22.0473	23.43843
8:40 AM	52.17757	286.2768	51.80166	634.4876	2455349	311.25	69.671873	312.02	22.0474	23.43843
8:41 AM	52.48333	289.3587	52.1609	636.8124	2455349	311.5	69.510837	312.19	22.0475	23.43843

8:42 AM	52.75403	292.8465	52.43318	639.6823	2455349	311.75	69.35025	312.37	22.0476	23.43843
8:43 AM	52.91789	296.555	52.51515	645.886	2455349	312	69.190114	312.55	22.0477	23.43843
8:44 AM	53.09585	299.2129	52.6101	646.0024	2455349	312.25	69.030434	312.73	22.0478	23.43843
8:45 AM	53.23993	301.6698	52.74983	646.8343	2455349	312.5	68.871213	312.91	22.0479	23.43843
8:46 AM	53.32503	304.6308	52.80582	651.2825	2455349	312.75	68.712454	313.09	22.0479	23.43843
8:47 AM	53.44476	307.4377	52.85392	654.9391	2455349	313	68.55416	313.27	22.048	23.43843
8:48 AM	53.39331	309.641	52.7651	657.52	2455349	313.25	68.396335	313.45	22.0481	23.43843
8:49 AM	53.32798	312.0421	52.7384	657.7206	2455349	313.5	68.238983	313.64	22.0482	23.43843
8:50 AM	53.40685	314.5036	52.85943	655.8493	2455349	313.75	68.082106	313.82	22.0483	23.43843
8:51 AM	53.73228	317.4949	53.233	657.8724	2455349	314	67.925709	314	22.0484	23.43843
8:52 AM	53.85616	319.4502	53.39672	657.6199	2455349	314.25	67.769795	314.19	22.0485	23.43843
8:53 AM	54.13516	322.4917	53.72771	659.1645	2455349	314.5	67.614367	314.37	22.0486	23.43843
8:54 AM	54.30449	325.4132	54.05671	661.1242	2455349	314.75	67.459429	314.56	22.0487	23.43843
8:55 AM	54.62882	327.7046	54.30178	662.6386	2455349	315	67.304985	314.75	22.0488	23.43843
8:56 AM	54.76461	329.9143	54.43039	663.5747	2455349	315.25	67.151037	314.93	22.0489	23.43843
8:57 AM	54.90127	332.275	54.65894	664.2335	2455349	315.5	66.99759	315.12	22.049	23.43843
8:58 AM	54.96955	334.4075	54.89154	665.0805	2455349	315.75	66.844647	315.31	22.0491	23.43843
8:59 AM	55.0576	336.6743	55.17006	666.7194	2455349	316	66.692213	315.5	22.0492	23.43843
9:00 AM	55.17754	339.4393	55.65739	669.1495	2455349	316.25	66.540289	315.69	22.0493	23.43843
9:01 AM	55.12795	342.1746	56.48578	672.864	2455349	316.5	66.388881	315.88	22.0494	23.43843
9:02 AM	55.00068	345.4123	60.20282	675.3953	2455349	316.75	66.237992	316.07	22.0495	23.43843
9:03 AM	54.93754	348.472	82.68886	680.796	2455349	317	66.087625	316.27	22.0496	23.43843
9:04 AM	54.85375	350.8649	159.1222	682.8135	2455349	317.25	65.937784	316.46	22.0496	23.43843
9:05 AM	54.78089	352.7903	271.2798	684.4501	2455349	317.5	65.788473	316.65	22.0497	23.43843
9:06 AM	54.60829	355.2138	332.7533	685.7647	2455349	317.75	65.639697	316.85	22.0498	23.43843
9:07 AM	54.77892	357.4419	342.9748	685.5198	2455349	318	65.491457	317.04	22.0499	23.43843
9:08 AM	54.78744	360.101	346.2179	690.2026	2455349	318.25	65.343759	317.24	22.05	23.43843
9:09 AM	54.8094	361.9991	348.378	692.436	2455349	318.5	65.196606	317.44	22.0501	23.43843
9:10 AM	54.85048	363.3532	349.9117	691.1286	2455349	318.75	65.050002	317.63	22.0502	23.43843
9:11 AM	54.98517	364.9042	351.6391	691.7709	2455349	319	64.903951	317.83	22.0503	23.43843
9:12 AM	54.92072	367.3733	354.4512	693.198	2455349	319.25	64.758457	318.03	22.0504	23.43843
9:13 AM	54.94999	369.8584	357.026	694.9828	2455349	319.5	64.613523	318.23	22.0505	23.43843
9:14 AM	54.9997	372.1267	359.5117	696.2735	2455349	319.75	64.469154	318.43	22.0506	23.43843
9:15 AM	55.0175	374.5668	362.2767	701.1979	2455349	320	64.325353	318.63	22.0507	23.43843
9:16 AM	54.83737	376.8382	364.721	700.9399	2455349	320.25	64.182124	318.84	22.0508	23.43843
9:17 AM	54.96562	380.3795	368.3056	701.9008	2455349	320.5	64.039471	319.04	22.0509	23.43843
9:18 AM	55.1499	382.5135	370.4446	703.2952	2455349	320.75	63.897399	319.24	22.051	23.43843
9:19 AM	55.20747	385.7032	373.5632	708.0308	2455349	321	63.755911	319.45	22.0511	23.43843
9:20 AM	55.06055	388.5695	376.3815	713.0828	2455349	321.25	63.615012	319.65	22.0512	23.43843
9:21 AM	54.99391	391.0467	378.9382	717.3132	2455349	321.5	63.474705	319.86	22.0513	23.43843
9:22 AM	54.95546	393.8372	381.8322	722.7861	2455349	321.75	63.334994	320.06	22.0513	23.43843

9:23 AM	54.64521	396.0625	383.872	725.4598	2455349	322	63.195883	320.27	22.0514	23.43843
9:24 AM	54.64412	397.6503	385.9715	727.9236	2455349	322.25	63.057377	320.48	22.0515	23.43843
9:25 AM	54.5233	399.9787	388.3376	728.8074	2455349	322.5	62.91948	320.69	22.0516	23.43843
9:26 AM	54.46737	401.9289	390.326	732.0228	2455349	322.75	62.782195	320.9	22.0517	23.43843
9:27 AM	54.34993	404.0159	392.6183	733.0394	2455349	323	62.645527	321.11	22.0518	23.43843
9:28 AM	54.17526	406.0858	395.1457	734.9791	2455349	323.25	62.50948	321.32	22.0519	23.43843
9:29 AM	53.86217	406.7472	396.1338	736.5826	2455349	323.5	62.374058	321.53	22.052	23.43843
9:30 AM	53.7006	408.7237	398.4093	739.5666	2455349	323.75	62.239266	321.74	22.0521	23.43843
9:31 AM	53.66062	412.484	402.6687	746.5908	2455349	324	62.105107	321.96	22.0522	23.43843
9:32 AM	53.65822	414.5412	405.0431	748.1035	2455349	324.25	61.971585	322.17	22.0523	23.43843
9:33 AM	53.88981	415.3401	405.9352	748.0802	2455349	324.5	61.838706	322.39	22.0524	23.43843
9:34 AM	53.84491	416.2798	406.9356	747.3829	2455349	324.75	61.706473	322.6	22.0525	23.43843
9:35 AM	53.91887	419.1053	409.9691	747.6455	2455349	325	61.57489	322.82	22.0526	23.43843
9:36 AM	54.04297	420.743	411.3405	748.4727	2455349	325.25	61.443962	323.04	22.0527	23.43843
9:37 AM	54.02844	422.4743	412.9005	747.3528	2455349	325.5	61.313693	323.25	22.0528	23.43843
9:38 AM	54.1793	426.0504	416.246	752.6581	2455349	325.75	61.184088	323.47	22.0529	23.43843
9:39 AM	54.1628	427.7094	417.3951	753.9952	2455349	326	61.05515	323.69	22.0529	23.43843
9:40 AM	54.13921	429.924	418.3425	755.3923	2455349	326.25	60.926884	323.91	22.053	23.43843
9:41 AM	53.95994	432.339	411.6602	757.6521	2455349	326.5	60.799294	324.13	22.0531	23.43843
9:42 AM	53.71568	434.2328	366.1304	759.1444	2455349	326.75	60.672385	324.36	22.0532	23.43843
9:43 AM	53.4913	436.5934	250.5758	762.8926	2455349	327	60.546161	324.58	22.0533	23.43843
9:44 AM	53.53674	438.5459	120.3298	763.936	2455349	327.25	60.420626	324.8	22.0534	23.43843
9:45 AM	53.4239	439.0014	62.99092	763.597	2455349	327.5	60.295785	325.03	22.0535	23.43843
9:46 AM	53.1367	440.6468	54.03521	766.2234	2455349	327.75	60.171642	325.25	22.0536	23.43843
9:47 AM	52.9097	443.3329	52.58776	768.0128	2455349	328	60.048202	325.48	22.0537	23.43843
9:48 AM	52.8518	446.3659	52.14427	770.6558	2455349	328.25	59.925468	325.71	22.0538	23.43843
9:49 AM	52.85988	450.0426	51.82742	773.36	2455349	328.5	59.803446	325.93	22.0539	23.43843
9:50 AM	52.90828	452.9351	51.58609	775.9855	2455349	328.75	59.68214	326.16	22.054	23.43843
9:51 AM	52.99349	453.7207	51.43587	774.5914	2455349	329	59.561554	326.39	22.0541	23.43843
9:52 AM	53.02812	454.1349	51.23309	773.5144	2455349	329.25	59.441693	326.62	22.0542	23.43843
9:53 AM	52.95187	454.7568	50.88227	772.7003	2455349	329.5	59.322561	326.85	22.0543	23.43843
9:54 AM	52.87015	455.3354	50.63076	771.0049	2455349	329.75	59.204163	327.08	22.0544	23.43843
9:55 AM	52.96552	457.7749	50.69382	772.3694	2455349	330	59.086503	327.31	22.0545	23.43843
9:56 AM	53.01501	461.025	50.72924	774.3996	2455349	330.25	58.969586	327.55	22.0546	23.43843
9:57 AM	52.97918	464.5576	50.66338	777.1843	2455349	330.5	58.853416	327.78	22.0546	23.43843
9:58 AM	52.70214	465.7851	50.30258	777.6742	2455349	330.75	58.737998	328.02	22.0547	23.43843
9:59 AM	52.18729	467.0152	49.81089	780.5815	2455349	331	58.623336	328.25	22.0548	23.43843
10:00 AM	51.85214	467.2303	49.24596	778.1244	2455349	331.25	58.509434	328.49	22.0549	23.43843
10:01 AM	51.87508	468.6258	49.10072	778.2072	2455349	331.5	58.396298	328.73	22.055	23.43843
10:02 AM	51.82035	470.5376	48.89731	780.476	2455349	331.75	58.283931	328.96	22.0551	23.43843

10:03 AM	51.86568	472.7604	48.87529	782.1838	2455349	332	58.172339	329.2	22.0552	23.43843
10:04 AM	51.8375	474.8468	48.81078	784.4553	2455349	332.25	58.061525	329.44	22.0553	23.43843
10:05 AM	51.72968	476.2568	48.50494	786.2301	2455349	332.5	57.951495	329.68	22.0554	23.43843
10:06 AM	51.60449	476.5438	48.17157	785.2018	2455349	332.75	57.842253	329.92	22.0555	23.43843
10:07 AM	51.56134	476.1017	48.19473	781.849	2455349	333	57.733803	330.17	22.0556	23.43843
10:08 AM	51.57947	477.7114	48.41788	782.2294	2455349	333.25	57.62615	330.41	22.0557	23.43843
10:09 AM	51.45734	477.8592	48.54857	779.2651	2455349	333.5	57.519299	330.65	22.0558	23.43843
10:10 AM	51.42522	480.5391	48.84641	780.7066	2455349	333.75	57.413253	330.9	22.0559	23.43843
10:11 AM	51.45657	484.2899	49.1322	785.1407	2455349	334	57.308018	331.14	22.056	23.43843
10:12 AM	51.51567	485.6951	49.23723	786.4836	2455349	334.25	57.203598	331.39	22.0561	23.43843
10:13 AM	51.54539	485.2088	49.47253	783.3865	2455349	334.5	57.099998	331.63	22.0562	23.43843
10:14 AM	51.52977	486.1381	49.71001	783.6587	2455349	334.75	56.997222	331.88	22.0562	23.43843
10:15 AM	51.71373	488.2821	50.01232	784.4695	2455349	335	56.895274	332.13	22.0563	23.43843
10:16 AM	52.02037	490.6594	50.5329	785.1043	2455349	335.25	56.79416	332.38	22.0564	23.43843
10:17 AM	52.27337	493.2794	51.12899	785.4397	2455349	335.5	56.693883	332.63	22.0565	23.43843
10:18 AM	52.24857	493.5752	51.89557	784.7866	2455349	335.75	56.594449	332.88	22.0566	23.43843
10:19 AM	52.3837	492.9164	56.23822	781.2196	2455349	336	56.495861	333.13	22.0567	23.43843
10:20 AM	52.14337	494.5683	82.107	781.6348	2455349	336.25	56.398124	333.38	22.0568	23.43843
10:21 AM	51.9333	494.8121	168.1859	781.3058	2455349	336.5	56.301243	333.63	22.0569	23.43843
10:22 AM	51.6307	496.0265	315.7944	779.9255	2455349	336.75	56.205222	333.89	22.057	23.43843
10:23 AM	51.56909	498.4471	439.1783	780.6922	2455349	337	56.110066	334.14	22.0571	23.43843
10:24 AM	51.40512	501.8438	484.0216	783.6611	2455349	337.25	56.015779	334.4	22.0572	23.43843
10:25 AM	51.22771	488.6323	490.923	793.4189	2455349	337.5	55.922365	334.65	22.0573	23.43843
10:26 AM	50.7701	508.8047	493.1174	811.4994	2455349	337.75	55.829829	334.91	22.0574	23.43843
10:27 AM	50.5064	510.8015	495.9304	812.7113	2455349	338	55.738176	335.17	22.0575	23.43843
10:28 AM	50.53261	513.9455	499.6324	815.9921	2455349	338.25	55.64741	335.42	22.0576	23.43843
10:29 AM	50.68774	516.8075	503.145	819.7597	2455349	338.5	55.557534	335.68	22.0577	23.43843
10:30 AM	50.56014	519.1713	506.2842	824.595	2455349	338.75	55.468554	335.94	22.0578	23.43843
10:31 AM	50.62285	520.6397	508.3987	827.1079	2455349	339	55.380475	336.2	22.0578	23.43843
10:32 AM	50.81347	521.7474	509.9968	827.7837	2455349	339.25	55.293299	336.46	22.0579	23.43843
10:33 AM	51.04288	521.03	509.7455	824.5702	2455349	339.5	55.207032	336.72	22.058	23.43843
10:34 AM	51.18249	519.3919	508.2922	818.3383	2455349	339.75	55.121678	336.99	22.0581	23.43843
10:35 AM	51.40884	520.0493	509.317	817.4486	2455349	340	55.037241	337.25	22.0582	23.43843

10:36 AM	51.58887	523.655	513.0481	821.7992	2455349	340.25	54.953725	337.51	22.0583	23.43843
10:37 AM	51.98268	526.9164	516.4743	824.4458	2455349	340.5	54.871135	337.78	22.0584	23.43843
10:38 AM	52.07619	529.3523	519.1147	825.8645	2455349	340.75	54.789475	338.04	22.0585	23.43843
10:39 AM	51.92271	530.3436	520.2095	825.3116	2455349	341	54.70875	338.31	22.0586	23.43843
10:40 AM	51.71067	529.9096	520.0263	823.804	2455349	341.25	54.628962	338.58	22.0587	23.43843
10:41 AM	51.56582	531.4347	521.6358	826.1597	2455349	341.5	54.550117	338.84	22.0588	23.43843
10:42 AM	51.33848	531.9115	522.1578	825.4913	2455349	341.75	54.472219	339.11	22.0589	23.43843
10:43 AM	51.3197	534.1988	524.4129	828.0997	2455349	342	54.395272	339.38	22.059	23.43843
10:44 AM	51.34821	536.7233	526.8264	831.7244	2455349	342.25	54.319279	339.65	22.0591	23.43843
10:45 AM	51.62339	539.3295	529.5002	833.9202	2455349	342.5	54.244245	339.92	22.0592	23.43843
10:46 AM	51.90785	541.2858	531.3368	836.2424	2455349	342.75	54.170174	340.19	22.0593	23.43843
10:47 AM	52.14796	542.7242	532.7702	835.7234	2455349	343	54.09707	340.46	22.0594	23.43843
10:48 AM	52.85792	544.4612	534.418	835.4158	2455349	343.25	54.024936	340.73	22.0594	23.43843
10:49 AM	53.76801	545.1623	535.1133	832.8693	2455349	343.5	53.953778	341	22.0595	23.43843
10:50 AM	54.24976	546.6412	536.5188	834.0821	2455349	343.75	53.883598	341.28	22.0596	23.43843
10:51 AM	54.48463	547.0403	536.6348	832.7591	2455349	344	53.8144	341.55	22.0597	23.43843
10:52 AM	54.31902	547.3025	536.7635	831.5072	2455349	344.25	53.746189	341.83	22.0598	23.43843
10:53 AM	54.25839	549.1587	538.4134	832.3985	2455349	344.5	53.678968	342.1	22.0599	23.43843
10:54 AM	54.53488	551.8618	540.8946	836.0829	2455349	344.75	53.612741	342.38	22.06	23.43843
10:55 AM	54.74823	553.2625	541.8736	837.6131	2455349	345	53.547512	342.65	22.0601	23.43843
10:56 AM	55.07278	552.6012	540.2853	836.044	2455349	345.25	53.483284	342.93	22.0602	23.43843
10:57 AM	55.74658	553.0497	536.3705	833.9802	2455349	345.5	53.420061	343.21	22.0603	23.43843
10:58 AM	55.99204	551.463	507.9137	827.7525	2455349	345.75	53.357846	343.48	22.0604	23.43843
10:59 AM	55.77597	552.1684	420.6909	826.2934	2455349	346	53.296644	343.76	22.0605	23.43843
11:00 AM	57.28863	556.2677	272.8772	826.4166	2455349	346.25	53.236457	344.04	22.0606	23.43843
11:01 AM	59.4315	560.8521	135.323	830.0495	2455349	346.5	53.177289	344.32	22.0607	23.43843
11:02 AM	60.84584	563.7968	74.02736	830.7008	2455349	346.75	53.119144	344.6	22.0608	23.43843
11:03 AM	61.47136	566.9474	62.86355	833.2653	2455349	347	53.062025	344.88	22.0609	23.43843
11:04 AM	61.69126	565.4843	61.7393	828.9	2455349	347.25	53.005934	345.16	22.061	23.43843
11:05 AM	62.74576	566.7653	62.57942	826.1479	2455349	347.5	52.950877	345.45	22.061	23.43843
11:06 AM	63.96129	567.8324	63.4075	825.4152	2455349	347.75	52.896855	345.73	22.0611	23.43843
11:07 AM	64.83227	566.7418	63.61205	824.357	2455349	348	52.843873	346.01	22.0612	23.43843
11:08 AM	66.95799	566.3765	65.29002	821.2927	2455349	348.25	52.791932	346.29	22.0613	23.43843

11:09 AM	71.79748	570.2477	69.76668	818.9257	2455349	348.5	52.741037	346.58	22.0614	23.43843
11:10 AM	78.39094	574.8232	76.07703	813.3187	2455349	348.75	52.69119	346.86	22.0615	23.43843
11:11 AM	84.23468	578.8767	81.69883	807.2436	2455349	349	52.642395	347.15	22.0616	23.43843
11:12 AM	88.73235	584.8731	86.06661	808.74	2455349	349.25	52.594654	347.43	22.0617	23.43843
11:13 AM	92.39531	590.9637	89.47065	810.3665	2455349	349.5	52.54797	347.72	22.0618	23.43843
11:14 AM	97.11878	598.94	93.77704	812.9543	2455349	349.75	52.502346	348	22.0619	23.43843
11:15 AM	97.02145	600.7759	93.50403	818.3147	2455349	350	52.457785	348.29	22.062	23.43843
11:16 AM	95.0491	596.7495	91.90522	813.2181	2455349	350.25	52.414289	348.58	22.0621	23.43843
11:17 AM	90.93607	594.1279	89.0523	812.1681	2455349	350.5	52.371861	348.86	22.0622	23.43843
11:18 AM	85.46998	592.1723	84.53845	814.4352	2455349	350.75	52.330505	349.15	22.0623	23.43843
11:19 AM	82.77642	591.7036	82.10783	815.0184	2455349	351	52.290222	349.44	22.0624	23.43843
11:20 AM	82.14555	586.1884	81.62933	806.9545	2455349	351.25	52.251014	349.73	22.0625	23.43843
11:21 AM	82.33967	586.3555	81.18958	806.6958	2455349	351.5	52.212885	350.02	22.0626	23.43843
11:22 AM	83.2018	588.85	81.29824	809.0814	2455349	351.75	52.175837	350.31	22.0626	23.43843
11:23 AM	86.06654	592.1226	83.95544	808.8013	2455349	352	52.139872	350.6	22.0627	23.43843
11:24 AM	88.89304	596.6969	86.91505	812.6224	2455349	352.25	52.104992	350.89	22.0628	23.43843
11:25 AM	91.89237	600.68	90.09812	807.4952	2455349	352.5	52.0712	351.18	22.0629	23.43843
11:26 AM	94.41616	597.8555	92.88383	794.6575	2455349	352.75	52.038497	351.47	22.063	23.43843
11:27 AM	96.43636	601.424	94.92425	796.3314	2455349	353	52.006886	351.76	22.0631	23.43843
11:28 AM	96.73251	603.8272	95.3586	801.5728	2455349	353.25	51.976368	352.05	22.0632	23.43843
11:29 AM	95.32581	602.403	93.95126	801.5474	2455349	353.5	51.946947	352.34	22.0633	23.43843
11:30 AM	92.77809	598.5324	91.65631	804.0091	2455349	353.75	51.918623	352.64	22.0634	23.43843
11:31 AM	89.1195	596.0155	87.68069	806.4795	2455349	354	51.891398	352.93	22.0635	23.43843
11:32 AM	87.45314	592.6902	86.00937	804.1882	2455349	354.25	51.865274	353.22	22.0636	23.43843
11:33 AM	87.80872	592.3208	86.77512	802.464	2455349	354.5	51.840253	353.51	22.0637	23.43843
11:34 AM	88.18669	592.6412	87.90259	798.1442	2455349	354.75	51.816336	353.81	22.0638	23.43843
11:35 AM	87.19664	592.165	91.03704	798.3351	2455349	355	51.793525	354.1	22.0639	23.438431
11:36 AM	86.56632	592.4304	112.5664	802.8939	2455349	355.25	51.771822	354.39	22.064	23.438431
11:37 AM	87.81014	595.4779	185.9976	807.001	2455349	355.5	51.751228	354.69	22.0641	23.438431
11:38 AM	89.45247	596.0957	320.1063	805.8568	2455349	355.75	51.731743	354.98	22.0642	23.438431
11:39 AM	88.6585	593.4979	463.3306	800.399	2455349	356	51.71337	355.27	22.0642	23.438431
11:40 AM	88.49224	593.6271	549.3182	800.4012	2455349	356.25	51.696109	355.57	22.0643	23.438431
11:41 AM	88.01256	591.4978	570.2772	797.0729	2455349	356.5	51.679963	355.86	22.0644	23.438431

11:42 AM	87.247	590.4351	571.8324	799.4072	2455349	356.75	51.66493	356.16	22.0645	23.438431
11:43 AM	86.08784	588.9477	570.8678	797.4916	2455349	357	51.651014	356.45	22.0646	23.438431
11:44 AM	84.13887	588.8979	571.2073	800.146	2455349	357.25	51.638214	356.75	22.0647	23.438431
11:45 AM	83.30515	589.4607	572.3023	803.344	2455349	357.5	51.626532	357.04	22.0648	23.438431
11:46 AM	83.99402	591.1274	574.3245	803.793	2455349	357.75	51.615968	357.34	22.0649	23.438431
11:47 AM	83.65843	592.3626	575.9687	806.0245	2455349	358	51.606523	357.63	22.065	23.438431
11:48 AM	84.10097	594.7516	578.5468	810.1582	2455349	358.25	51.598197	357.93	22.0651	23.438431
11:49 AM	83.92891	597.0759	581.2045	812.4457	2455349	358.5	51.590992	358.22	22.0652	23.438431
11:50 AM	83.39636	596.7479	581.1507	811.0797	2455349	358.75	51.584907	358.52	22.0653	23.438431
11:51 AM	82.81105	596.1526	580.7248	813.2599	2455349	359	51.579943	358.81	22.0654	23.438431
11:52 AM	83.95884	598.4909	583.0897	815.0051	2455349	359.25	51.5761	359.11	22.0655	23.438431
11:53 AM	88.47192	601.7055	585.9802	811.8473	2455349	359.5	51.573379	359.41	22.0656	23.438431
11:54 AM	93.39082	600.9393	584.7659	798.8301	2455349	359.75	51.57178	359.7	22.0657	23.438431
11:55 AM	95.62732	599.2117	582.4783	792.9532	2455349	180	51.571302	359.93	22.0657	23.438431
11:56 AM	98.17536	595.5021	578.6468	784.3442	2455349	0.2476	51.571946	359.71	22.0658	23.438431
11:57 AM	100.4032	593.7483	576.9106	778.2588	2455349	0.4976	51.573712	359.41	22.0659	23.438431
11:58 AM	103.0478	597.7396	580.8445	780.4359	2455349	0.7476	51.5766	359.12	22.066	23.438431
11:59 AM	102.0711	600.437	583.4141	785.2254	2455349	0.9975	51.580609	358.82	22.0661	23.438431
12:00 PM	99.02067	597.1363	580.0249	782.7538	2455349	1.2475	51.58574	358.52	22.0662	23.438431
12:01 PM	99.44136	595.4751	578.1031	780.2425	2455349	1.4975	51.591991	358.23	22.0663	23.438431
12:02 PM	98.56667	590.7124	573.1978	773.086	2455349	1.7475	51.599363	357.93	22.0664	23.438431
12:03 PM	94.17288	584.6814	567.1538	771.9787	2455349	1.9974	51.607855	357.64	22.0665	23.438431
12:04 PM	89.17893	582.5915	564.8589	777.304	2455349	2.2474	51.617466	357.34	22.0666	23.438431
12:05 PM	87.18375	583.5451	565.8258	781.0539	2455349	2.4974	51.628196	357.05	22.0667	23.438431
12:06 PM	85.58981	579.5465	561.4046	777.0925	2455349	2.7474	51.640044	356.75	22.0668	23.438431
12:07 PM	84.55967	575.4835	557.0329	770.0538	2455349	2.9973	51.65301	356.46	22.0669	23.438431
12:08 PM	82.31313	572.1851	553.1357	763.9839	2455349	3.2473	51.667092	356.16	22.067	23.438431
12:09 PM	80.49263	567.5146	547.6328	760.3298	2455349	3.4973	51.682289	355.87	22.0671	23.438431
12:10 PM	80.98574	568.5747	547.9583	764.9436	2455349	3.7473	51.698602	355.57	22.0672	23.438431
12:11 PM	82.11485	568.286	547.4327	765.4991	2455349	3.9972	51.716027	355.28	22.0672	23.438431
12:12 PM	82.92695	564.8568	543.4405	759.6058	2455349	4.2472	51.734565	354.99	22.0673	23.438431
12:13 PM	83.72114	565.3747	538.7798	756.7422	2455349	4.4972	51.754215	354.69	22.0674	23.438431
12:14 PM	85.44234	564.6608	510.4348	752.6452	2455349	4.7472	51.774974	354.4	22.0675	23.438431

12:15 PM	86.33298	565.74	434.3915	753.9567	2455349	4.9971	51.796842	354.11	22.0676	23.438431
12:16 PM	86.67753	565.8944	310.0115	754.1012	2455349	5.2471	51.819817	353.81	22.0677	23.438431
12:17 PM	87.24853	567.7162	185.6889	757.1321	2455349	5.4971	51.843897	353.52	22.0678	23.438431
12:18 PM	86.95117	564.1967	112.4827	752.8257	2455349	5.747	51.869082	353.23	22.0679	23.438431
12:19 PM	84.78951	559.7089	90.31618	748.5073	2455349	5.997	51.895369	352.93	22.068	23.438431
12:20 PM	83.63516	560.6899	86.6035	753.0535	2455349	6.247	51.922757	352.64	22.0681	23.438431
12:21 PM	84.03258	569.6363	86.13497	767.0917	2455349	6.497	51.951244	352.35	22.0682	23.438431
12:22 PM	84.52591	574.9799	85.76379	775.6295	2455349	6.7469	51.980828	352.06	22.0683	23.438431
12:23 PM	83.9666	575.7797	84.70352	778.1786	2455349	6.9969	52.011508	351.77	22.0684	23.438431
12:24 PM	82.31509	572.773	82.72938	777.4776	2455349	7.2469	52.043281	351.48	22.0685	23.438431
12:25 PM	81.63977	571.2749	81.6339	778.5412	2455349	7.4969	52.076145	351.18	22.0686	23.438431
12:26 PM	81.76168	569.4073	81.39278	775.4231	2455349	7.7468	52.110098	350.89	22.0687	23.438431
12:27 PM	80.87956	567.5909	80.37345	773.0304	2455349	7.9968	52.145139	350.6	22.0687	23.438431
12:28 PM	78.07774	566.6024	77.1509	775.463	2455349	8.2468	52.181265	350.31	22.0688	23.438431
12:29 PM	75.56356	564.7483	74.4429	777.8081	2455349	8.4968	52.218473	350.03	22.0689	23.438431
12:30 PM	74.99573	562.555	73.73492	776.071	2455349	8.7467	52.256762	349.74	22.069	23.438431
12:31 PM	74.811	559.8933	73.60039	769.8227	2455349	8.9967	52.296129	349.45	22.0691	23.438431
12:32 PM	74.74316	557.2123	73.69866	767.5261	2455349	9.2467	52.336571	349.16	22.0692	23.438431
12:33 PM	75.17827	555.1894	73.99328	765.7239	2455349	9.4967	52.378086	348.87	22.0693	23.438431
12:34 PM	75.60354	555.2568	74.37351	766.7511	2455349	9.7466	52.420671	348.58	22.0694	23.438431
12:35 PM	76.0865	553.0929	74.79944	762.3956	2455349	9.9966	52.464325	348.3	22.0695	23.438431
12:36 PM	76.11064	548.0169	74.85502	753.935	2455349	10.247	52.509043	348.01	22.0696	23.438431
12:37 PM	75.89248	542.0431	74.66293	746.2194	2455349	10.497	52.554824	347.73	22.0697	23.438431
12:38 PM	75.93454	540.6138	74.70449	745.2178	2455349	10.747	52.601664	347.44	22.0698	23.438431
12:39 PM	75.98283	541.5742	74.88463	748.0388	2455349	10.996	52.649562	347.15	22.0699	23.438431
12:40 PM	76.19181	540.3105	75.15743	745.62	2455349	11.246	52.698513	346.87	22.07	23.438431
12:41 PM	76.7048	533.2227	75.88682	733.6185	2455349	11.496	52.748514	346.59	22.0701	23.438431
12:42 PM	77.88166	526.6461	77.2043	721.6908	2455349	11.746	52.799564	346.3	22.0702	23.438431
12:43 PM	78.30191	528.4696	77.81131	723.7675	2455349	11.996	52.851658	346.02	22.0702	23.438431
12:44 PM	78.037	530.5075	77.79229	728.3652	2455349	12.246	52.904794	345.74	22.0703	23.438431
12:45 PM	77.54913	532.3405	77.60187	733.3401	2455349	12.496	52.958969	345.45	22.0704	23.438431
12:46 PM	77.04017	534.494	77.40937	738.75	2455349	12.746	53.014179	345.17	22.0705	23.438431
12:47 PM	76.93912	536.4419	77.59242	744.4354	2455349	12.996	53.070421	344.89	22.0706	23.438431

12:48 PM	77.03351	539.1377	78.01845	749.9909	2455349	13.246	53.127691	344.61	22.0707	23.438431
12:49 PM	76.6173	538.534	77.98656	750.4932	2455349	13.496	53.185987	344.33	22.0708	23.438431
12:50 PM	75.27571	540.6796	77.50027	758.3218	2455349	13.746	53.245305	344.05	22.0709	23.438431
12:51 PM	74.29735	542.0859	83.65344	764.2698	2455349	13.996	53.305642	343.77	22.071	23.438431
12:52 PM	73.79801	543.5784	116.8841	770.4972	2455349	14.246	53.366994	343.49	22.0711	23.438431
12:53 PM	72.87153	542.1745	197.8365	770.4655	2455349	14.496	53.429357	343.22	22.0712	23.438431
12:54 PM	72.31025	541.4165	317.2182	769.2943	2455349	14.746	53.492728	342.94	22.0713	23.438431
12:55 PM	71.80392	540.2159	433.1262	770.284	2455349	14.996	53.557103	342.66	22.0714	23.438431
12:56 PM	70.92803	537.6818	498.9398	771.8105	2455349	15.246	53.62248	342.39	22.0715	23.438431
12:57 PM	70.15023	536.5879	516.4096	772.6224	2455349	15.496	53.688853	342.11	22.0716	23.438431
12:58 PM	69.73806	536.1532	517.7959	773.4503	2455349	15.746	53.756219	341.83	22.0717	23.438431
12:59 PM	69.74986	534.7547	516.964	773.1076	2455349	15.996	53.824575	341.56	22.0717	23.438431
1:00 PM	70.69829	536.5765	519.1811	776.2225	2455349	16.246	53.893917	341.29	22.0718	23.438431
1:01 PM	70.51127	537.1128	520.4558	778.4927	2455349	16.496	53.964241	341.01	22.0719	23.438431
1:02 PM	69.26592	538.7792	522.5854	786.2428	2455349	16.746	54.035543	340.74	22.072	23.438431
1:03 PM	68.5185	536.0098	520.3852	785.7199	2455349	16.996	54.107818	340.47	22.0721	23.438431
1:04 PM	67.28527	535.2633	520.0781	788.19	2455349	17.246	54.181064	340.2	22.0722	23.438431
1:05 PM	66.25688	536.7125	521.797	793.0289	2455349	17.496	54.255277	339.93	22.0723	23.438431
1:06 PM	65.95592	537.6577	522.8512	796.5012	2455349	17.746	54.330451	339.66	22.0724	23.438431
1:07 PM	65.70641	536.7039	522.0883	795.1262	2455349	17.996	54.406584	339.39	22.0725	23.438431
1:08 PM	65.18588	533.988	519.4449	794.1407	2455349	18.246	54.483671	339.12	22.0726	23.438431
1:09 PM	64.65431	531.1554	516.7737	791.2609	2455349	18.496	54.561707	338.85	22.0727	23.438431
1:10 PM	64.4142	530.6259	516.1567	791.8828	2455349	18.746	54.64069	338.59	22.0728	23.438431
1:11 PM	64.26662	527.6301	513.175	789.7452	2455349	18.996	54.720615	338.32	22.0729	23.438431
1:12 PM	64.10385	524.9197	510.2976	785.7157	2455349	19.246	54.801477	338.05	22.073	23.438431
1:13 PM	63.97046	520.8637	506.3032	777.7362	2455349	19.496	54.883273	337.79	22.0731	23.438431
1:14 PM	63.85128	518.8972	504.1318	776.4767	2455349	19.746	54.965998	337.52	22.0732	23.438431
1:15 PM	63.57152	514.5039	499.5847	771.2109	2455349	19.996	55.049648	337.26	22.0732	23.438431
1:16 PM	63.36756	513.588	498.6744	772.5559	2455349	20.246	55.134219	337	22.0733	23.438431
1:17 PM	63.16962	512.16	497.2317	772.3538	2455349	20.495	55.219706	336.74	22.0734	23.438431
1:18 PM	62.99538	509.7842	494.8399	771.0592	2455349	20.745	55.306106	336.47	22.0735	23.438431
1:19 PM	62.80453	508.8031	493.7866	770.4427	2455349	20.995	55.393413	336.21	22.0736	23.438431
1:20 PM	62.84528	509.7777	494.7329	773.4349	2455349	21.245	55.481624	335.95	22.0737	23.438431
1:21 PM	62.77897	509.7186	494.6176	775.7287	2455349	21.495	55.570734	335.69	22.0738	23.438431
1:22 PM	62.44087	507.4673	491.9999	774.5678	2455349	21.745	55.660739	335.44	22.0739	23.438431
1:23 PM	62.08802	507.5907	491.8577	778.0278	2455349	21.995	55.751634	335.18	22.074	23.438431
1:24 PM	61.74675	507.8406	491.8318	780.5837	2455349	22.245	55.843416	334.92	22.0741	23.438431
1:25 PM	61.26183	506.6712	490.261	781.2822	2455349	22.495	55.936079	334.66	22.0742	23.438431

1:26 PM	60.61228	505.0446	488.2237	781.9857	2455349	22.745	56.029619	334.41	22.0743	23.438431
1:27 PM	60.07536	501.5877	484.5114	778.0801	2455349	22.995	56.124033	334.15	22.0744	23.438431
1:28 PM	59.62584	499.6342	481.2934	777.1721	2455349	23.245	56.219314	333.9	22.0745	23.438431
1:29 PM	59.24863	496.9529	466.7684	776.2147	2455349	23.495	56.31546	333.65	22.0746	23.438431
1:30 PM	59.04686	495.7703	419.3563	777.4104	2455349	23.745	56.412464	333.39	22.0747	23.438431
1:31 PM	58.90201	495.3819	327.9978	779.9763	2455349	23.995	56.510324	333.14	22.0747	23.438431
1:32 PM	58.83712	494.5627	214.5098	781.1684	2455349	24.245	56.609034	332.89	22.0748	23.438431
1:33 PM	59.08094	493.918	117.898	780.3897	2455349	24.495	56.708591	332.64	22.0749	23.438431
1:34 PM	59.21771	492.249	70.64711	779.0997	2455349	24.745	56.808988	332.39	22.075	23.438431
1:35 PM	59.38136	490.5023	61.04326	775.7886	2455349	24.995	56.910223	332.14	22.0751	23.438431
1:36 PM	59.61786	488.3904	60.29715	772.8025	2455349	25.245	57.01229	331.89	22.0752	23.438431
1:37 PM	59.5828	485.7734	59.83226	770.7555	2455349	25.495	57.115185	331.65	22.0753	23.438431
1:38 PM	59.39905	484.2419	59.7184	768.4664	2455349	25.745	57.218903	331.4	22.0754	23.438431
1:39 PM	59.24284	481.7681	58.75174	767.7751	2455349	25.995	57.32344	331.16	22.0755	23.438431
1:40 PM	58.73181	479.0316	57.74238	765.7181	2455349	26.245	57.428791	330.91	22.0756	23.438431
1:41 PM	58.18462	476.9299	56.9033	765.0742	2455349	26.495	57.534953	330.67	22.0757	23.438431
1:42 PM	57.64224	474.5492	56.06223	764.233	2455349	26.745	57.641919	330.42	22.0758	23.438431
1:43 PM	57.38115	472.3612	55.64285	762.7358	2455349	26.995	57.749687	330.18	22.0759	23.438431
1:44 PM	57.33341	474.1235	55.35768	768.2615	2455349	27.245	57.85825	329.94	22.076	23.438431
1:45 PM	57.36662	475.7369	55.26262	773.3986	2455349	27.495	57.967605	329.7	22.0761	23.438431
1:46 PM	57.33877	474.6391	55.13848	772.9798	2455349	27.745	58.077747	329.46	22.0761	23.438431
1:47 PM	57.52076	471.4006	55.23904	769.5481	2455349	27.995	58.188672	329.22	22.0762	23.438431
1:48 PM	57.70232	470.4894	55.26003	771.4852	2455349	28.245	58.300375	328.98	22.0763	23.438431
1:49 PM	57.61908	470.6629	55.0776	773.5649	2455349	28.495	58.412851	328.74	22.0764	23.438431
1:50 PM	57.52317	467.5239	54.9839	769.4103	2455349	28.745	58.526097	328.51	22.0765	23.438431
1:51 PM	57.55812	464.5855	55.07074	765.6225	2455349	28.995	58.640107	328.27	22.0766	23.438431
1:52 PM	56.98188	461.4481	54.65146	763.8955	2455349	29.245	58.754876	328.03	22.0767	23.438431
1:53 PM	56.43338	459.4766	54.051	765.7483	2455349	29.495	58.870402	327.8	22.0768	23.438431
1:54 PM	56.31256	458.3815	53.83388	766.9833	2455349	29.745	58.986678	327.57	22.0769	23.438431
1:55 PM	56.46375	456.8924	53.9736	765.7381	2455349	29.994	59.103701	327.33	22.077	23.438431
1:56 PM	56.37646	455.1773	53.90421	765.7506	2455349	30.244	59.221465	327.1	22.0771	23.438431
1:57 PM	56.04055	450.875	53.741	759.8293	2455349	30.494	59.339967	326.87	22.0772	23.438431
1:58 PM	55.96178	446.4376	53.81871	753.7501	2455349	30.744	59.459202	326.64	22.0773	23.438431
1:59 PM	56.22702	444.8675	54.35362	752.5569	2455349	30.994	59.579166	326.41	22.0774	23.438431
2:00 PM	56.25968	447.4695	54.55318	761.2289	2455349	31.244	59.699853	326.18	22.0775	23.438431
2:01 PM	56.23139	446.1252	54.65863	760.4093	2455349	31.494	59.82126	325.95	22.0776	23.438431
2:02 PM	56.24002	443.1444	54.89725	757.6841	2455349	31.744	59.943383	325.72	22.0776	23.438431
2:03 PM	56.37624	438.7446	55.32765	752.3893	2455349	31.994	60.066216	325.5	22.0777	23.438431
2:04 PM	56.39787	435.1111	55.64399	747.662	2455349	32.244	60.189755	325.27	22.0778	23.438431
2:05 PM	56.54	434.2836	56.29629	747.6252	2455349	32.494	60.313996	325.05	22.0779	23.438431
2:06 PM	56.94222	434.2668	58.37671	749.74	2455349	32.744	60.438934	324.82	22.078	23.438431

2:07 PM	57.45729	433.2741	71.19439	749.187	2455349	32.994	60.564566	324.6	22.0781	23.438431
2:08 PM	57.74733	431.2354	115.4541	747.8397	2455349	33.244	60.690886	324.38	22.0782	23.438431
2:09 PM	57.69052	430.6952	195.6619	750.0666	2455349	33.494	60.81789	324.15	22.0783	23.438431
2:10 PM	57.77562	429.1083	290.0916	749.7005	2455349	33.744	60.945575	323.93	22.0784	23.438431
2:11 PM	57.80435	426.6544	366.9965	747.6095	2455349	33.994	61.073934	323.71	22.0785	23.438431
2:12 PM	57.7718	422.9632	400.0089	741.4834	2455349	34.244	61.202966	323.49	22.0786	23.438431
2:13 PM	57.72876	420.3337	403.5284	738.6749	2455349	34.494	61.332664	323.27	22.0787	23.438431
2:14 PM	57.39295	417.9294	401.6564	737.6856	2455349	34.744	61.463024	323.06	22.0788	23.438431
2:15 PM	57.26317	416.5624	401.2772	737.0345	2455349	34.994	61.594043	322.84	22.0789	23.438431
2:16 PM	56.767	411.9545	397.2589	730.7946	2455349	35.244	61.725716	322.62	22.079	23.438431
2:17 PM	56.35767	408.3547	394.1772	727.9965	2455349	35.494	61.858039	322.41	22.079	23.438431
2:18 PM	56.15656	406.4343	392.5702	728.0708	2455349	35.744	61.991007	322.19	22.0791	23.438431
2:19 PM	56.13843	404.8516	391.2072	728.2235	2455349	35.994	62.124616	321.98	22.0792	23.438431
2:20 PM	55.85484	401.2291	387.9172	723.732	2455349	36.244	62.258863	321.77	22.0793	23.438431
2:21 PM	55.60162	398.8983	386.0507	722.5214	2455349	36.494	62.393742	321.55	22.0794	23.438431
2:22 PM	55.7244	399.6929	387.0527	726.5433	2455349	36.744	62.52925	321.34	22.0795	23.438431
2:23 PM	55.61647	400.957	388.4174	731.9776	2455349	36.994	62.665382	321.13	22.0796	23.438431
2:24 PM	55.5104	397.807	385.4692	729.2447	2455349	37.244	62.802135	320.92	22.0797	23.438431
2:25 PM	55.15471	391.9497	379.8506	719.9775	2455349	37.494	62.939504	320.71	22.0798	23.438431
2:26 PM	55.00953	388.5666	376.7084	716.7674	2455349	37.744	63.077484	320.5	22.0799	23.438431
2:27 PM	54.98932	387.6969	375.7518	717.6675	2455349	37.994	63.216073	320.29	22.08	23.438431
2:28 PM	54.90335	386.4562	374.5479	717.6155	2455349	38.244	63.355266	320.09	22.0801	23.438431
2:29 PM	54.4737	383.8412	372.0101	716.1689	2455349	38.494	63.495058	319.88	22.0802	23.438431
2:30 PM	54.12064	382.2437	370.5263	716.5845	2455349	38.744	63.635446	319.67	22.0803	23.438431
2:31 PM	54.03925	378.5274	366.9428	712.5361	2455349	38.994	63.776426	319.47	22.0804	23.438431
2:32 PM	54.11583	375.1281	363.6949	707.7048	2455349	39.244	63.917993	319.27	22.0804	23.438431
2:33 PM	54.08262	372.7761	361.3944	705.8039	2455349	39.493	64.060144	319.06	22.0805	23.438431
2:34 PM	53.99228	370.4522	359.0336	704.5269	2455349	39.743	64.202874	318.86	22.0806	23.438431
2:35 PM	53.75512	368.2513	356.8253	703.6193	2455349	39.993	64.34618	318.66	22.0807	23.438431
2:36 PM	53.58896	365.1441	353.6723	700.7611	2455349	40.243	64.490058	318.46	22.0808	23.438431
2:37 PM	53.34797	361.7453	350.343	697.6609	2455349	40.493	64.634503	318.26	22.0809	23.438431
2:38 PM	53.2407	360.3144	348.8719	698.0007	2455349	40.743	64.779512	318.06	22.081	23.438431
2:39 PM	52.97502	359.9914	348.5024	702.8186	2455349	40.993	64.925082	317.86	22.0811	23.438431
2:40 PM	52.50179	357.6074	345.9107	702.7707	2455349	41.243	65.071207	317.66	22.0812	23.438431
2:41 PM	52.00027	354.086	342.2733	700.2193	2455349	41.493	65.217884	317.46	22.0813	23.438431
2:42 PM	51.75065	350.6916	338.7128	698.2518	2455349	41.743	65.36511	317.27	22.0814	23.438431
2:43 PM	51.54189	348.3541	336.2387	697.667	2455349	41.993	65.51288	317.07	22.0815	23.438431
2:44 PM	51.50606	346.3833	333.1216	694.973	2455349	42.243	65.661191	316.87	22.0816	23.438431
2:45 PM	51.47187	343.3045	319.1918	691.6544	2455349	42.493	65.810039	316.68	22.0817	23.438431
2:46 PM	51.41146	340.7404	278.3073	689.6441	2455349	42.743	65.95942	316.49	22.0818	23.438431
2:47 PM	51.09575	338.3824	211.5035	688.9386	2455349	42.993	66.10933	316.29	22.0818	23.438431

2:48 PM	50.81664	335.9366	137.2932	689.2242	2455349	43.243	66.259766	316.1	22.0819	23.438431
2:49 PM	50.45877	333.2512	79.07529	687.5041	2455349	43.493	66.410724	315.91	22.082	23.438431
2:50 PM	50.11804	329.1969	54.75888	683.2701	2455349	43.743	66.5622	315.72	22.0821	23.438431
2:51 PM	49.69615	325.7219	50.52012	680.7189	2455349	43.993	66.714191	315.53	22.0822	23.438431
2:52 PM	49.39935	321.9087	49.41384	677.3553	2455349	44.243	66.866692	315.34	22.0823	23.438431
2:53 PM	48.82102	319.5291	48.43315	677.3858	2455349	44.493	67.019701	315.15	22.0824	23.438431
2:54 PM	48.53066	317.6667	47.77586	677.7546	2455349	44.743	67.173214	314.96	22.0825	23.438431
2:55 PM	48.23648	316.6332	47.29414	679.4124	2455349	44.993	67.327226	314.78	22.0826	23.438431
2:56 PM	48.18502	314.8335	47.02414	681.1625	2455349	45.243	67.481735	314.59	22.0827	23.438431
2:57 PM	48.10997	312.802	46.80868	678.6221	2455349	45.493	67.636736	314.4	22.0828	23.438431
2:58 PM	48.06246	311.3679	46.70417	678.2102	2455349	45.743	67.792227	314.22	22.0829	23.438431
2:59 PM	47.9211	308.8153	46.49962	676.7704	2455349	45.993	67.948204	314.03	22.083	23.438431
3:00 PM	47.69737	305.509	46.17093	673.5677	2455349	46.243	68.104663	313.85	22.0831	23.438431
3:01 PM	47.44721	302.0179	45.77252	668.4155	2455349	46.493	68.261601	313.67	22.0832	23.438431
3:02 PM	47.31645	298.199	45.6089	662.8343	2455349	46.743	68.419014	313.48	22.0832	23.438431
3:03 PM	46.79122	295.6031	45.1196	662.693	2455349	46.993	68.576899	313.3	22.0833	23.438431
3:04 PM	46.36452	291.9433	44.63476	659.4859	2455349	47.243	68.735252	313.12	22.0834	23.438431
3:05 PM	46.01397	289.3401	44.18743	658.722	2455349	47.493	68.894071	312.94	22.0835	23.438431
3:06 PM	45.65839	286.3977	43.77916	657.4053	2455349	47.743	69.05335	312.76	22.0836	23.438431
3:07 PM	45.31406	282.8474	43.44527	654.1913	2455349	47.993	69.213088	312.58	22.0837	23.438431
3:08 PM	45.15479	280.3153	43.21204	652.2867	2455349	48.243	69.373281	312.4	22.0838	23.438431
3:09 PM	44.84924	277.3339	43.01404	650.0786	2455349	48.493	69.533926	312.22	22.0839	23.438431
3:10 PM	44.62267	275.1911	42.84803	650.0558	2455349	48.742	69.695018	312.05	22.084	23.438431
3:11 PM	44.3925	272.6605	42.77011	649.3195	2455349	48.992	69.856555	311.87	22.0841	23.438431
3:12 PM	44.26043	270.2874	42.60161	648.7489	2455349	49.242	70.018534	311.69	22.0842	23.438431
3:13 PM	43.90878	268.5288	42.37742	650.0196	2455349	49.492	70.180951	311.52	22.0843	23.438431
3:14 PM	43.55921	266.412	42.03377	650.5691	2455349	49.742	70.343802	311.34	22.0844	23.438431
3:15 PM	43.2765	264.7112	41.89009	651.7796	2455349	49.992	70.507086	311.17	22.0845	23.438431
3:16 PM	43.0401	262.9193	41.71993	652.8978	2455349	50.242	70.670798	311	22.0846	23.438431
3:17 PM	42.73106	260.7788	41.57189	653.3121	2455349	50.492	70.834935	310.82	22.0846	23.438431
3:18 PM	42.61777	259.159	41.62498	655.0365	2455349	50.742	70.999494	310.65	22.0847	23.438431
3:19 PM	42.55955	256.8612	41.79618	653.0613	2455349	50.992	71.164472	310.48	22.0848	23.438431
3:20 PM	42.35876	254.6093	41.8314	652.5068	2455349	51.242	71.329866	310.31	22.0849	23.438431
3:21 PM	42.08173	252.0467	41.70601	650.8294	2455349	51.492	71.495672	310.14	22.085	23.438431
3:22 PM	41.75837	249.2177	42.0214	647.4412	2455349	51.742	71.661888	309.97	22.0851	23.438431
3:23 PM	41.52023	245.4075	47.75976	641.3977	2455349	51.992	71.828509	309.8	22.0852	23.438431
3:24 PM	41.28809	241.5354	72.27844	636.4139	2455349	52.242	71.995534	309.63	22.0853	23.438431
3:25 PM	40.88193	238.0518	116.7001	632.5786	2455349	52.492	72.162959	309.46	22.0854	23.438431
3:26 PM	40.58654	235.0948	166.4597	629.7699	2455349	52.742	72.330781	309.3	22.0855	23.438431
3:27 PM	40.32163	232.059	204.6112	626.5621	2455349	52.992	72.498996	309.13	22.0856	23.438431
3:28 PM	39.99905	228.9596	217.8414	622.3643	2455349	53.242	72.667602	308.96	22.0857	23.438431

3:29 PM	39.69197	225.737	216.6027	618.2988	2455349	53.492	72.836596	308.8	22.0858	23.438431
3:30 PM	39.39953	221.8788	213.2012	612.4489	2455349	53.742	73.005975	308.63	22.0859	23.438431
3:31 PM	39.11463	218.6611	210.475	608.1238	2455349	53.992	73.175735	308.47	22.086	23.438431
3:32 PM	38.86742	215.8263	207.953	605.1869	2455349	54.242	73.345874	308.31	22.086	23.438431
3:33 PM	38.64063	212.8098	205.1468	601.1774	2455349	54.492	73.516389	308.14	22.0861	23.438431
3:34 PM	38.39593	209.1652	201.8398	595.4949	2455349	54.742	73.687276	307.98	22.0862	23.438431
3:35 PM	38.0303	205.9533	198.9791	591.7287	2455349	54.992	73.858533	307.82	22.0863	23.438431
3:36 PM	37.7004	203.261	196.6907	589.485	2455349	55.242	74.030156	307.66	22.0864	23.438431
3:37 PM	37.51075	200.6914	194.3081	586.3053	2455349	55.492	74.202144	307.5	22.0865	23.438431
3:38 PM	37.43363	198.7573	192.6255	585.148	2455349	55.742	74.374491	307.34	22.0866	23.438431
3:39 PM	37.23743	196.2965	190.3182	582.1746	2455349	55.992	74.547197	307.18	22.0867	23.438431
3:40 PM	37.20674	193.2021	187.0924	577.3191	2455349	56.242	74.720258	307.02	22.0868	23.438431
3:41 PM	36.89223	189.6991	183.3285	571.7922	2455349	56.492	74.89367	306.86	22.0869	23.438431
3:42 PM	36.88295	186.4462	179.6063	566.0392	2455349	56.742	75.067431	306.7	22.087	23.438431
3:43 PM	36.89387	183.1261	175.7772	559.1349	2455349	56.992	75.241539	306.54	22.0871	23.438431
3:44 PM	36.76486	179.985	171.7266	554.2397	2455349	57.242	75.415989	306.39	22.0872	23.438431
3:45 PM	36.38317	176.8934	167.4846	550.127	2455349	57.492	75.59078	306.23	22.0873	23.438431
3:46 PM	36.13159	173.7025	163.04	544.3274	2455349	57.742	75.765908	306.08	22.0874	23.438431
3:47 PM	35.7736	170.9789	159.1679	542.0526	2455349	57.992	75.94137	305.92	22.0874	23.438431
3:48 PM	35.39093	168.3393	155.3844	539.7328	2455349	58.241	76.117164	305.77	22.0875	23.438432
3:49 PM	35.1364	165.3566	151.4851	536.1711	2455349	58.491	76.293286	305.61	22.0876	23.438432
3:50 PM	34.80168	163.1797	148.6997	534.929	2455349	58.741	76.469734	305.46	22.0877	23.438432
3:51 PM	34.33807	160.9259	146.0844	534.8331	2455349	58.991	76.646505	305.31	22.0878	23.438432
3:52 PM	33.82048	157.9898	143.2513	531.9197	2455349	59.241	76.823596	305.15	22.0879	23.438432
3:53 PM	33.37882	154.981	140.4532	527.4265	2455349	59.491	77.001003	305	22.088	23.438432
3:54 PM	33.0109	152.3301	137.9889	523.7498	2455349	59.741	77.178725	304.85	22.0881	23.438432
3:55 PM	32.62855	149.4034	135.268	520.0294	2455349	59.991	77.356758	304.7	22.0882	23.438432
3:56 PM	32.30422	146.3395	132.372	515.5418	2455349	60.241	77.535099	304.55	22.0883	23.438432
3:57 PM	31.91412	143.4241	129.6391	510.994	2455349	60.491	77.713745	304.4	22.0884	23.438432
3:58 PM	31.47671	140.5241	126.7755	506.6416	2455349	60.741	77.892693	304.25	22.0885	23.438432
3:59 PM	31.07711	137.3513	123.6971	501.6889	2455349	60.991	78.071941	304.1	22.0886	23.438432
4:00 PM	30.79363	134.113	120.5487	494.5296	2455349	61.241	78.251486	303.95	22.0887	23.438432
4:01 PM	30.40222	131.0886	116.0189	489.8556	2455349	61.491	78.431324	303.8	22.0887	23.438432
4:02 PM	30.10782	128.2617	103.0056	485.2273	2455349	61.741	78.611452	303.65	22.0888	23.438432
4:03 PM	29.73279	125.4332	80.02564	481.2378	2455349	61.991	78.791869	303.51	22.0889	23.438432
4:04 PM	29.34542	122.8079	55.03127	476.576	2455349	62.241	78.97257	303.36	22.089	23.438432
4:05 PM	29.00241	119.9657	36.7684	471.0274	2455349	62.491	79.153552	303.22	22.0891	23.438432
4:06 PM	28.7175	117.0706	29.86372	464.8023	2455349	62.741	79.334814	303.07	22.0892	23.438432
4:07 PM	28.49454	113.8257	28.69739	455.4915	2455349	62.991	79.516351	302.92	22.0893	23.438432
4:08 PM	28.16136	111.235	28.22409	449.966	2455349	63.241	79.698161	302.78	22.0894	23.438432
4:09 PM	28.01782	108.9308	27.75826	445.8084	2455349	63.491	79.880241	302.64	22.0895	23.438432

4:10 PM	27.67174	106.2187	27.24724	439.5255	2455349	63.741	80.062587	302.49	22.0896	23.438432
4:11 PM	27.25848	103.1507	26.7167	432.4937	2455349	63.991	80.245197	302.35	22.0897	23.438432
4:12 PM	26.77094	100.4039	26.06845	427.3989	2455349	64.241	80.428069	302.21	22.0898	23.438432
4:13 PM	26.40749	97.33057	25.42955	420.1736	2455349	64.491	80.611198	302.06	22.0899	23.438432
4:14 PM	26.03269	94.31688	24.83262	412.5885	2455349	64.741	80.794582	301.92	22.09	23.438432
4:15 PM	25.63691	91.56919	24.4071	406.2401	2455349	64.991	80.978217	301.78	22.0901	23.438432
4:16 PM	25.28155	89.0037	24.01462	400.4031	2455349	65.241	81.162102	301.64	22.0901	23.438432
4:17 PM	25.02461	86.33643	23.629	392.9175	2455349	65.491	81.346234	301.5	22.0902	23.438432
4:18 PM	24.53215	83.54124	23.0891	385.8677	2455349	65.741	81.530608	301.36	22.0903	23.438432
4:19 PM	24.11278	80.58586	22.67065	377.0543	2455349	65.991	81.715224	301.22	22.0904	23.438432
4:20 PM	23.59246	77.9456	22.18197	370.9751	2455349	66.241	81.900078	301.08	22.0905	23.438432
4:21 PM	23.23371	75.49042	21.81182	364.8697	2455349	66.491	82.085167	300.94	22.0906	23.438432
4:22 PM	22.87704	72.90181	21.42526	358.2166	2455349	66.741	82.270489	300.8	22.0907	23.438432
4:23 PM	22.46203	70.31319	20.93762	350.1396	2455349	66.991	82.456043	300.67	22.0908	23.438432
4:24 PM	22.03447	67.54678	20.50524	340.466	2455349	67.241	82.641825	300.53	22.0909	23.438432
4:25 PM	21.66403	64.64354	20.16388	329.7453	2455349	67.491	82.827835	300.39	22.091	23.438432
4:26 PM	21.31424	62.08809	19.92286	320.1844	2455349	67.74	83.014072	300.26	22.0911	23.438432
4:27 PM	20.90557	59.45902	19.58409	310.9041	2455349	67.99	83.200533	300.12	22.0912	23.438432
4:28 PM	20.44905	56.71962	19.16636	299.7975	2455349	68.24	83.38722	299.98	22.0913	23.438432
4:29 PM	20.00335	53.59172	18.76983	285.673	2455349	68.49	83.574131	299.85	22.0914	23.438432
4:30 PM	19.43912	50.62025	18.32852	270.5358	2455349	68.74	83.761268	299.71	22.0914	23.438432
4:31 PM	19.00499	47.83374	17.92586	257.9667	2455349	68.99	83.948634	299.58	22.0915	23.438432
4:32 PM	18.49145	45.11005	17.36498	245.198	2455349	69.24	84.136229	299.44	22.0916	23.438432
4:33 PM	18.03799	42.68327	16.73802	234.2405	2455349	69.49	84.32406	299.31	22.0917	23.438432
4:34 PM	17.34595	40.30788	16.06432	224.7021	2455349	69.74	84.512131	299.18	22.0918	23.438432
4:35 PM	16.7957	37.96943	15.54146	214.4421	2455349	69.99	84.70045	299.04	22.0919	23.438432
4:36 PM	16.05133	35.71127	14.874	205.4646	2455349	70.24	84.889027	298.91	22.092	23.438432
4:37 PM	15.5509	33.96224	14.4757	197.7707	2455349	70.49	85.077875	298.78	22.0921	23.438432
4:38 PM	14.95794	31.92635	13.98504	188.3527	2455349	70.74	85.267007	298.65	22.0922	23.438432
4:39 PM	14.40409	29.8147	13.47039	176.9381	2455349	70.99	85.456445	298.52	22.0923	23.438432
4:40 PM	13.72144	26.83808	13.10928	152.4915	2455349	71.24	85.64621	298.39	22.0924	23.438432
4:41 PM	13.07965	21.85384	12.91948	97.63617	2455349	71.49	85.836332	298.26	22.0925	23.438432
4:42 PM	12.1144	18.03249	12.89164	64.32463	2455349	71.74	86.026844	298.13	22.0926	23.438432
4:43 PM	11.3768	16.41828	12.79949	55.82213	2455349	71.99	86.217787	298	22.0927	23.438432
4:44 PM	10.87276	14.14542	11.56491	28.18378	2455349	72.24	86.409209	297.87	22.0928	23.438432
4:45 PM	10.48714	12.68299	10.45198	12.77548	2455349	72.49	86.601167	297.74	22.0928	23.438432
4:46 PM	10.0245	12.65874	10.25532	21.06199	2455349	72.74	86.793726	297.61	22.0929	23.438432
4:47 PM	9.517954	12.94157	9.911564	42.0642	2455349	72.99	86.986962	297.48	22.093	23.438432
4:48 PM	8.942363	12.7619	8.86834	52.26264	2455349	73.24	87.180959	297.35	22.0931	23.438432
4:49 PM	8.375183	11.79717	8.052419	47.28886	2455349	73.49	87.375812	297.22	22.0932	23.438432
4:50 PM	7.893321	10.77137	7.553973	38.52527	2455349	73.74	87.571623	297.1	22.0933	23.438432

4:51 PM	7.2299	9.585244	6.946863	28.54751	2455349	73.99	87.7685	296.97	22.0934	23.438432
4:52 PM	6.57063	8.401758	6.304016	18.06262	2455349	74.24	87.966554	296.84	22.0935	23.438432
4:53 PM	5.826043	7.397321	5.621276	12.87343	2455349	74.49	88.165889	296.72	22.0936	23.438432
4:54 PM	5.195941	6.483478	5.118987	8.217102	2455349	74.74	88.366602	296.59	22.0937	23.438432
4:55 PM	4.790984	5.871568	4.627814	2.316301	2455349	74.99	88.568766	296.47	22.0938	23.438432
4:56 PM	4.34681	5.305269	4.225359	0.090435	2455349	75.24	88.772427	296.34	22.0939	23.438432
4:57 PM	4.022474	4.868514	3.838903	0.156675	2455349	75.49	88.977591	296.22	22.094	23.438432
4:58 PM	3.53362	4.28877	3.338899	0.031476	2455349	75.74	89.184224	296.09	22.0941	23.438432
4:59 PM	3.262265	3.934064	2.925536	0.092431	2455349	75.99	89.392257	295.97	22.0941	23.438432
5:00 PM	2.831637	3.46087	2.513732	-0.03394	2455349	76.24	89.601661	295.84	22.0942	23.438432
5:01 PM	2.53472	3.158936	2.207268	-0.10653	2455349	76.49	89.812927	295.72	22.0943	23.438432
5:02 PM	2.304112	3.000744	1.943501	-0.09302	2455349	76.74	90.016101	295.6	22.0944	23.438432
5:03 PM	1.976935	2.572533	1.5318	-0.1131	2455349	76.989	90.220457	295.47	22.0945	23.438432
5:04 PM	1.47967	2.093937	1.173913	-0.25216	2455349	77.239	90.438529	295.35	22.0946	23.438432
5:05 PM	1.243163	1.89114	0.918769	-0.27577	2455349	77.489	90.649724	295.23	22.0947	23.438432
5:06 PM	0.838097	1.565961	0.597657	-0.2659	2455349	77.739	90.859738	295.11	22.0948	23.438432
5:07 PM	0.509609	1.215401	0.218888	-0.06718	2455349	77.989	91.068747	294.98	22.0949	23.438432
5:08 PM	0.220667	0.921508	-0.09329	-0.05379	2455349	78.239	91.276705	294.86	22.095	23.438432
5:09 PM	-0.0295	0.751505	-0.35498	-0.15374	2455349	78.489	91.483566	294.74	22.0951	23.438432
5:10 PM	-0.31156	0.419416	-0.6016	-0.21387	2455349	78.739	91.68932	294.62	22.0952	23.438432
5:11 PM	-0.54905	0.280825	-0.73707	-0.08092	2455349	78.989	91.893996	294.5	22.0953	23.438432
5:12 PM	-0.67424	0.146255	-0.826	-0.05579	2455349	79.239	92.097659	294.38	22.0954	23.438432
5:13 PM	-0.69106	0.158946	-0.78683	0.063539	2455349	79.489	92.300396	294.26	22.0954	23.438432
5:14 PM	-0.72438	0.102781	-0.77187	0.387577	2455349	79.739	92.502309	294.14	22.0955	23.438432
5:15 PM	-0.76119	0.119995	-0.65199	0.645844	2455349	79.989	92.703509	294.02	22.0956	23.438432
5:16 PM	-0.80467	0.10743	-0.65209	0.276589	2455349	80.239	92.904106	293.9	22.0957	23.438432
5:17 PM	-0.81112	-0.01546	-0.71359	0.153034	2455349	80.489	93.104206	293.79	22.0958	23.438432
5:18 PM	-1.02217	-0.19702	-1.01237	-0.03852	2455349	80.739	93.303907	293.67	22.0959	23.438432
5:19 PM	-1.11601	-0.2616	-1.11511	-0.00059	2455349	80.989	93.503301	293.55	22.096	23.438432
5:20 PM	-1.17358	-0.34466	-1.27302	0.111575	2455349	81.239	93.702466	293.43	22.0961	23.438432
5:21 PM	-1.18592	-0.34893	-1.3019	0.202832	2455349	81.489	93.901473	293.31	22.0962	23.438432
5:22 PM	-1.15533	-0.31437	-1.28881	0.300313	2455349	81.739	94.100384	293.2	22.0963	23.438432
5:23 PM	-1.2247	-0.45862	-1.35114	0.325212	2455349	81.989	94.299251	293.08	22.0964	23.438432
5:24 PM	-1.21837	-0.49292	-1.32081	0.273183	2455349	82.239	94.498118	292.96	22.0965	23.438432
5:25 PM	-1.06991	-0.23773	-1.25733	0.24711	2455349	82.489	94.697022	292.85	22.0966	23.438432
5:26 PM	-1.00032	-0.20745	-1.14825	0.348584	2455349	82.739	94.895996	292.73	22.0967	23.438432
5:27 PM	-0.80773	0.030407	-0.93269	0.48224	2455349	82.989	95.095064	292.61	22.0967	23.438432
5:28 PM	-0.71389	0.131303	-0.80335	0.726061	2455349	83.239	95.294249	292.5	22.0968	23.438432
5:29 PM	-0.62115	0.234586	-0.70726	0.534269	2455349	83.489	95.493568	292.38	22.0969	23.438432
5:30 PM	-0.67773	0.173772	-0.65417	0.496333	2455349	83.739	95.693035	292.27	22.097	23.438432
5:31 PM	-0.61383	0.268637	-0.60805	0.539319	2455349	83.989	95.892661	292.15	22.0971	23.438432

5:32 PM	-0.65359	0.245518	-0.61054	0.47073	2455349	84.239	96.092456	292.04	22.0972	23.438432
5:33 PM	-0.52403	0.319148	-0.54114	0.63915	2455349	84.489	96.292426	291.92	22.0973	23.438432
5:34 PM	-0.45095	0.50247	-0.50281	0.692471	2455349	84.739	96.492577	291.81	22.0974	23.438432
5:35 PM	-0.43172	0.466785	-0.54821	0.569503	2455349	84.989	96.692914	291.7	22.0975	23.438432
5:36 PM	-0.4752	0.402327	-0.6522	0.540611	2455349	85.239	96.893438	291.58	22.0976	23.438432
5:37 PM	-0.38781	0.472565	-0.58509	0.62764	2455349	85.489	97.094151	291.47	22.0977	23.438432
5:38 PM	-0.33919	0.574969	-0.49574	0.622472	2455349	85.739	97.295056	291.36	22.0978	23.438432
5:39 PM	-0.42233	0.53162	-0.53003	0.639619	2455349	85.989	97.496153	291.24	22.0979	23.438432
5:40 PM	-0.30336	0.581251	-0.42271	0.793123	2455349	86.239	97.697441	291.13	22.098	23.438432
5:41 PM	-0.24951	0.710921	-0.38448	0.710205	2455349	86.488	97.89892	291.02	22.098	23.438432
5:42 PM	-0.11208	0.702502	-0.30231	0.783963	2455349	86.738	98.100589	290.91	22.0981	23.438432
5:43 PM	0.005244	0.779525	-0.19541	0.827418	2455349	86.988	98.302448	290.79	22.0982	23.438432
5:44 PM	0.131745	0.932314	-0.04613	0.896125	2455349	87.238	98.504495	290.68	22.0983	23.438432
5:45 PM	0.241423	1.056078	0.056202	0.806747	2455349	87.488	98.706729	290.57	22.0984	23.438432
5:46 PM	0.32379	1.051806	0.066383	0.798056	2455349	87.738	98.909148	290.46	22.0985	23.438432
5:47 PM	0.307514	1.159236	0.196968	0.937467	2455349	87.988	99.11175	290.35	22.0986	23.438432
5:48 PM	0.347714	1.200951	0.195929	0.84527	2455349	88.238	99.314534	290.24	22.0987	23.438432
5:49 PM	0.277581	1.171298	0.163309	0.801462	2455349	88.488	99.517498	290.13	22.0988	23.438432
5:50 PM	0.266548	1.17758	0.158219	0.792419	2455349	88.738	99.720639	290.01	22.0989	23.438432
5:51 PM	0.176424	1.141268	0.142012	0.694585	2455349	88.988	99.923957	289.9	22.099	23.438432
5:52 PM	-0.01005	1.010468	0.038334	0.538967	2455349	89.238	100.12745	289.79	22.0991	23.438432
5:53 PM	-0.13393	0.915226	-0.01922	0.529806	2455349	89.488	100.33111	289.68	22.0992	23.438432
5:54 PM	-0.14322	0.879039	-0.09952	0.743561	2455349	89.738	100.53495	289.57	22.0993	23.438432
5:55 PM	-0.16353	0.891227	-0.15053	0.834935	2455349	89.988	100.73895	289.47	22.0993	23.438432
5:56 PM	-0.00721	0.956564	-0.01621	0.786664	2455349	90.238	100.94312	289.36	22.0994	23.438432
5:57 PM	0.092199	1.06525	0.113755	0.744383	2455349	90.488	101.14745	289.25	22.0995	23.438432
5:58 PM	0.167576	1.042885	0.125079	0.771748	2455349	90.738	101.35195	289.14	22.0996	23.438432
5:59 PM	0.171071	1.033838	0.074798	0.641499	2455349	90.988	101.55661	289.03	22.0997	23.438432

Appendix D: Removing outliers

```
% The following script identifies outliers by the method of box and
whisker plots through use of the upper and lower quartiles.
% define data set
Ig = xlsread('hcCORRECT.xlsx','final','d2:d2462');
Id = xlsread('hcCORRECT.xlsx','final','c2:c2462');
Ib = xlsread('hcCORRECT.xlsx','final','e2:e2462');
NIg = size(Ig,1);

% Compute the mean
mId = mean(Id);

% Compute the standard deviation
sigma = std(Id);

% Compute the median
medianId = median(Id);

% STEP 1 - Data ranking
y = sort(Id);

% Compute the first quartile
Q(1) = median(y(find(y<median(y))));

% Compute the second quartile
Q(2) = median(y);

% Compute the third quartile
Q(3) = median(y(find(y>median(y))));

% Compute the interquartile range (IQR)
IQR = Q(3)-Q(1);

% compute Semi Interquartile Deviation (SID)
SID = IQR/2;

% Determine extreme Q1 outliers (e.g., Id < Q1 - 3*IQR)
iy = find(y<Q(1)-3*IQR);
if ~isempty(iy),
    outliersQ1 = y(iy);
else
    outliersQ1 = [];
end

% Determine extreme Q3 outliers (e.g. Id > Q1 + 3*IQR)
iy = find(y>Q(1)+3*IQR);
if ~isempty(iy),
    outliersQ3 = y(iy);
else
    outliersQ3 = [];
end

% Compute total number of outliers
```

```
Noutliers = length(outliersQ1)+length(outliersQ3);
Id(any(outliersQ1),:) = [];
Id(any(outliersQ3),:) = [];

% Display results
disp(['Mean:                                ',num2str(mId)]);
disp(['Standard Deviation:                  ',num2str(sigma)]);
disp(['Median:                              ',num2str(medianId)]);
disp(['25th Percentile:                     ',num2str(Q(1))]);
disp(['50th Percentile:                     ',num2str(Q(2))]);
disp(['75th Percentile:                     ',num2str(Q(3))]);
disp(['Semi Interquartile Deviation:        ',num2str(SID)]);
disp(['Number of outliers:                  ',num2str(Noutliers)]);
```

Appendix E: Lookup table by Le Baron et al. [25]

Shadow band correction ratios for the parameterized categories from Le Baron et al. (*i*= zenith, *j* =geometric, *k* =epsilon, *l*=delta)

i =	*j*= (, 1)	(, 2)	(, 3)	(, 4)	*i* =	*j*= (, 1)	(, 2)	(, 3)	(, 4)
(*i*, *j*, 1, 1)					(*i*, *j*, 1, 3)				
(1,)	1.051	1.082	1.117	1.173	(1,)	1.051	1.082	1.117	1.182
(2,)	1.051	1.104	1.115	1.163	(2,)	1.051	1.082	1.128	1.159
(3,)	1.069	1.082	1.119	1.140	(3,)	1.076	1.088	1.131	1.129
(4,)	1.047	1.063	1.074	1.030	(4,)	1.060	1.085	1.103	1.156
(*i*, *j*, 2, 1)					(*i*, *j*, 2, 3)				
(1,)	1.051	1.082	1.117	1.248	(1,)	1.051	1.082	1.117	1.221
(2,)	1.051	1.082	1.117	1.184	(2,)	1.051	1.171	1.180	1.213
(3,)	1.161	1.161	1.147	1.168	(3,)	1.135	1.148	1.176	1.197
(4,)	1.076	1.078	1.104	1.146	(4,)	1.092	1.119	1.143	1.182
(*i*, *j*, 3, 1)					(*i*, *j*, 3, 3)				
(1,)	1.051	1.082	1.117	1.156	(1,)	1.051	1.082	1.117	1.238
(2,)	1.051	1.082	1.117	1.156	(2,)	1.051	1.160	1.207	1.230
(3,)	1.051	1.082	1.117	1.156	(3,)	1.169	1.191	1.193	1.210
(4,)	1.187	1.167	1.139	1.191	(4,)	1.150	1.133	1.180	1.156
(*i*, *j*, 4, 1)					(*i*, *j*, 4, 3)				
(1,)	1.051	1.082	1.117	1.181	(1,)	1.051	1.082	1.117	1.156
(2,)	1.051	1.082	0.990	1.104	(2,)	1.051	1.082	1.117	1.156
(3,)	1.015	1.016	0.946	1.027	(3,)	1.051	1.082	1.117	1.156
(4,)	0.925	0.967	0.947	1.150	(4,)	1.089	1.194	1.216	1.064
(*i*, *j*, 1, 2)					(*i*, *j*, 1, 4)				
(1,)	1.051	1.082	1.117	1.176	(1,)	1.051	1.082	1.117	1.191
(2,)	1.051	1.095	1.130	1.162	(2,)	1.051	1.105	1.143	1.168
(3,)	1.073	1.089	1.115	1.142	(3,)	1.085	1.093	1.117	1.156
(4,)	1.058	1.076	1.117	1.156	(4,)	1.069	1.082	1.117	1.156
(*i*, *j*, 2, 2)					(*i*, *j*, 2, 4)				
(1,)	1.051	1.082	1.117	1.211	(1,)	1.051	1.082	1.117	1.238
(2,)	1.051	1.082	1.186	1.194	(2,)	1.051	1.148	1.195	1.230
(3,)	1.086	1.130	1.168	1.177	(3,)	1.132	1.160	1.183	1.210
(4,)	1.074	1.102	1.118	1.174	(4,)	1.118	1.116	1.150	1.185
(*i*, *j*, 3, 2)					(*i*, *j*, 3, 4)				
(1,)	1.051	1.082	1.117	1.237	(1,)	1.051	1.082	1.117	1.232
(2,)	1.051	1.082	1.203	1.212	(2,)	1.051	1.206	1.210	1.238
(3,)	1.080	1.195	1.211	1.185	(3,)	1.144	1.178	1.226	1.216
(4,)	1.140	1.098	1.191	1.181	(4,)	1.117	1.155	1.178	1.167
(*i*, *j*, 4, 2)					(*i*, *j*, 4, 4)				
(1,)	1.051	1.082	1.117	1.217	(1,)	1.051	1.082	1.117	1.156
(2,)	1.051	1.082	1.120	1.180	(2,)	1.051	1.082	1.117	1.156
(3,)	1.182	1.115	1.081	1.111	(3,)	1.051	1.082	1.117	1.156
(4,)	1.057	1.119	1.133	1.033	(4,)	1.024	1.025	1.162	1.142

Boundaries for the parameters in the above table—index (3, 4, 1, 3) would be (*i*) 50–60 zenith angle, (*j*) geometric screening >13.2%, (*k*) overcast skies and (*l*) average to high sky brightness

Cuts	1	2	3	4	
i	0.000	35.00	50.00	60.00	90.00
j	1.000	1.068	1.100	1.132	–
k	0.000	1.253	2.134	5.980	–
l	0.000	0.120	0.200	0.300	

Appendix F: Shadow band correction models

```
% The script calculates the different shadow band corrections for each of
the models: Drummond, Batlles, Le Baron and Muneer and Zhang. These
% corrections are used to correct the measured diffuse irradiance at
STARlab.

b = 0.076; % width of shadow band (m)
r = 0.317; % radius of shadow band (m)
Ig = xlsread('1 hr MLAZI.xlsx', 3,'d2:d2621'); % Global horizontal
irradiance
Id = xlsread('1 hr MLAZI.xlsx', 3,'c2:c2621'); % Diffuse horizontal
irradiance
Ib = xlsread('1 hr MLAZI.xlsx', 3,'e2:e2621'); % Direct normal irradiance
h = xlsread('1 hr MLAZI.xlsx', 3,'b2:b2621');
zen = xlsread('1 hr MLAZI.xlsx', 3,'g2:g2621');% Zenith angle
n = xlsread('1 hr MLAZI.xlsx', 3,'k2:k2621'); % Day number of the year
alpha = (90-zen)*(pi/180);% Solar altitude
lat = -29.97*(pi/180); %  in radians
deltaD = 23.45*sin(((2*pi)/365)*(284+n));  % In degrees
deltaR = deltaD*(pi./180);
omegaS = acos(-tan(lat)*tan(deltaR)); %in radians
omegaSD = omegaS*(180/pi);
Eo = 1+0.033*cos(((2*pi)*n)/365);
Isc = 1367;
omegaI = (12-(h-0.5)).*15; % in degrees
omegaIR = omegaI*(pi./180);
Io = Isc*Eo.*sin(deltaR).*sin(lat)+
Isc*Eo.*cos(omegaIR)*cos(lat).*cos(deltaR);
N = length(n);

%Uncorrected and filtered data
idf = Ig - Ib.*cos(zen*(pi/180));
x = 0:1:800;
z = 0:1:800;
subplot(3,2,1)
axis square
plot(x,z);
hold on;
scatter(Id,idf,'.')
title('Uncorrected and filtered')
xlabel('Diffuse measured (W/m^2)')
ylabel('Diffuse modelled W/m^2)')

% Drummond
b = 0.076;
r = 0.317;
a =(deltaD).*(omegaS.*sin(lat).*sin(deltaR))+
(cos(lat).*cos(deltaR).*sin(omegaS*(pi/180)));
f = ((2*b)/(pi*r)).*(cos(a*(pi/180))).^3;
CD = 1./(1-f);
id = CD.*Id;
x = 0:1:800;
z = 0:1:800;
subplot(3,2,2)
axis square
```

```
plot(x,z);
hold on;
scatter(Id,id,'.')
title('Drummond')
xlabel('Diffuse measured (W/m^2)')
ylabel('Diffuse corrected W/m^2)')

% Batlles
m = 1./cos(zen*(pi/180));
del = (m.*Id)./Io;
In = (Ig-Id)./cos(zen*(pi/180));
eps = (In+Id)./Id;

 for i=1:N
    if eps(i)<= 3.5
        CB = 1.178.*CD + 0.207.*log(del)+ 0.122./exp(-1./sin(alpha));

    elseif eps(i) > 11
        CB = 1.384*CD + 0.363*log(del);
    elseif eps(i) <=8 && eps(i)> 3.5
        CB = 1.454.*CD + 0.655.*log(del)+ 0.4756.*exp(-1./sin(alpha));
    else
        CB = 1.38*CD + 0.363*log(del);
        fprintf('%f\n',CB);
    end
 end
IdB = CB.*Id;
x = 0:100:800;
z = 0:100:800;
subplot(3,2,3)
axis square
plot(x,z);
hold on;
scatter(Id,IdB,'.');
title('Batlles')
xlabel('Measured diffuse(W/m^2)')
ylabel('Corrected diffuse(W/m^2)')


%Le Baron
%N=length(zen);
a=zeros(1,N);
for i=1:N
    if zen(i)<= 35;
        a(i) = 1;
    elseif zen(i) > 35 && zen(i)<= 50;
        a(i) =2;
        elseif zen(i)> 50 && zen(i)< 60;
        a(i) = 3;
    else
        a(i) = 4;
    end
end
```

```
b=zeros(1,N);
for i=1:N
    if CD(i)<= 1.068;
        b(i) = 1;
    elseif CD(i) > 1.068 && CD(i)<= 1.100;
        b(i) =2;
    elseif CD(i)> 1.100 && CD(i)< 1.;
        b(i) = 3;
    else
        b(i) = 4;
    end
end

c=zeros(1,N);
for i=1:N
    if eps(i)<= 1.253;
        c(i) =1;
    elseif eps(i) > 1.253 && CD(i)<= 2.134;
        c(i) =2;
    elseif eps(i)> 2.134 && CD(i)< 5.980;
        c(i) =3;
    else
        c(i) =4 ;
    end
end

d=zeros(1,N);
v=zeros(N,4);
for i=1:N
    if del(i)<= 0.120;
        d(i) = 1;
    elseif del(i) > 0.120 && del(i)<= 0.200;
        d(i) =2;
    elseif del(i)> 0.200 && del(i)< 0.300;
        d(i) = 3;
    else
        d(i)= 4;
    end
   v(i,:)  = [a(i) b(i) c(i) d(i)];
end

for i=1:2620
v(i,:);
end

A=zeros(4,4,4,4);
for g=1:4
    for h=1:4
        cellrange=sprintf('%s%d:%s%d',char('a'+2+5*(g-
1)),6*h,char('a'+5+5*(g-1)),6*h+3);
        A(:,:,g,h)=xlsread('look_up_table.xlsx',1,cellrange);
    end
```

```
end

for i=1:2620
A(v(i,1),v(i,2),v(i,3),v(i,4));
end

for i=1:2620
y = (A(v(i,1),v(i,2),v(i,3),v(i,4)))-1;
end
IdLeBaron = (Id.* y) + Id;
x = 0:1:800;
z = 0:1:800;
subplot(3,2,4)
axis square
plot(x,z);
hold on;
scatter(Id,IdLeBaron,'.')
title('Le Baron')
xlabel('Diffuse measured (W/m^2)')
ylabel('Diffuse modelled (W/m^2)')

% Muneer and Zhang
b = 0.076;  % width of shadowband
r = 0.317;
Kt = Ig./Io;
b1=zeros(N,1);
b2=zeros(N,1);
for i=1:N
if Kt(i) > 0.2
   b1(i) = (3.6-10.462*Kt(i))./(-0.4+6.974*Kt(i));
 else b1(i) = 1.68;
end
end
for i=1:N
if Kt(i) > 0.2
    b2(i) = (1.565+0.990.*Kt(i))./(0.957-0.660*Kt(i));
else b2(i) = 1.68;
end
end
I1 = cos(lat).*cos(deltaR).*sin(omegaS) + omegaS*sin(lat).*sin(deltaR);
I2a =
((omegaS.*(sin(lat))^2.*(sin(deltaR)).^2)+(2*sin(omegaS).*sin(lat).*cos(l
at).*sin(deltaR).*cos(deltaR)))*(pi/180);
I2b = (deltaR.*((omegaS/2)+(sin(2*omegaS))/4))*(pi/180);
I2c = (cos(lat)^2.*cos(I2b).^2)*(pi/180);
I2 = I2a + I2b + I2c;
D = (pi/6).*((3+2.*b1)./(1+b1)+(3+2.*b2)./(1+b2));
F = ((2*b)/r).*cos((deltaR).*((I1+b1.*I2)./(1+b1))).^3;
CM = 1./(1-F./D);
IdMuneer = CM.*Id;
x = 0:100:800;
z = 0:100:800;
subplot(3,2,5)
axis square
```

```
plot(x,z);
hold on;
scatter(IdMuneer,Id,'.')
title('Muneer and Zhang')
xlabel('Diffuse measured (W/m^2)')
ylabel('Diffuse corrected W/m^2)')
```

Appendix G: Beam irradiance estimation models

```
% Plots of diffuse fraction,k vs clearness index,Kt for models: Erbs,
% Orgill and Hollands, Reindl-A, Reindl-B, Boland and Skartveit.

% The following code estimates the beam irradiance from k vs Kt
% correlations for Howard College station. The modelled beam irradiance
is plotted against the measured irradiance.

%Declaration of constants
Ig = xlsread('hcCORRECT.xlsx', 'final','d2:d2462'); % Global horizontal
irradiance
Id = xlsread('hcCORRECT.xlsx', 'final','c2:c2462');% Diffuse horizontal
irradiance
Ib = xlsread('hcCORRECT.xlsx', 'final','e2:e2462');% Direct normal
irradiance
h = xlsread('hcCORRECT.xlsx', 'final','b2:b2462');% Hour
thetaZ = xlsread('hcCORRECT.xlsx', 'final','g2:g2462');% Zenith angle
n = xlsread('hcCORRECT.xlsx', 'final','k2:k2462');% Day number
alpha = (90-thetaZ)*(pi/180);% Solar altitude
lat = -29.52*(pi/180) ; %  Geographical latitude in radians
deltaD = 23.45*sin(((2*pi)/365)*(284+n));   % Declination in degrees
deltaR = deltaD*(pi./180);% Declination in radians
omegaS = acos(-tan(lat)*tan(deltaR)); % Sunset hour
omegaSD = omegaS*(180/pi);Sunset % Hour angle in radians
Eo = 1+0.033*cos(((2*pi)*n)/365);
Isc = 1367; %Solar constant
omegaI = (12-(h-0.5)).*15;
omegaIR = omegaI*(pi./180);
Io = Isc.*Eo.*(sin(deltaR).*sin(lat)+
cos(omegaIR).*cos(lat).*cos(deltaR));% Extraterrestrial solar radiation

% Calculation of Kt, the clearness index
Kt = Ig./Io;
N = length(Ig);

%*********************************************************************

% Erbs model
k=zeros(N,1);
for i=1:N
    if Kt(i)<=0.22
        k(i) = 1.0-0.09*Kt(i);
    elseif Kt(i) > 0.8
        k(i) = 0.165;
    else
        k(i) = 0.9511-0.16041.*Kt(i)+ 4.388.*(Kt(i))^2-16.638.*(Kt(i))^3+
12.336.*(Kt(i))^4;
    end
end
Ibm = (Ig.*(1-k))./sin(alpha);
a = 0:1:1200;
b = 0:1:1200;
hold on
subplot(3,2,1)
```

```
plot(a,b);
hold on;
scatter(Ibm,Ib)
title('Erbs')
xlabel('Direct measured (W/m^2)')
ylabel('Direct modelled (W/m^2)')

%************************************************************************

% Orgill and Hollands model
ko=zeros(N,1);
for i=1:N
    if Kt(i)< 0.35
        ko(i) = 1.0-0.249*Kt(i);
    elseif Kt(i) > 0.75
        ko(i) = 0.177;
        fprintf('%f\n',k(i))
    else
        ko(i) = 1.577-1.84*Kt(i);
    end
end
Ibmo = (Ig.*(1-ko))./sin(alpha);
a = 0:1:2000;
b = 0:1:2000;
subplot(3,2,2)
plot(a,b);
hold on;
scatter(Ibmo,Ib)
title('Orgill and Hollands')
xlabel('Direct measured (W/m^2)')
ylabel('Direct modelled (W/m^2)')

%************************************************************************

% Reindl-A model
kr1 =zeros(N,1);
for i=1:N
    if Kt(i)<=0.30
        kr1(i) = 1.020-0.248*Kt(i);
    elseif Kt(i) >= 0.78
        kr1(i) = 0.147;
    else
        kr1(i) = 1.450-1.670*Kt(i);
    end
end
Ibmr1 = (Ig.*(1-kr1))./sin(alpha);
a = 0:1:1200;
b = 0:1:1200;
subplot(3,2,3)
plot(a,b);
hold on;
scatter(Ibmr1,Ib)
title('Reindl-A')
xlabel('Direct measured (W/m^2)')
```

```
ylabel('Direct modelled (W/m^2)')


%*********************************************************************

% Reindl-B model
kr2=zeros(N,1);
for i=1:N
    if Kt(i)<= 0.30
        kr2(i) = 1.020-0.254*Kt(i)+ 0.0123*sin(alpha(i));
    elseif Kt(i) >= 0.78
        kr2(i) = 0.486*Kt(i)-0.182*sin(alpha(i));
%         fprintf('%f\n',k(i))
    else
        kr2(i) =1.400-1.749*Kt(i)+ 0.177*sin(alpha(i)) ;
    end
end
Ibmr2 = (Ig.*(1-kr2))./sin(alpha);
a = 0:1:1200;
b = 0:1:1200;
subplot(3,2,4)
plot(a,b);
hold on;
scatter(Ibmr2,Ib)
title('Reindl-B')
xlabel('Direct measured (W/m^2)')
ylabel('Direct modelled W/m^2)')


%*********************************************************************

% Boland model
kb=zeros(N,1);

for i=1:N
    kb(i) = 1./(1+exp(7.997*(Kt(i)-0.586)));
end
Ibmb = (Ig.*(1-kb))./sin(alpha);
a = 0:1:1200;
b = 0:1:1200;
subplot(3,2,5)
plot(a,b);
hold on;
scatter(Ibmb,Ib)
title('Boland')
xlabel('Direct measured (W/m^2)')
ylabel('Direct modelled (W/m^2)')


%*********************************************************************
% Skartveit and Olseth model
k0 = 0.2;
k1 = 0.87-0.56*exp(-0.06*alpha);
```

```
d1 = 0.15+0.43*exp(-0.06*alpha);
a = 0.27;
aP = Kt-k0;
bP = k1-k0;
aPP = 1.09*k1-k0;
q = 0.5*(1+sin(pi*((aP./bP)-0.5)));
qP = 0.5*(1+sin(pi*(aPP./bP-0.5)));
e = 1-(1-d1).*(a*qP.^(0.5)+(1-a)*qP.^2);
N = length(Kt);
ks =zeros(N,1);
for i=1:N
if Kt(i) > 1.09*k1(i)
        ks(i) =1-((1.09*k1(i).*(1-e(i))./Kt(i));
elseif Kt(i)< k0
        ks(i) =1;
    else
        ks(i) = 1-((1-d1(i)).*(a.*q(i).^(0.5)+(1-a).*q(i).^2));
 end
end
Ibms = (Ig.*(1-ks))./sin(alpha);
a = 0:1:1200;
b = 0:1:1200;
subplot(3,2,6)
plot(a,b);
hold on;
scatter(Ibms,Ib)
title('Skartveit & Olseth')
xlabel('Direct measured (W/m^2)')
ylabel('Direct modelled (W/m^2)')
```

```
% Plots of diffuse fraction,k vs clearness index,Kt for models: Erbs,
% Orgill and Hollands, Reindl-A, Reindl-B, Boland and Skartveit for
STARlab.

% The following code estimates the beam irradiance from k vs Kt
% correlations. The modelled beam irradiance is plotted against the
% measured irradiance.

%Declaration of constants
Ig = xlsread('1 hr MLAZI.xlsx',3,'d2:d2621'); % Global horizontal
irradiance
Id = xlsread('1 hr MLAZI.xlsx',3,'c2:c2621');% Diffuse horizontal
irradiance
Ib = xlsread('1 hr MLAZI.xlsx',3,'e2:e2621');% Direct normal irradiance
h = xlsread('1 hr MLAZI.xlsx',3,'b2:b2621');% Hour
thetaZ = xlsread('1 hr MLAZI.xlsx',3,'g2:g2621');% Zenith angle
n = xlsread('1 hr MLAZI.xlsx',3,'k2:k2621');% Day number
alpha = (90-thetaZ)*(pi/180);% Solar altitude
lat = -29.97*(pi/180) ; %  Geographical latitude in radians
deltaD = 23.45*sin(((2*pi)/365)*(284+n));   % Declination in degrees
deltaR = deltaD*(pi./180);% Declination in radians
omegaS = acos(-tan(lat)*tan(deltaR)); % Sunset hour
omegaSD = omegaS*(180/pi);Sunset % Hour angle in radians
Eo = 1+0.033*cos(((2*pi)*n)/365);
Isc = 1367; %Solar constant
omegaI = (12-(h-0.5)).*15;
omegaIR = omegaI*(pi./180);
Io = Isc.*Eo.*(sin(deltaR).*sin(lat)+
cos(omegaIR).*cos(lat).*cos(deltaR));% Extraterrestrial solar radiation

% Calculation of Kt, the clearness index
Kt = Ig./Io;
N = length(Ig);

%*********************************************************************

% Erbs model
k=zeros(N,1);
for i=1:N
    if Kt(i)<=0.22
        k(i) = 1.0-0.09*Kt(i);
    elseif Kt(i) > 0.8
        k(i) = 0.165;
    else
        k(i) = 0.9511-0.16041.*Kt(i)+ 4.388.*(Kt(i))^2-16.638.*(Kt(i))^3+
12.336.*(Kt(i))^4;
    end
end
Ibm = (Ig.*(1-k))./sin(alpha);
a = 0:1:1200;
b = 0:1:1200;
hold on
subplot(3,2,1)
```

```
plot(a,b);
hold on;
scatter(Ibm,Ib)
title('Erbs')
xlabel('Direct measured (W/m^2)')
ylabel('Direct modelled (W/m^2)')

%************************************************************************

% Orgill and Hollands model
ko=zeros(N,1);
for i=1:N
    if Kt(i)< 0.35
        ko(i) = 1.0-0.249*Kt(i);
    elseif Kt(i) > 0.75
        ko(i) = 0.177;
        fprintf('%f\n',k(i))
    else
        ko(i) = 1.577-1.84*Kt(i);
    end
end
Ibmo = (Ig.*(1-ko))./sin(alpha);
a = 0:1:2000;
b = 0:1:2000;
subplot(3,2,2)
plot(a,b);
hold on;
scatter(Ibmo,Ib)
title('Orgill and Hollands')
xlabel('Direct measured (W/m^2)')
ylabel('Direct modelled (W/m^2)')

%************************************************************************

% Reindl-A model
kr1 =zeros(N,1);
for i=1:N
    if Kt(i)<=0.30
        kr1(i) = 1.020-0.248*Kt(i);
    elseif Kt(i) >= 0.78
        kr1(i) = 0.147;
    else
        kr1(i) = 1.450-1.670*Kt(i);
    end
end
Ibmr1 = (Ig.*(1-kr1))./sin(alpha);
a = 0:1:1200;
b = 0:1:1200;
subplot(3,2,3)
plot(a,b);
hold on;
scatter(Ibmr1,Ib)
title('Reindl-A')
xlabel('Direct measured (W/m^2)')
```

```
ylabel('Direct modelled (W/m^2)')


%*********************************************************************

% Reindl-B model
kr2=zeros(N,1);
for i=1:N
    if Kt(i)<= 0.30
        kr2(i) = 1.020-0.254*Kt(i)+ 0.0123*sin(alpha(i));
    elseif Kt(i) >= 0.78
        kr2(i) = 0.486*Kt(i)-0.182*sin(alpha(i));
%         fprintf('%f\n',k(i))
    else
        kr2(i) =1.400-1.749*Kt(i)+ 0.177*sin(alpha(i)) ;
    end
end
Ibmr2 = (Ig.*(1-kr2))./sin(alpha);
a = 0:1:1200;
b = 0:1:1200;
subplot(3,2,4)
plot(a,b);
hold on;
scatter(Ibmr2,Ib)
title('Reindl-B')
xlabel('Direct measured (W/m^2)')
ylabel('Direct modelled W/m^2)')


%*********************************************************************

% Boland model
kb=zeros(N,1);

for i=1:N
    kb(i) = 1./(1+exp(7.997*(Kt(i)-0.586)));
end
Ibmb = (Ig.*(1-kb))./sin(alpha);
a = 0:1:1200;
b = 0:1:1200;
subplot(3,2,5)
plot(a,b);
hold on;
scatter(Ibmb,Ib)
title('Boland')
xlabel('Direct measured (W/m^2)')
ylabel('Direct modelled (W/m^2)')


%*********************************************************************
% Skartveit and Olseth model
k0 = 0.2;
k1 = 0.87-0.56*exp(-0.06*alpha);
```

```
d1 = 0.15+0.43*exp(-0.06*alpha);
a = 0.27;
aP = Kt-k0;
bP = k1-k0;
aPP = 1.09*k1-k0;
q = 0.5*(1+sin(pi*((aP./bP)-0.5)));
qP = 0.5*(1+sin(pi*(aPP./bP-0.5)));
e = 1-(1-d1).*(a*qP.^(0.5)+(1-a)*qP.^2);
N = length(Kt);
ks =zeros(N,1);
for i=1:N
if Kt(i) > 1.09*k1(i)
        ks(i) =1-((1.09*k1(i).*(1-e(i))./Kt(i));
elseif Kt(i)< k0
        ks(i) =1;
    else
        ks(i) = 1-((1-d1(i)).*(a.*q(i).^(0.5)+(1-a).*q(i).^2));
 end
end
Ibms = (Ig.*(1-ks))./sin(alpha);
a = 0:1:1200;
b = 0:1:1200;
subplot(3,2,6)
plot(a,b);
hold on;
scatter(Ibms,Ib)
title('Skartveit & Olseth')
xlabel('Direct measured (W/m^2)')
ylabel('Direct modelled (W/m^2)')
```

Appendix H: Sample calculation of a data point (Erbs et al. [29])

Sample calculation of the Erbs et al. [29] model

The following is a sample calculation of how the predictive model by Erbs et al. [29] was used to estimate DNI. Measurements of GHI and DHI are known and obtained from an unshaded pyranometer and NIP respectively and read in real time. For example, an extract of the data file for 2 January 2011 for the Howard College station is shown below. The file shows the minute values at which the irradiance values were recorded. A sample calculation of the model is used for the data highlighted in the figure below for 9:30 am.

From the figure below,

$I_g = 915.4$ W/m^2

$I_d = 258.2$ W/m^2

$I_b = 739.1$ W/m^2

$\theta_Z = 34.4°$

	A	B	C	D	E	F	G	H	I	J	K
1	Time	DHI	GHI	Perforate	DNI	Julian Day	Hour angl	Zenith angl	Azimuth ang	Declination	Obliquity
197	08:22 AM	243.0082	624.9022	581.4734	520.8863	2455564	305.1761	49.16486	264.101147	-22.940667	23.437807
198	08:23 AM	248.2607	714.4821	671.2711	650.3136	2455564	305.426	48.948644	264.205154	-22.940606	23.437807
258	09:23 AM	293.5742	805.1935	748.6718	541.9695	2455564	320.4211	35.926505	271.036529	-22.936942	23.437807
259	09:24 AM	296.7828	1010.585	949.0685	794.8989	2455564	320.6711	35.709158	271.165559	-22.936881	23.437807
260	09:25 AM	287.3231	910.6162	846.7951	663.4656	2455564	320.921	35.49182	271.295322	-22.936819	23.437807
261	09:26 AM	269.7161	586.1537	529.0964	272.7981	2455564	321.1709	35.274493	271.425832	-22.936758	23.437807
262	09:27 AM	260.7538	398.1975	346.2233	68.77988	2455564	321.4208	35.057178	271.557107	-22.936697	23.437807
263	09:28 AM	261.1912	682.618	630.4957	425.025	2455564	321.6707	34.839876	271.689162	-22.936636	23.437807
264	09:29 AM	255.3563	636.0449	593.9628	387.3327	2455564	321.9207	34.622589	271.822014	-22.936575	23.437807
265	09:30 AM	258.1769	915.4213	873.2893	739.0575	2455564	322.1706	34.405317	271.95568	-22.936513	23.437807
266	09:31 AM	259.3859	927.4253	886.7039	755.1066	2455564	322.4205	34.188063	272.090177	-22.936452	23.437807
267	09:32 AM	255.9922	946.0175	900.6557	773.3127	2455564	322.6704	33.970826	272.225522	-22.936391	23.437807
268	09:33 AM	246.7116	881.935	827.7926	686.7435	2455564	322.9203	33.753609	272.361736	-22.93633	23.437807
269	09:34 AM	239.9773	661.3212	608.2108	422.7865	2455564	323.1702	33.536413	272.498835	-22.936268	23.437807

The time in hours, h at which each measurement is taken is calculated from the known stored minute values of each daily file. Here, the value of h is 9:30 am and is calculated in hours to be

$h = 9.50$

The day number of the year, n is known and is an input in calculating the solar declination angle using the equation by Cooper [39],

$\delta = \left[23.45 \sin\left(\frac{284+n}{365} 2\pi\right)\right]$ = -22.93°

where n = 2 for 2 January 2011.

The site geographical latitude is known, that is -29.52° for the Howard College station.

$I_{SC} = 1367$ W/m^2

The hourly horizontal extraterrestrial solar irradiation is calculated at the middle of every hour from ω_i , the hour angle at the middle of the i[th] hour.

$$E_0 = 1 + 0.033\cos(\frac{2\pi n}{365}) = 1.033$$

$\omega_i = [12 - (h - 0.5)]15 = 107.7°$

The terrestrial irradiance is calculated as

$I_o = I_{SC} E_0 \sin\delta \sin\Phi + \cos\omega_i \cos\Phi \cos\delta = 1071$ W/m^2

$I_{SC} = 1367$ W/m^2 is the solar constant and the clearness index is calculated to be,

$$k_t = \frac{I_g}{I_o} = 0.855$$

The diffuse fraction by the model of Erbs et al. [29] is calculated when the following conditions are met for the range of the clearness index, k_t.

$k = 0.165$

$k = 1.0 - 0.098k_t \quad when \;\; k_t < 0.35$

$k = 0.9511 - 0.1604k_t + 4.388{k_t}^2 - 16.638{k_t}^3 + 12.336{k_t}^4 \quad when \;\; 0.35 \leq k_t \leq 0.75$

$k = 0.165 \quad when \;\; k_t > 0.75$

From the above clearness intervals, the corresponding diffuse fraction is $k = 0.165$.

The diffuse fraction, k is defined as the ratio of the measured diffuse horizontal (after correction for the shadow band effect) to the global horizontal irradiance,

$$k = \frac{I_d}{I_g} \rightarrow I_g = \frac{I_d}{k}$$

Therefore, from equation 1.1, the direct normal irradiance, is given as

$$I_b = \frac{I_g(1-k)}{\cos\theta_z} = 926.4 \text{ W/m}^2$$

where the parameter, k is the diffuse fraction calculated from the model by Erbs et al. [29].

Compared with the measured DNI from the NIP (739.1 W/m^2), the model by Erbs et al. [29] overestimates the DNI.

4.2.3 Comparison between measured direct normal data and predictive models

Due to the high cost of radiometric instruments, various mathematical models have been developed to estimate the missing component of irradiance as calculated from equation 1.1. Examples are those linking the diffuse fraction, k and the clearness index, k_t. Orgill and Hollands, Skartveit and Olseth, Reindl et al. and Boland et al. [29, 33, 31, and 32] established hourly correlations between the diffuse fraction, k and clearness index, k_t under diverse climatic conditions. In [29], [31] and [33], the data were split into regions defined for different values of the clearness index before attempting any regression. Boland et al. [32] constructed a continuous model for the whole range of the clearness index, that is, from zero (fully overcast) to unity (clear sky). They showed that this empirical relationship does not require splitting the clearness interval into three sub intervals as done by the other authors (Fig. 4-19). This allows for greater flexibility for altering the relationship to cater for location differences [60]. Using this proposed model, they showed that it can be adopted for 15 minute data as well as hourly data as experimental validation showed similarity. Figure 4-19 is an illustration of the clearness index split into three different regions that describe the condition of the sky: overcast, partly cloudy and clear.

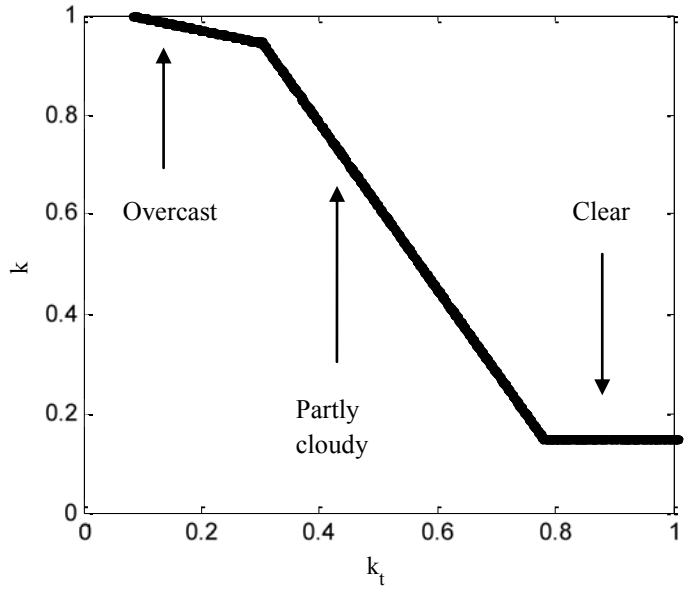

Fig. 4-19 Splitting the clearness index into three sub-regions: overcast, partly cloudy and clear skies using a correlation between diffuse fraction and clearness index.

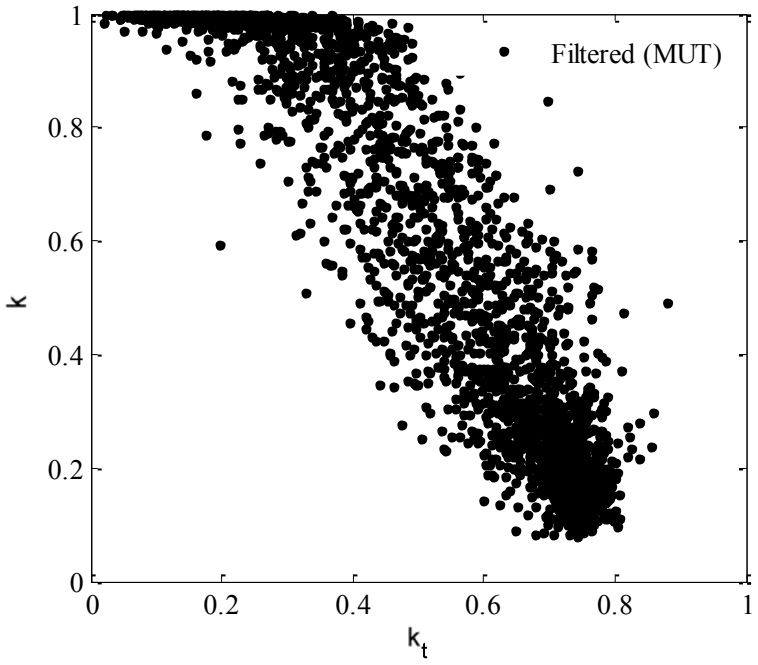

Fig. 4-23 Filtered data from STARlab after the removal of outliers.

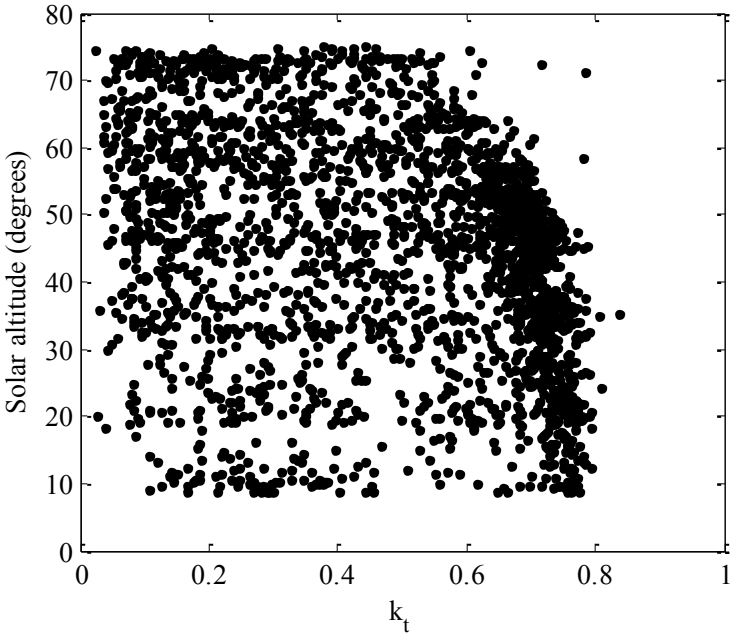

Fig. 4-24 Solar altitude versus clearness index.